Title
Mechanisms of Cohesin Function Revealed by Analysis of Smc3

Author
Robison, Brett

Publication Date
2017

Peer reviewed|Thesis/dissertation

Mechanisms of Cohesin Function Revealed by Analysis of Smc3

By

Brett R Robison

A dissertation submitted in partial satisfaction of the

requirements for the degree of

Doctor of Philosophy

In

Molecular and Cell Biology

in the

Graduate Division

of the

University of California, Berkeley

Committee in charge:

Professor Douglas E Koshland, Chair
Professor Elçin Ünal
Professor Jasper Rine
Professor Kathleen R Ryan

Spring 2017

Abstract

Mechanisms of Cohesin Function Revealed by Analysis of Smc3

by

Brett R Robison

Doctor of Philosophy in Molecular and Cell Biology

University of California, Berkeley

Professor Douglas E Koshland, Chair

A central problem in biology is how genetic material is organized and inherited during cell divisions without loss of information. The conserved protein complex cohesin functions to ensure chromosomes are partitioned equally when cells divide. Cohesin mediates sister chromatid cohesion, chromosome condensation, efficient repair of DNA damage and regulation of transcription. The activity by which cohesin performs these functions is through DNA tethering. Tethering can occur between two sister chromatids or within a single chromatid to bring together two separate positions along its length. Within this dissertation, I will describe novel insights into the mechanism by which cohesin performs these critical activities on chromosomes. I chose to study this problem in the budding yeast *Saccharomyces cerevisiae* because of the unparalleled genetic tools available in this model eukaryote.

Cohesin consists of four core subunits referred to in yeast as Mcd1p, Scc3p, Smc1p, and Smc3p, whereas spatiotemporal control of cohesin activity depends on auxiliary factors. To better understand cohesin architecture and regulation, I performed a genetic screen to identify novel mutants of the Smc3p subunit. Characterization of these mutants has revealed functions for previously undescribed regions of Smc3p and new activities for previously described domains that further our understanding of this complex molecular machine. First, I describe a series of mutations at the interface between Smc3p and Mcd1p termed the DNA “exit gate”. This investigation revealed an unexpected role for this interface in loading cohesin on chromosomes. Second, I reveal a novel role for the Smc3p hinge domain in cohesion maintenance that is independent of its ability to stably bind chromosomes. This discovery lends additional weight against a simple “embrace” model for DNA tethering by cohesin still supported by many in this field. Moreover, this observation suggests that communication between the Smc3p hinge, Mcd1p, and regulator Pds5p is required for cohesion maintenance. Finally, I show that a specific region in the middle of the cohesin ring is critical for a step in the process of cohesin loading onto chromosomes. This result is surprising since it suggests that a contortion of the cohesin ring is critical for it to productively bind chromosomes. In sum, this dissertation advances our understanding of the mechanism by which cohesin functions and supports a variation of the “handcuff” model in which an activity after DNA binding is required for cohesin to achieve tethering.

This dissertation is dedicated to my nephew, Magnus Ryan Walker,
who was born September 4th, 2016

Acknowledgements

It is fair to say that you are reading these words thanks to a tremendous group effort. I wish to especially acknowledge those who encouraged me to continue my studies in the face of both internal and external obstacles.

First, I'd like to thank my advisor Doug Koshland. Doug has been instrumental in helping me view perceived failures as learning moments. He has provided imagination and positivity when all I could see is negative results though a lens of dogged skepticism. Doug has cultivated a pleasant lab culture and advocates a work-hard/play-hard philosophy that I appreciate. Many mentor-mentee relationships are complicated and ours has been no different. My appreciation for Doug grows together with my perspective and maturity. Thanks Doug.

I thank members of the Koshland and Weis labs who have provided welcome relief from the routines of work. In no particular order, I thank Hugo Tapia for making me excited about science at a point when I desperately needed it and for reminding me that a certain fiery rebelliousness can be a refreshing relief. Speaking of which, Vinny Guacci, no stranger to enlivening conversations, thank you for patiently fielding my questions about protocol minutiae and allowing to grow as a critical thinker. Thomas Eng, I appreciate your patience with me during my rotation and your very generous willingness to step up and help me out; you were a welcome voice of calm reason when I could not provide one for myself. Also cats. Michelle Bloom has provided levity in many a dull situation and was a great partner with whom to gripe. Thanks Rebecca Lamothe for your willingness to listen and for helping me gain perspective and appreciation for my work when I sorely needed it. Jeremy Amon, without you my bad puns and obscure musical references would have fallen on deaf ears, you are a very literally a gentleman and a scholar. It has been a pleasure to see Skylar Kim grow as scientist. Skylar, I admire your thoughtfulness and boundless enthusiasm for science and life. I thank Anjali Zimmer for her warm presence and willingness to put up with philosophical babble. To my present and past baymates Lorenzo Costantino and Lamia Wahba, you both set a high fashion bar and your wardrobes, though vast, have nothing on your scientific talents. Lorenzo has taught me the virtue of rejecting outright that which does not make sense to or interest me. I thank Gamze Camdere for showing me what is possible in a test tube and Martin Kupiec for showing me what is possible in a well-run suppressor screen. Ryan Holly it has been a pleasure seeing you grow and hearing your snarky retorts. Thanks Heba Farag for your cheerful spirit and wit. I appreciate the guidance of Chris Mugler, Leon Chan and Karsten Weis. I thank Karsten for being a patient listener, providing a space for me to develop my scientific voice, and giving me honest feedback and encouragement.

I thank my thesis committee for staying with me despite the dizzying dance of my various projects. Jasper Rine, it is embarrassing to admit but I have watched your undergraduate lectures online for the shear enjoyment of it. Kathleen Ryan and Elçin Ünal I thank you for your helpful advice and direction.

I owe my opportunity to pursue a PhD in large part to Brian Kennedy, Matt Kaeberlein and Marion Schmidt who have collectively showed me the importance of collaboration, communication, and common ground. Thanks Brian for giving me a very long leash to pursue my curiosities and inviting me to the Buck Institute. Mark

McCormick has been a great friend and provided a lot of advice and good humor as I navigated personal and professional obstacles.

I have met the most amazing and supportive friends while pursuing my PhD. I had a great time getting to know the entire MCB 2011 cohort through the years. Big head nod to Jonathan Braverman for being a sort of Jiminy Cricket in scientific and personal matters. You were always willing to discuss science and help with strategy of any kind. I appreciate Thornton Thompson for being an awesome roommate, fearless, and a model citizen. Thanks Jesse Niebaum for encouraging my antics with humor and only a little judgement. Thank you, Jorge Santiago Ortiz, for your constant willingness to help, your amazing attitude and sense of humor, and for letting me help get kids excited about science at SMART. Thanks Caleb Cassidy-Amstutz, you have been a source of boundless and, some might say, trivial knowledge and are a reliable confidant. I thank Cody Little for encouraging personal growth and moral rigor and Ryan Hyde for reminding me that now is the time to have an adventure. I appreciate the support of Cameron McCool for teaching me that true friendship persists even when people are separated by long distances.

I am especially grateful for my loving family. I thank the Kensington Ream contingent for adopting me while at Berkeley and showing me what courage looks like. I thank my sister Amber and her husband Hall for sharing their home and young family with me. I look forward to seeing little Eleanora and Magnus grow through the years. Thanks Jan Robison, Erik and Roxanne Gillett for always making me feel welcome and appreciated and for helping care for Dad. I am grateful for my father, John Robison, who has inspired my curiosity and taught me the importance of challenging my own beliefs to gain a deeper understanding of the world. Thanks Dad for giving me the freedom to choose my own adventure, make mistakes and grow through experience. Thanks Bob Carey for spending time with and supporting my Mom. I am immensely grateful for my mother, Cheryl Robison, whose support I could always count on. Thanks, Mom, for always seeing the best in me and reminding me of the Anacortes community that nurtured my growth and supports me still.

Finally, I'd like to thank Rachel Hood for accompanying me on this journey. When I struggled, you reminded me how much I have to appreciate. You helped me get out of my head and see the beauty that is all around and right in front of me. I am inspired by how you confront your fears with grace and your genuine and expansive curiosity for the subtle pleasures of life. I look forward to evolving together in love as monkey companions do.

Table of Contents

Chapter One: Introduction to Cohesin

Chromosomes and the discovery of cohesin

A central problem in biology is how genetic material is organized and inherited during cell divisions without loss of information. Linear DNA molecules are hierarchically organized by chromatin proteins to form the chromosomes of eukaryotic cells. Chromatin proteins orchestrate DNA metabolic processes like replication and transcription, but also serve structural functions. These structural functions include condensation of chromosomes and cohesion of replicated sister chromatids in preparation for cell division. Condensation shortens chromosomes and is thought to prevent their tangling during anaphase and severing of lagging arms during cytokinesis. Sister chromatid cohesion pairs replicated chromosomes together during and after their synthesis in S phase. Cohesion helps ensure that sister chromatids engage with microtubules from opposite poles of the mitotic spindle and provides resistance between opposing spindle forces to allow metaphase congression and orderly segregation during anaphase.

Early studies of sister chromatid pairing produced two possible cohesion mechanisms. In the first, regions of replicated chromatids were thought to be held together by DNA catenations that were resolved upon anaphase onset. This model arose from the observation that Topoisomerase II, which can decatenate intertwined DNA, was required for proper chromosome segregation. In the second, proteinaceous bridges were proposed to link replicated chromatids. This was consistent with an observed requirement for ubiquitin-dependent proteolysis in segregation at anaphase. The development of fluorescence *in situ* hybridization (FISH) in the genetically tractable yeast *Saccharomyces cerevisiae* permitted screens that ultimately helped distinguish between these two proposed mechanisms of chromatid pairing. Discovery of the evolutionarily conserved cohesin complex, a member of the SMC complex family, confirmed that sister chromatid cohesion was achieved by protein linkages (Guacci et al. 1997; Michaelis et al. 1997). Subsequent investigation has revealed that in addition to sister chromatid cohesion, cohesin is also involved in shaping the higher-order structure of chromosomes in the process of condensation, repairing DNA double-strand breaks, and facilitating enhancer-promoter interactions that underlie transcription.

Cohesin architecture: Smc folding, ATPases, and interfaces of the core trimer

Cohesin shares structural and functional similarities with other members of the SMC complex family. Cohesin's structural features underlie its functions on chromosomes and are important targets of regulators. Cohesin is composed of four highly conserved proteins referred to in yeast as Smc1p, Smc3p, Mcd1p (also called Scc1p) and Scc3p (Figure 1). Its Smc1p and Smc3p subunits, which are approximately ~1200 amino acids in length, share an unusual folding and domain architecture with other SMC proteins (Strunnikov et al. 1993; Haering et al. 2002). Their N and C-termini form a bi-lobed globular "head" domain. Within the head domain are key motifs that make up the

ATPase active site, which resembles those of ABC-like transporters (Lowe et al. 2001). Extending from the head domain are long, N and C-terminal alpha helices that fold back upon themselves to form a ~45nm long antiparallel coiled coil (Figure 1). At the transition between N and C-terminal stretches of coiled coil, opposite the head domain, is a globular dimerization domain that links Smc1p and Smc3p together called the hinge. The V-shaped dimer formed by Smc1p and Smc3p is joined by Mcd1p. Mcd1p binds to Smc3p at its N-terminus and Smc1p at its C-terminus. Mcd1p is uniquely poised to regulate the Smc ATPase heads, and the structurally undefined “linker” between its Smc contact points is constitutively bound by Scc3p and binds regulators Pds5p and Scc2p in a cell cycle-dependent manner (Figures 1 and 2). Cohesin therefore consists of a core trimer of the Smc heterodimer and Mcd1p which binds regulators. This core architecture is shared with condensin, a protein complex involved in chromosome condensation in eukaryotes, and BsSMC-ScpAB, a complex with condensin-like activity found in prokaryotes that is well-characterized biochemically.

The head domains of Smc1p and Smc3p form a composite ATPase resembling ABC-like transporters and serve critical mechanistic roles in DNA loading/unloading and cohesion establishment (Melby et al. 1998; Hirano et al. 2001; Murayama and Uhlmann 2015; Çamdere et al. 2015). Each Smc head contains a Walker A motif that allows nucleotide binding and Walker B, D-loop, and Signature motifs that promote hydrolysis of ATP held on the opposite Smc head. This arrangement requires that Smc1p and Smc3p heads come together for ATP to be hydrolyzed. The ATP hydrolysis rate of purified cohesin is very low, so it has been speculated to couple hydrolysis to ring opening or conformational changes rather than serving as a motor to allow cohesin movement on DNA (Arumugam et al. 2006). Divergence between Smc1p and Smc3p may have allowed specialized roles for each of their ATPase functions. Recent work has demonstrated a critical role of the Smc1p ATPase in supporting cohesin binding to chromosomes while the Smc3p ATPase appears to be involved in the process of cohesion establishment (Çamdere et al. 2015; Elbatsh et al. 2016). Since cohesion establishment occurs after cohesin binds to chromosomes, the requirement of the Smc3p ATPase in this process is intriguing. It suggests that a conformational change coupled to the Smc3p ATPase cycle may underlie the critical step by which cohesin tethers sister chromatids.

On the opposite end of the coiled coil from the ATPase head domains is the hinge dimer, which joins Smc1p and Smc3p together. The hinge dimer is toroidal in shape and consists of two sites of contact between Smc1p and Smc3p, termed “North” and “South” (Mishra et al. 2010). Initial observations of Smc1p/Smc3p dimers by electron microscopy suggested the hinge merely dimerizes the Smcs, but subsequent mutant analysis has revealed that dimerization may not be its only function. Mutations that impair the hinge interfaces can support cohesin assembly and loading on DNA but increase cohesin turnover on DNA and fail to support cohesion (Mishra et al. 2010). Opening of the hinge appears to be essential for loading of cohesin onto chromosomes (Gruber et al. 2006). In contrast, the other two interfaces of cohesin, those between Smc1p/Mcd1p and Smc3p/Mcd1p are not required to open for cohesin to load onto

chromosomes. A crystal structure of the mouse Smc1p/Smc3p hinge dimer showed that a positively charged channel is a conserved feature of the hinge (Kurze et al. 2011). This channel does not appear to be large enough for a DNA double helix to pass through. Neutralization of the positive charges within the channel preserves the strong interface, allows cohesin assembly and localization on chromosomes, but impairs cohesion. Histones and other DNA interacting proteins have strong positive charges, and the hinge may serve as a sensor of DNA binding. Hinge domains of cohesin, condensin, and BsSMC-ScpAB complexes all bind DNA (Arumugam et al. 2003; Chiu et al. 2004; Griese et al. 2010; Hirano and Hirano 2006). Moreover, crosslinking between coiled coils emerging from the BsSMC hinge is reduced in the presence of DNA (Soh et al. 2015). The loss of crosslinking upon DNA binding to the BsSMC hinge raises the interesting possibility that a general function of SMC complex hinge domains is to sense DNA and promote conformational changes necessary for complex function. The roles that hinge opening and DNA-dependent conformations play in cohesin function on chromosomes await further investigation.

Opposite the hinge, the other two interfaces that comprise the core trimer of cohesin involve binding of Smc heads to Mcd1p. This uniquely positions Mcd1p to communicate with the ATPase. The first interface of cohesin to be crystalized was the Smc1p head together with the C-terminal winged-helix domain of Mcd1p (Haering et al. 2004). This C-terminal domain of Mcd1p stimulates ATP hydrolysis by Smc1p/Smc3p head heterodimers, showing that this interface not only acts to close the cohesin ring but also serves to modulate its compound ATPase (Arumugam et al. 2006). Due to the structural conservation between Smc1p and Smc3p, it was supposed that Mcd1p would bind in a similar, symmetric manner to Smc3p. A clue that an alternative mode of binding was possible came from the crystal structure of the BsSMC head with its Mcd1p-like ScpA subunit. ScpA bound not to the head domain but to the base of the BsSMC coiled-coil (Burmann et al. 2013). Instead, a crystal structure between the N-terminus of Mcd1p and Smc3p head shows that Mcd1p forms a helix bundle along the coiled coil emerging from the head of Smc3p (Gligoris et al. 2014). The asymmetry in Mcd1p-Smc interactions has important regulatory consequences. The Mcd1p/Smc1p interface regulates the Smc1p ATPase while the Mcd1p/Smc3p interface is disrupted by the action of Wpl1p (Beckouet et al. 2016). Wpl1p is the yeast homolog of Wapl, a protein originally identified as an antagonist of cohesin in metazoans (Kueng et al. 2006). Furthermore, the Mcd1p/Smc3p interface is subject to post-translational modification in response to DNA double-stranded breaks. In yeast, DNA damage can trigger cohesion generation in M phase in addition to the cohesion that normally occurs in S phase (Ünal et al. 2007). Modulation of the Smc3p/Mcd1p interface allows cohesion generation to occur outside of S phase to help repair DNA damage. The effects of these modifications on the stability of the Mcd1p/Smc3p interface, and subsequent cohesin function in response to DNA damage, will be important to resolve.

The cohesin coiled coils or “arms”, which are about 45 nm long and connect the head and hinge domains, were considered primarily as a barrier to prevent escape of pairs of DNA molecules from with cohesin (Haering et al. 2002). Although initial electron

microscopy images showed cohesin's coiled coils as flexible rings, recent scanning force microscopy suggests that, like condensin and the BsSMC-ScpAB complex, cohesin's coiled coils can be seen collapsed into a "rod" shape (Kulemzina et al. 2016; Soh et al. 2015; Anderson et al. 2002). Mutating all arm lysines to arginines prevents any possible acetylation of the coiled coils by Eco1p (Kulemzina et al. 2016). It was found that the absence of acetylation-competent arms prevents "rod" formation and impairs cohesin loading, implying that the cohesin loading reaction requires close arm juxtaposition to bind DNA or interact with Scc2p/Scc4p. Extensive crosslinking interactions have been observed between Smc1p and Smc3p coiled coils in human and yeast cohesin, suggesting that rod formation occurs in cells (Huis in t Veld et al. 2014; Chao et al. 2017). Paradoxically, flexible coiled-coil conformations may be necessary for DNA loading and cohesion establishment. It has been suggested that the ATPase controls loading of DNA through the hinge, and evidence from both budding yeast and *S. pombe* cohesin supports that a juxtaposition between the hinge and heads may be enforced by Scc2p/Scc4p (Mc Intyre et al. 2007; Murayama and Uhlmann 2015). To achieve this, cohesin's coiled coils would have to bend considerably. A similar contortion has been proposed to accompany the cohesion establishment step in which Eco1p acetylates Smc3p-K112, K113 (Kurze et al. 2011). Whether the cohesin coiled coils dynamically alternate between rigid rods and flexible flaps awaits identification and characterization of mutants that can specifically disrupt these functions.

Models for tethering of DNA by cohesin

The core activity of cohesin is its ability to tether two DNA duplexes. The dual roles of cohesin in sister chromatid cohesion and condensation suggest that the complex must be able to form interstrand tethers between sister chromatids as well as intrastrand tethers within a single chromatid. Models for how cohesin may mediate these forms of tethering are illustrated in Figure 3. Early electron microscopy images of SMC complexes inspired a simple model of DNA tethering, the "embrace," by which two DNA duplexes pass through a ring formed by the Smc1p/Smc3p/Mcd1p trimer (Haering et al. 2002). This model supposes that a single cohesin bound prior to replication can achieve tethering between sisters following passage of the replication fork through the large Smc loop of cohesin. The "embrace" model raises important considerations for the regulation of cohesin-DNA interactions. Through which portion of cohesin does DNA bind? The architecture of cohesin suggests two topologically distinct loops are possible within one complex. The first is the large ~45 nm diameter ring formed by the Smcs and the second is the smaller diameter ring formed by the Mcd1p linker spanning the Smc heads. The Mcd1p ring is expected to be topologically distinct from the larger coiled-coil ring only if the Smc heads are engaged together while ATP bound (Eng et al. 2014). Recent single-molecule studies showed that cohesin could not bypass a ~20 nm obstacle when bound to a single DNA duplex. This observation suggests that the loop through which DNA is bound is much smaller than that observed for Smc coiled coils by electron microscopy and therefore unlikely to accommodate the large DNA replication fork.

The “handcuff” models provide an alternative to the simple “embrace” model. Two variations of the handcuff model are depicted in Figure 3. The intramolecular handcuff model predicts that after the initial topological binding of cohesin to a single DNA duplex, tethering is mediated by a second duplex binding event at a second site in cohesin. The illustration depicts the Mcd1p loop as the second duplex binding site, however it could also be the location of the first duplex binding event. Answering how a second strand may be captured awaits the development of tools that allow modulation of one or more cohesin interfaces at will. The intermolecular handcuff model dispenses with the second duplex binding requirement. This model predicts that cohesin independently binds each sister chromatid, or two positions on the same chromatid in the case of intrastrand compaction, and that tethering is achieved by direct cohesin-cohesin interactions. Evidence in support of this model emerged after investigation of a peculiar genetic interaction between two hypomorphic cohesin mutants, termed interallelic complementation (Eng et al. 2015). Introduction of *mcd1-Q266*, a hypomorphic allele that cannot support viability on its own, restored viability to the temperature-sensitive *mcd1-1* strain at the non-permissive temperature. Interestingly, while the product of *mcd1-1* is normally degraded at the restrictive temperature, the presence of Mcd1-Q266p prevented its degradation and supported its chromosome binding. An interallelic complementing pair was also found among *SMC3* hypomorphic alleles, showing that this phenomenon is not limited to a single cohesin subunit. How can interallelic complementation be reconciled with the apparent stoichiometry of cohesin? Cohesin-cohesin physical interactions may have been missed by previous biochemical characterizations on soluble cohesin if such interactions occur only after cohesin is bound to chromosomes. Crosslinking of cohesin *in vivo* and mapping of contacts by mass spectrometry suggests the possibility of cohesin-cohesin interactions (Huis in t Veld et al. 2014), and initial investigations show the ability of differentially-epitope tagged cohesin subunits (Smc3-FLAGp and Smc3-MYCp) to co-immunoprecipitate. Further confirmation of functional cohesin-cohesin interactions *in vivo* await the identification of mutants whose restoration or inhibition of interallelic complementation correlates with detection of cohesin-cohesin interactions.

Loading and localization of cohesin on chromosomes and the roles of Scc2p and Scc4p

The core cohesin complex is directed to its chromosome functions by the activity of highly conserved and specialized regulatory factors. Mcd1p, but no other cohesin subunit, is destroyed in anaphase by Esp1p, which causes release of cohesin from chromatin. Cohesin reloading onto chromosomes occurs in late G1 only after additional Mcd1p expression. This process requires the dedicated cohesin loader complex comprising Scc2p and Scc4p (Ciosk et al. 2000). Cohesin is enriched near yeast centromeres, within pericentromeres, and at roughly regular intervals along chromosome arms termed cohesin associated regions or CARs (Laloraya et al. 2000). Cohesin chromatin immunoprecipitation shows approximately 1 kb wide CAR peaks, suggesting multiple cohesins may bind at a single CAR. Cohesin is not recruited to a discernable DNA sequence motif, but seems to enrich at sites of convergent transcription and at AT-rich regions (Legronne et al. 2004). Evidence suggests that the

mechanism of cohesin loading is complex and involves the ATPases, Scc3p, and the Smc hinge heterodimer (Hu et al. 2011; Murayama and Uhlmann 2014; Murayama and Uhlmann 2015). The loader complex and cohesin are mutually dependent for chromosome binding, implying that a loader-cohesin complex recognizes sites of loading on chromosomes. Interestingly, Scc2p and Scc4p homologs have been shown to mediate juxtaposition of the Smc hinge heterodimer with the Smc heads in a process that may promote loading (Murayama and Uhlmann 2015). Additional investigation will be needed to assess the structural underpinnings of cohesin loading.

Establishment of sister chromatid cohesion and the role of Eco1p

During DNA replication, chromosome-bound cohesin is converted to a form capable of tethering sister chromatids by the acetyltransferase Eco1p, an essential regulator of cohesin (Skibbens et al. 1999; Toth et al. 1999). Although multiple subunits of cohesin can be acetylated by Eco1p *in vitro* (Ivanov et al. 2002), the critical targets of Eco1p were revealed to be lysines 112 and 113 (K112, K113) of Smc3p (Ünal et al. 2008; Ben-Shahar et al. 2008; Zhang et al. 2008). This regulation ultimately gives rise to cohesion establishment, but multiple mechanistic outcomes of acetylation have been discovered and their consequences on cohesion establishment are under active investigation (Rowland et al. 2009; Guacci et al. 2015; Çamdere et al. 2015). It has been proposed that the role of Smc3p acetylation is to disrupt the activity of Wpl1p, which is recruited to cohesin by Pds5p (Sutani et al. 2009; Rowland et al. 2009). Wpl1p is thought to destabilize cohesin-DNA binding by releasing the N-terminus of Mcd1p from Smc3p (Chan et al. 2013; Beckouet et al. 2016). The fact that *wpl1*Δ (and mutations within *PDS5*, *SMC3*, and *SCC3* that phenocopy *wpl1*Δ) restore viability to *eco1*Δ cells seems to support this model. However, *eco1*Δ *wpl1*Δ cells appear to survive because cohesin function in condensation and not cohesion is restored (Guacci and Koshland 2012). Since condensation function can remain in the absence of cohesion, these two functions of cohesin on chromosomes must be subject to at least partially distinct regulation. Additional factors beyond inhibition of Wpl1p must support cohesion establishment.

Recent studies have revealed an additional role for Eco1p in regulating the cohesin ATPases (Çamdere et al. 2015; Elbatsh et al. 2016). A mutation that reduces the rate of cohesin ATP hydrolysis *in vitro*, *SMC1-D1164E*, restores viability and cohesion to *eco1*Δ cells. Therefore, a second role of Eco1p may be to promote cohesion through downregulating the ATPase of cohesin. Does Eco1p promote capture of a second DNA duplex or prevent loss of a second DNA duplex? The ability of *eco1*Δ to be suppressed by *SMC1-D1164E* suggests that cohesion establishment may be possible without Eco1p and that Eco1p acts to mark cohesive structures after they form rather than promote them in the first place. Since reducing the ATP hydrolysis rate enhances an Eco1p-independent capacity of cohesin to become cohesive, one intermediate of the cohesin ATPase cycle may adopt a cohesion-competent conformation. Further investigation of the conformational dynamics of cohesin may lend critical insight into the cohesive state. While Smc3p acetylation accompanies cohesion establishment, the fact

that this modification persists until cohesin is released from chromosomes in anaphase suggests that it might also help maintain cohesion following S phase (Beckouet et al. 2010).

Cohesion maintenance and the role of Pds5p

Once cohesion is established in S phase, the regulator Pds5p is recruited to cohesin and helps promote cohesion maintenance through mitosis. How Pds5p functions to maintain cohesion is not well understood but its ability to interact with every subunit of cohesin implies that its effect on cohesin activity on DNA is major. Two models have emerged for the essential function of Pds5p in cohesion maintenance. The first model is based on observations that Mcd1p is degraded by a polySUMO-dependent pathway in *pds5* cells, suggesting that Pds5p functions to protect Mcd1p until anaphase onset (Noble et al. 2006; D'Ambriosio et al. 2014). Although the temperature sensitive *pds5-1* mutant can be partially suppressed by deleting the factors responsible for Mcd1p polySUMOylation and degradation, the *pds5*Δ mutant cannot be (D'Ambrosio et al. 2014). This suggests an additional essential function of Pds5p exists beyond protecting Mcd1p. The second model for Pds5p function emerged from the fact that *pds5* mutants are defective in the Eco1p-dependent acetylation of Smc3p at K112 and K113, a phenotype that can be partially restored by deletion of the Hos1p deacetylase (Chan et al. 2013). However, *hos1*Δ cannot restore viability to a *pds5* temperature sensitive mutant despite restoring K112, K113 acetylation. In addition to the requirement of Pds5p for Smc3p-K112, K113 acetylation, Pds5p's stable chromosome binding is impaired in the temperature sensitive *eco1-1* mutant (Chan et al. 2012). This apparent codependence supports the notion that Eco1p and Pds5p functions may be reciprocally reinforcing (Noble et al. 2006). Since neither restoring Mcd1p stability nor Smc3p-K112, K113 acetylation restores *pds5* mutant viability, an additional role of Pds5p in cohesion maintenance may exist. Pds5p can be crosslinked to all cohesin subunits, implying that its association with cohesin is extensive and/or dynamic (Huis in t Veld et al. 2014). Moreover, Pds5p shows strong FRET interaction with the Smc hinge heterodimer (Mc Intyre et al. 2007). The significance of Pds5p-hinge proximity on cohesin function is poorly understood, but may suggest a role for Pds5p and the hinge following cohesin loading onto chromosomes.

In the course of the work I present in subsequence chapters, I have been motivated by a desire to better understand the underlying architecture of cohesin and its regulation. Cohesin is a complicated molecular machine. While an inventory of its parts is available, it is still quite unclear how these parts function individually or as a whole. To what extent are the interfaces of cohesin regulated? Each has been crystallized, but do we know the complete story of how the Smc3p/Mcd1p interface, termed the "exit gate", is regulated? In Chapter 2 I will describe my data that support a role for this interface in cohesin loading on chromosome. Is the Smc hinge merely a dimerization domain or is it involved in cohesin function after chromosome binding? I investigate a novel function of the hinge in Chapter 3. The Smc coiled coils appear as either rigid rods or flexible rings when observed by electron microscopy. Can analyzing coiled-coil mutants inform our

understanding of these dynamic domains? In Chapter 4 I present a panel of mutants in an uninvestigated region of Smc3p that suggest a new role for its coiled coil.

References

Anderson, D. E., Losada, A., Erickson, H. P., & Hirano, T. (2002). Condensin and cohesin display different arm conformations with characteristic hinge angles. *The Journal of Cell Biology*, *156*(3), 419–424.

Arumugam, P., Gruber, S., Tanaka, K., Haering, C. H., Mechtler, K., & Nasmyth, K. (2003). ATP hydrolysis is required for cohesin's association with chromosomes. *Current Biology : CB*, *13*(22), 1941–1953.

Arumugam, P., Nishino, T., Haering, C. H., Gruber, S., & Nasmyth, K. (2006). Cohesin's ATPase activity is stimulated by the C-terminal Winged-Helix domain of its kleisin subunit. *Current Biology : CB*, *16*(20), 1998–2008.

Beckouët, F., Srinivasan, M., Roig, M. B., Chan, K.-L., Scheinost, J. C., Batty, P., et al. (2016). Releasing Activity Disengages Cohesin's Smc3p/Scc1p Interface in a Process Blocked by Acetylation. *Molecular Cell*, *61*(4), 563–574.

Bürmann, F., Shin, H.-C., Basquin, J., Soh, Y.-M., Giménez-Oya, V., Kim, Y.-G., et al. (2013). An asymmetric SMC–kleisin bridge in prokaryotic condensin. *Nature Structural & Molecular Biology*, *20*(3), 371–379.

Çamdere, G., Guacci, V., Stricklin, J., & Koshland, D. (2015). The ATPases of cohesin interface with regulators to modulate cohesin-mediated DNA tethering. *eLife*, *4*, 13115.

Chan, K.-L., Gligoris, T., Upcher, W., Kato, Y., Shirahige, K., Nasmyth, K., & Beckouët, F. (2013). Pds5p promotes and protects cohesin acetylation. *Proceedings of the National Academy of Sciences of the United States of America*, *110*(32), 13020–13025.

Chao, W. C. H., Murayama, Y., Muñoz, S., Jones, A. W., Wade, B. O., Purkiss, A. G., et al. (2017). Structure of the cohesin loader Scc2p. *Nature Communications*, *8*, 13952.

Chiu, A., Revenkova, E., & Jessberger, R. (2004). DNA Interaction and Dimerization of Eukaryotic SMC Hinge Domains. *Journal of Biological Chemistry*, *279*(25), 26233–26242.

Ciosk, R., Shirayama, M., Shevchenko, A., Tanaka, T., Tóth, A., Shevchenko, A., & Nasmyth, K. (2000). Cohesin's Binding to Chromosomes Depends on a Separate Complex Consisting of Scc2p and Scc4p Proteins. *Molecular Cell*, *5*(2), 243–254.

Eckert, C. A., Gravdahl, D. J., & Megee, P. C. (2007). The enhancement of pericentromeric cohesin association by conserved kinetochore components promotes high-fidelity chromosome segregation and is sensitive to microtubule-based tension. *Genes & Development*, *21*(3), 278–291.

Eng, T., Guacci, V., & Koshland, D. (2014). ROCC, a conserved region in cohesin's Mcd1p subunit, is essential for the proper regulation of the maintenance of cohesion and establishment of condensation. *Molecular Biology of the Cell*, *25*(16), 2351–2364.

Eng, T., Guacci, V., & Koshland, D. (2015). Interallelic complementation provides functional evidence for cohesin-cohesin interactions on DNA. *Molecular Biology of the Cell*, *26*(23), 4224–4235.

Gligoris, T. G., Scheinost, J. C., Bürmann, F., Petela, N., Chan, K.-L., Uluocak, P., et al. (2014). Closing the cohesin ring: structure and function of its Smc3p-kleisin interface. *Science*, *346*(6212), 963–967.

Griese, J. J., Witte, G., & Hopfner, K. P. (2010). Structure and DNA binding activity of the mouse condensin hinge domain highlight common and diverse features of SMC proteins. *Nucleic Acids Research*.

Gruber, S., Arumugam, P., Katou, Y., Kuglitsch, D., Helmhart, W., Shirahige, K., & Nasmyth, K. (2006). Evidence that loading of cohesin onto chromosomes involves opening of its SMC hinge. *Cell*, *127*(3), 523–537.

Guacci, V., & Koshland, D. (2012). Cohesin-independent segregation of sister chromatids in budding yeast. *Molecular Biology of the Cell*, *23*(4), 729–739.

Guacci, V., Koshland, D., & Strunnikov, A. (1997). A Direct Link between Sister Chromatid Cohesion and Chromosome Condensation Revealed through the Analysis of MCD1 in S. cerevisiae. *Cell*, *91*(1), 47–57.

Guacci, V., Stricklin, J., Bloom, M. S., Guō, X., Bhatter, M., & Koshland, D. (2015). A novel mechanism for the establishment of sister chromatid cohesion by the ECO1 acetyltransferase. *Molecular Biology of the Cell*, *26*(1), 117–133.

Haering, C. H., Löwe, J., Hochwagen, A., & Nasmyth, K. (2002). Molecular architecture of SMC proteins and the yeast cohesin complex. *Molecular Cell*, *9*(4), 773–788.

Haering, C. H., Schoffnegger, D., Nishino, T., Helmhart, W., Nasmyth, K., & Löwe, J. (2004). Structure and stability of cohesin's Smc1p-kleisin interaction. *Molecular Cell*, *15*(6), 951–964.

Hirano, M., & Hirano, T. (2006). Opening closed arms: long-distance activation of SMC ATPase by hinge-DNA interactions. *Molecular Cell*, *21*(2), 175–186.

Hirano, M., Anderson, D. E., Erickson, H. P., & Hirano, T. (2001). Bimodal activation of SMC ATPase by intra- and inter-molecular interactions. The EMBO Journal, 20(12), 3238–3250.

Hu, B., Itoh, T., Mishra, A., Katoh, Y., Chan, K.-L., Upcher, W., et al. (2011). ATP hydrolysis is required for relocating cohesin from sites occupied by its Scc2p/4 loading complex. *Current Biology : CB*, *21*(1), 12–24.

Huis in t Veld, P. J., Herzog, F., Ladurner, R., Davidson, I. F., Piric, S., Kreidl, E., et al. (2014). Characterization of a DNA exit gate in the human cohesin ring. *Science*, *346*(6212), 968–972.

Intyre, J. M., Muller, E. G., Weitzer, S., Snydsman, B. E., Davis, T. N., & Uhlmann, F. (2007). In vivo analysis of cohesin architecture using FRET in the budding yeast Saccharomyces cerevisiae. *The EMBO Journal*, *26*(16), 3783–3793.

Kueng, S., Hegemann, B., Peters, B. H., Lipp, J. J., Schleiffer, A., Mechtler, K., & Peters, J.-M. (2006). Wapl Controls the Dynamic Association of Cohesin with Chromatin. *Cell*, *127*(5), 955–967.

Kulemzina, I., Ang, K., Zhao, X., Teh, J.-T., Verma, V., Suranthran, S., et al. (2016). A Reversible Association between Smc Coiled Coils Is Regulated by Lysine Acetylation and Is Required for Cohesin Association with the DNA. *Molecular Cell*, *63*(6), 1044–1054.

Laloraya, S., Guacci, V., & Koshland, D. (2000). Chromosomal addresses of the cohesin component Mcd1pp. *The Journal of Cell Biology*, *151*(5), 1047–1056.

Lengronne, A., Katou, Y., Mori, S., Yokobayashi, S., Kelly, G. P., Itoh, T., et al. (2004). Cohesin relocation from sites of chromosomal loading to places of convergent transcription. *Nature*, *430*(6999), 573–578.

Löwe, J., Cordell, S. C., & van den Ent, F. (2001). Crystal structure of the SMC head domain: an ABC ATPase with 900 residues antiparallel coiled-coil inserted. *Journal of Molecular Biology*, *306*(1), 25–35.

Melby, T. E., Ciampaglio, C. N., Briscoe, G., & Erickson, H. P. (1998). The symmetrical structure of structural maintenance of chromosomes (SMC) and MukB proteins: long, antiparallel coiled coils, folded at a flexible hinge. *The Journal of Cell Biology*, *142*(6), 1595–1604.

Michaelis, C., Ciosk, R., & Nasmyth, K. (1997). Cohesins: Chromosomal Proteins that Prevent Premature Separation of Sister Chromatids. *Cell*, *91*(1), 35–45.

Mishra, A., Hu, B., Kurze, A., Beckouët, F., Farcas, A.-M., Dixon, S. E., et al. (2010). Both interaction surfaces within cohesin's hinge domain are essential for its stable chromosomal association. *Current Biology : CB*, *20*(4), 279–289.

Murayama, Y., & Uhlmann, F. (2014). Biochemical reconstitution of topological DNA binding by the cohesin ring. *Nature*, *505*(7483), 367–371.

Murayama, Y., & Uhlmann, F. (2015). DNA Entry into and Exit out of the Cohesin Ring by an Interlocking Gate Mechanism. *Cell*, *163*(7), 1628–1640.

Ng, T. M., Waples, W. G., Lavoie, B. D., & Biggins, S. (2009). Pericentromeric sister chromatid cohesion promotes kinetochore biorientation. *Molecular Biology of the Cell*, *20*(17), 3818–3827.

Rolef Ben-Shahar, T., Heeger, S., Lehane, C., East, P., Flynn, H., Skehel, M., & Uhlmann, F. (2008). Eco1p-dependent cohesin acetylation during establishment of sister chromatid cohesion. *Science*, *321*(5888), 563–566.

Rowland, B. D., Roig, M. B., Nishino, T., Kurze, A., Uluocak, P., Mishra, A., et al. (2009). Building sister chromatid cohesion: smc3 acetylation counteracts an antiestablishment activity. *Molecular Cell*, *33*(6), 763–774.

Skibbens, R. V., Corson, L. B., Koshland, D., & Hieter, P. (1999). Ctf7p is essential for sister chromatid cohesion and links mitotic chromosome structure to the DNA replication machinery. *Genes & Development*, *13*(3), 307–319.

Soh, Y.-M., Bürmann, F., Shin, H.-C., Oda, T., Jin, K. S., Toseland, C. P., et al. (2015). Molecular Basis for SMC Rod Formation and Its Dissolution upon DNA Binding. Molecular Cell, 57(2), 290–303.

Strunnikov, A. V., Larionov, V. L., & Koshland, D. (1993). SMC1: an essential yeast gene encoding a putative head-rod-tail protein is required for nuclear division and defines a new ubiquitous protein family. *The Journal of Cell Biology*, *123*(6 Pt 2), 1635–1648.

Tóth, A., Ciosk, R., Uhlmann, F., Galova, M., Schleiffer, A., & Nasmyth, K. (1999). Yeast cohesin complex requires a conserved protein, Eco1pp(Ctf7), to establish cohesion between sister chromatids during DNA replication. *Genes & Development*, *13*(3), 320–333.

Ünal, E., Heidinger-Pauli, J. M., & Koshland, D. (2007). DNA double-strand breaks trigger genome-wide sister-chromatid cohesion through Eco1 (Ctf7). *Science*, *317*(5835), 245–248.

Ünal, E., Heidinger-Pauli, J. M., Kim, W., Guacci, V., Onn, I., Gygi, S. P., & Koshland, D. E. (2008). A molecular determinant for the establishment of sister chromatid cohesion. *Science*, *321*(5888), 566–569.

Zhang, J., Shi, X., Li, Y., Kim, B.-J., Jia, J., Huang, Z., et al. (2008). Acetylation of Smc3p by Eco1p Is Required for S Phase Sister Chromatid Cohesion in Both Human and Yeast. *Molecular Cell*, *31*(1), 143–151.

Figure Legends

Figure 1: The cohesin complex and the folding of Smc proteins

Smcs have a globular head and hinge domain separated by a coiled coil. The coiled coil is formed by the antiparallel association of long N- and C-terminal helices. Within cohesin, the hinge domains of Smc1p and Smc3p associate to form a heterodimer. Likewise, the head domains of Smc1p and Smc3p associate to form a heterodimer. The distance between Smc head and hinge domains has been estimated to be ~45 nm. Heterodimerization of Smc1p and Smc3p generates a large topological loop observed by electron microscopy. Mcd1p binds Smc1p at its globular head, and Smc3p at the head-proximal base of its coiled coil, creating a second topological loop of cohesin. Mcd1p contains a large unstructured linker domain connecting its two ends that binds Scc3p and the cohesin regulator Pds5p.

Figure 2: Cell cycle dependent regulation of cohesin by accessory factors generates cohesion and condensation

Top: Cell cycle regulation of cohesion. Mcd1p expression allows assembly of soluble cohesin in G1. Soluble cohesin is loaded onto chromosomes by the Scc2p/Scc4p complex in late G1. During DNA replication in S phase, Eco1p acetylates Smc3p at K112, K113 to convert bound cohesin into a tethering state in the process of cohesion establishment. Association of Pds5p with cohesin ensures maintenance of cohesion from its establishment in S phase until M phase. At anaphase onset, Mcd1p is subject to proteolysis by the action of Esp1p. Bottom: Condensation is established following S phase and maintained until anaphase in a process requiring both cohesin and condensin function.

Figure 3: Models of cohesin DNA tethering

Cohesin topologically entraps DNA duplex to bind chromosomes. Duplex-bound cohesin exhibits interstrand tethering to generate sister chromatid cohesion, left, and intrastrand tethering to generate chromosome condensation, right. Illustrations depict tethering according to the embrace model and two versions of the handcuff model. The embrace model predicts that tethering occurs when two DNA duplexes are co-entrapped within the Smc loop. The intermolecular handcuff model predicts that tethering occurs by physical interaction between two cohesin complexes. Alternatively, the intramolecular handcuff model predicts that two distinct DNA duplex binding sites within a single cohesin mediate tethering.

Figure 1

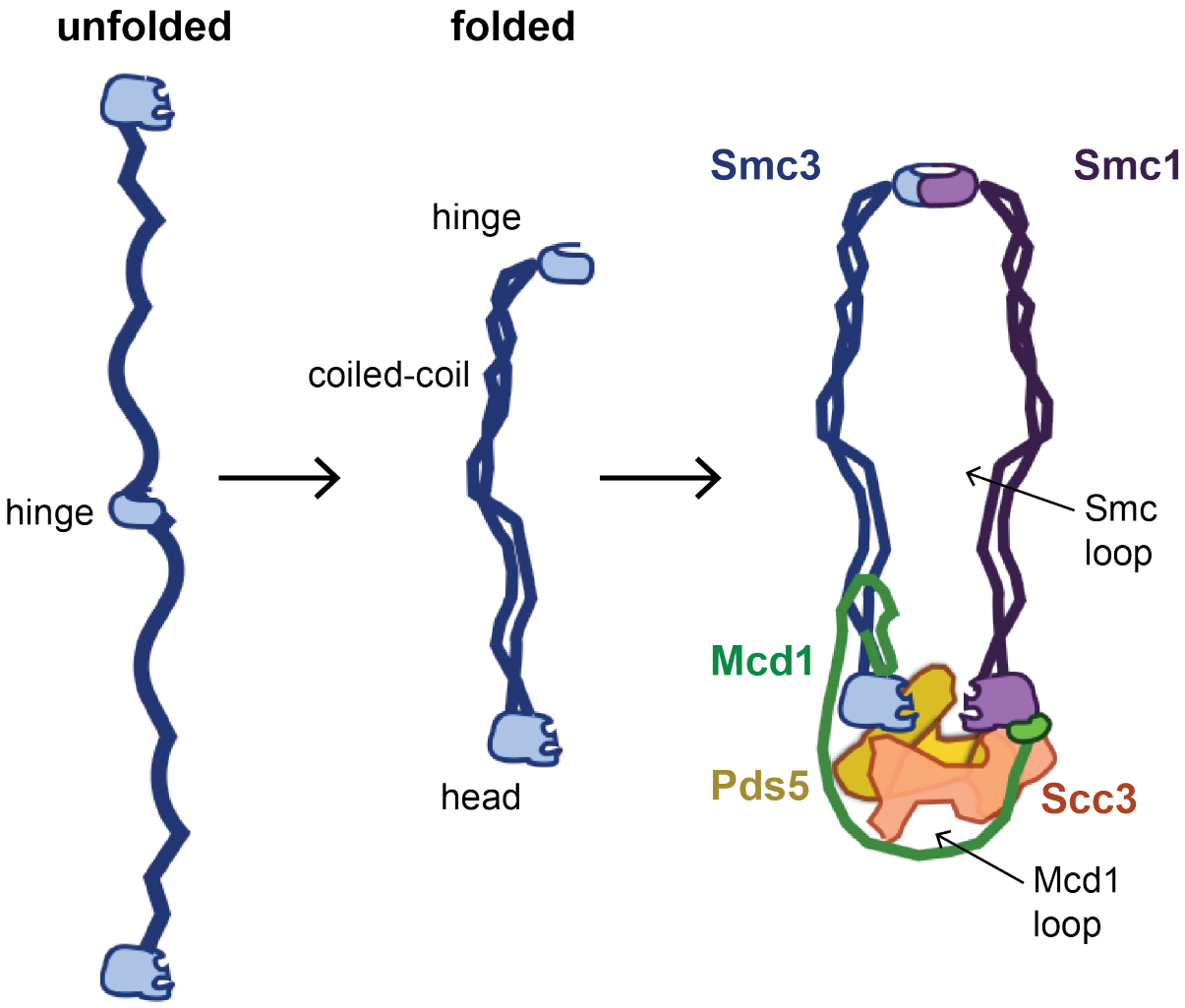
unfolded
folded
hinge
hinge
coiled-coil
head
Smc3
Smc1
Smc
loop
Mcd1
Pds5
Scc3
Mcd1
loop

Figure 2

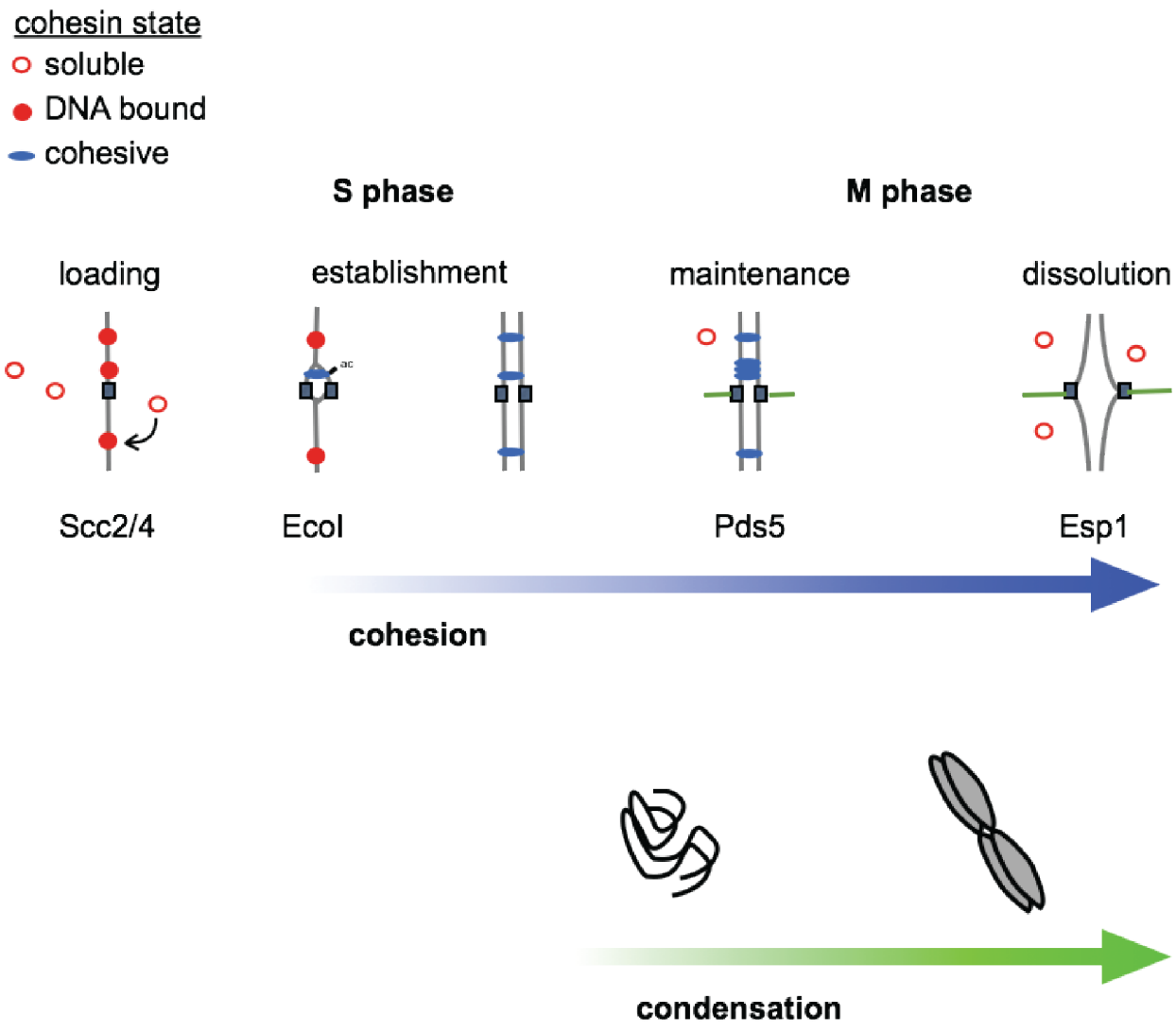
cohesin state
soluble
DNA bound
cohesive
S phase
M phase
loading
establishment
maintenance
dissolution
Scc2/4
Eco1
Pds5
Esp1
cohesion
condensation

Figure 3

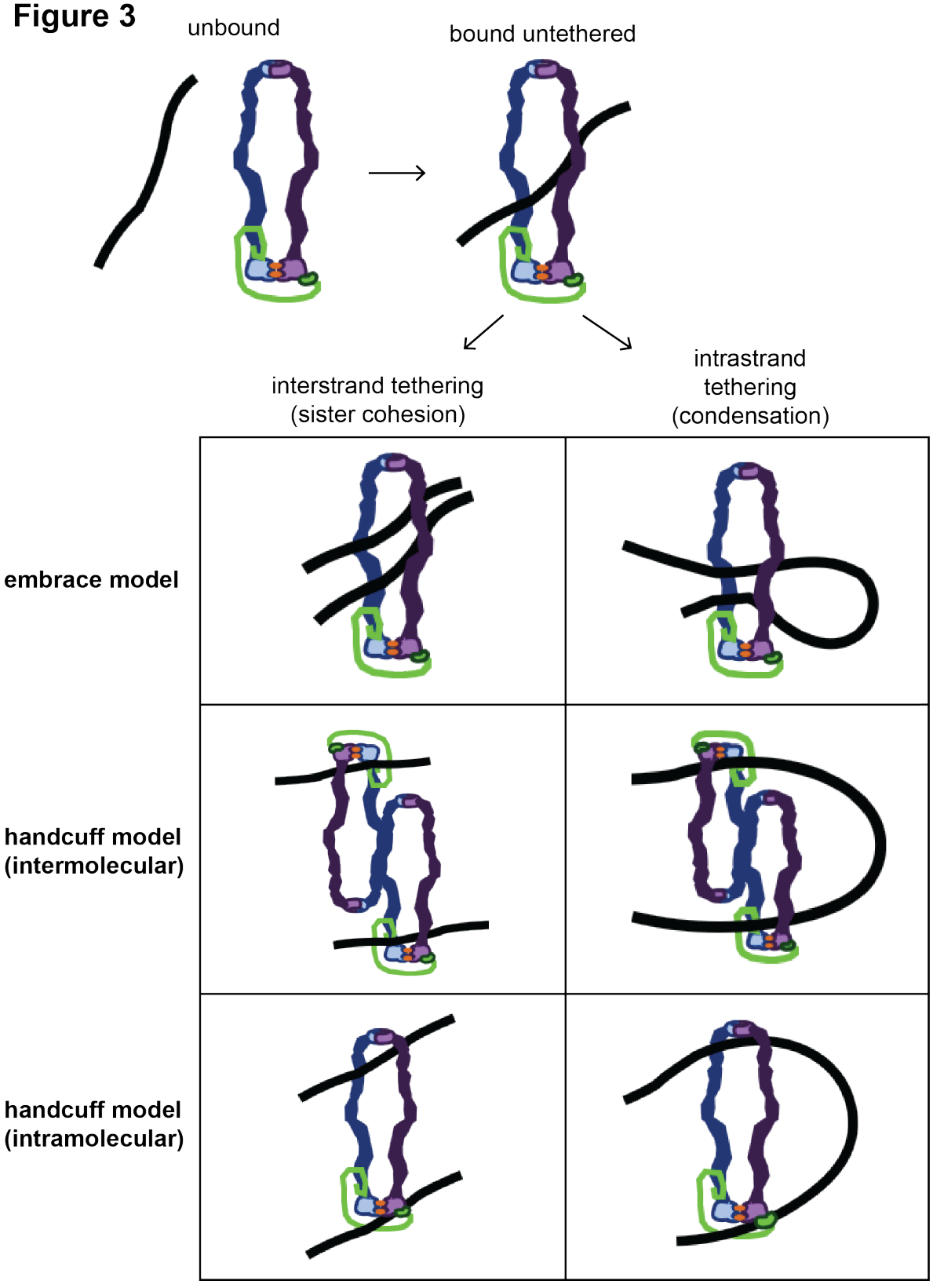
unbound
bound untethered
interstrand tethering
(sister cohesion)
intrastrand
tethering
(condensation)
embrace model
handcuff model
(intermolecular)
handcuff model
(intramolecular)

Chapter Two: Insertion mutagenesis screen of cohesin subunit Smc3p

Introduction

Among the unanswered questions on how cohesin tethers sister chromatids is: what occurs to cohesin once bound to DNA to toggle it from bound to tethering? Activation of cohesin into the cohesive form is complex. The regulators Eco1p and Pds5p act to promote establishment and maintenance of the cohesive state, respectively. Moreover, the core Smc1p/Smc3p ATPases and acetylated lysines of Smc3p also promote the cohesive state. What connects these regulatory factors, post-translational modifications, and enzymatic functions is that they all impact the tethering activity intrinsic to the core SMC subunits. The cascade of events leading to tethering produce an outcome at the level of the core complex, its configuration, and interaction with DNA. Understanding the interplay between regulatory factors and cohesin is key to understanding the tethering state of cohesin.

Mutants that allow cohesin to bind chromosomes but fail to function in either cohesion or condensation provide valuable insight and serve as essential tools to investigate the mechanism of tethering. One such mutant was identified in *MCD1*. This mutant defines a motif referred to as "ROCC" for Regulator of Cohesion and Condensation (Eng et al. 2014). The discovery of ROCC is significant for two reasons. First, it is the first cohesin mutant that is unable to maintain cohesion while remaining stably bound to chromosomes, showing that cohesin's stable binding to DNA is not sufficient to ensure tethering. Since it is known that Mcd1p plays critical roles in loading cohesin onto chromosomes and supporting association with regulatory factors, it was surprising that this mutation disrupted neither of these activities. Instead, ROCC is required for a previously unknown transition in the activity of cohesin once it loads on chromosomes. Second, the discovery of ROCC by a random insertion dominant screen (RID screening, described below) underscores the utility of this mutagenesis strategy to pinpoint interaction surfaces and identify regulated functions of cohesin. RID screening, therefore, is a versatile tool for providing insight into cohesin function.

The Smc3p subunit of cohesin is an attractive candidate for investigation by RID screening and mutant analysis. Smc3p has a domain architecture typical of SMC proteins. The Smc3p polypeptide folds back on itself to form a large dumbbell shaped structure with two globular domains, referred to as the head and hinge, separated by a long coiled coil. The hinge forms a globular domain where polypeptide chain folds back on itself. The N and C-termini come together to form the head domain. The head domains of Smc1p and Smc3p heterodimerize to form a compound ATPase with two ATP binding sites. Smc3p is directly involved in the transition of cohesin that is DNA bound to a state that mediates sister chromatid tethering. Acetylation by Eco1p at lysines K112 and K113 of Smc3p in S phase provides temporal control to tethering, but its consequence on cohesin function remains poorly understood. I reasoned that identification and characterization of RID mutants of *SMC3* could reveal unappreciated aspects of Smc3p's structure, function, and regulation.

Results

RID screen of *SMC3*

SMC3 is essential for cell growth. Thus, impaired growth is a powerful phenotypic consequence of loss of Smc3p function. However, I suspected that a considerable portion of loss-of-function *SMC3* alleles would encode proteins that cannot fold properly or abolish cohesin assembly. To identify alleles that impair some but not all *SMC3* function, I chose to perform a RID screen. Key to this approach is the assumption that overexpression under the galactose-inducible *GAL1* promoter of either wild-type *SMC3* or insertions that cause complete loss-of-function cause no phenotype in otherwise wild-type yeast. On the other hand, rare alleles produced by random mutagenesis may eliminate 1) an activity of Smc3p needed to assemble cohesin, 2) a function of cohesin needed for DNA binding, or 3) a critical aspect of cohesin regulation. When overexpressed, these alleles may titrate one or more cohesin subunits from wild-type Smc3p expressed at normal levels, forcing the assembly of defective complexes and impairing growth.

I sought a mutagenesis strategy that allowed me to easily generate a complex library of synthetic alleles to screen. Of the numerous available mutagenesis approaches I decided to choose an option based on its ability to allow 1) rapid library construction 2) simple identification of the location and nature of the mutant residues and 3) ease of troubleshooting. Therefore, I generated random insertion alleles of *SMC3* using the MuA transposon system to target a *pGAL-SMC3* plasmid (Figure 1A). This system generates a single random insertion of 15 bp (a 10 bp Not1 site between and a 5 bp duplication of the insertion site, details in Materials and Methods). Because of the nature of the transposition reaction, it has the potential to generate three different insertions within a codon. Therefore, it was possible to obtain three unique five amino acid insertions that follow a particular Smc3p amino acid. I generated an insertion library of *pGAL-SMC3* in which approximately 2,118 plasmids were expected to contain an insertion within *SMC3*. The library was expected to contain plasmids that harbor an insertion for every 1.7 base pairs within the *SMC3* coding sequence. Therefore, I had generated a dense library of insertion alleles expected to perturb Smc3p at every amino acid position in the polypeptide.

The mutagenized *pGAL-SMC3 URA3 ARS/CEN* plasmid library was transformed into both a wild-type strain VG3349-1B and the temperature-sensitive *smc3-42* strain VG3358-3B. The temperature-sensitive *smc3-42* allele, I reasoned, would be more susceptible to dominant interaction with *SMC3* insertion alleles, maximizing screen hits. A total of 3,382 URA^+ colonies were obtained by transforming wild-type cells with the RID library in uninducing conditions in which glucose-repression prevents expression of genes under *GAL1* promoter control. These transformants were then screened for growth impairment upon replica plating to plates containing galactose that induced the mutant *SMC3*. In parallel, a total of 1,811 colonies were screened in the *smc3-42* background. All colonies that appeared growth impaired were retested. The growth impairment was demonstrated to be linked to the overexpressed *SMC3* alleles because impaired growth disappeared upon loss of the plasmid. These steps eliminated a few

false screen hits and gave us confidence that the vast majority of galactose-sensitive colonies contained *pGAL-SMC3* plasmids with *SMC3* insertion alleles.

As an initial characterization of the galactose sensitive RIDs, I determined the DNA sequence of the mutated *SMC3* alleles. I obtained 13 galactose-sensitive *SMC3-RID* alleles from the screen in wild type cells and 49 from the screen in *smc3-42* cells, indicating that the sensitized background was more susceptible to dominant RIDs. Sequencing revealed that a significant number of sites of insertion were hit multiple times in the *smc3-42* background indicating that the screen was close to saturation (Table 2). RIDs mapped to the Smc3p head, hinge and coiled coil domains, which indicated that all three domains had the potential to give a RID phenotype.

To further narrow alleles for subsequent studies, I assessed the function of RID alleles in a more physiologically relevant context. I placed them under the native *SMC3* promoter and assessed their ability to support viability as the sole copy of *SMC3* in haploid yeast. Plasmids encoding RID alleles of *SMC3* were generated by site directed mutagenesis of pVG419 (*SMC3 LEU2*) and integrated into an *smc3*Δ strain (3464-16C) supported by the plasmid pEU42 (*SMC3 URA3 CEN ARS*). These strains were treated with 5-FOA to select for progeny that had lost the *SMC3 URA3* plasmid, thereby revealing the viability of cells containing solely the integrated *SMC3* RID allele. Most *SMC3* RID alleles failed to support viability. These results showed that when expressed at physiological levels, most RID alleles were recessive hypomorphs. These phenotypes coupled with the original overexpression-dominant phenotype were consistent with the model that these alleles eliminated only a portion of *SMC3* function, and therefore identified interesting alleles to pursue further.

Although I primarily focused my analyses on inviable RIDs, the RIDs that were viable at normal expression levels represent mutants that retain cohesin function despite disrupting the Smc3p polypeptide. Their toxicity when overexpressed may have resulted from an off target defect. These functional RID alleles defined regions of Smc3p whose functions were less constrained by sequence or structure. The majority of the viable RIDs map to the Smc3p coiled coil (Figure 1B). The fact that viable RIDs were obtained at many positions along the length of the coiled coil indicated that many positions within the coiled coil were tolerant to localized disruptions (discussed in greater detail in Chapter 4 of this dissertation).

Distribution of inviable RID alleles in *SMC3* defines novel candidate functional regions

Do inviable RIDs map only to known functional regions or also to poorly understood regions of the protein? Within the Smc3p head domain are conserved motifs responsible for its ATPase activity and two lysine residues (K112, K113) that undergo Eco1p-dependent acetylation to regulate cohesin function. Most of the RIDs that mapped to the Smc3p head domain were within or near key motifs of the ATPase, and this suggested that they directly impaired one or more steps of the ATP hydrolysis cycle. Similarly, an insertion following L111 likely disrupted acetylation. Since simple point mutations that impair ATP binding, ATP hydrolysis, and lysine acetylation have been well characterized (Arumugam et al. 2003; Ünal et al. 2008; Guacci and Koshland 2012), I focused my attention on RID mutations within Smc3p's head domain that were

more distal to these motifs and might identify novel regions necessary for Smc3p function.

RIDs following D84, D127, and R1199 lie in poorly understood regions of the Smc3p head (Figure 1C). Using the Smc3p structure (Gligoris et al. 2014) as a guide, D84 lies at the boundary of a conserved unstructured loop that is 16-23 residues long in different organisms while D127 is an absolutely conserved residue in species from humans to yeast that is part of an alpha helix with a highly-conserved sequence. The loop and alpha helix lie on opposite sides of the loop that contains the K112, K113 residues. Thus, these RIDs may define new regions of Smc3p necessary for acetylation of K112 and K113. Alternatively, these regions may respond to the acetylation state of K112 and K113 to change cohesin function. The R1199 RID lies within a nearly perfectly conserved 25-residue sequence of Smc3p that is homologous to the winged-helix binding domain of Smc1p (Figure 1D). This putative winged-helix binding domain was initially proposed to be the binding site for the Mcd1p N-terminal domain based upon binding of the C-terminus of Mcd1p to Smc1p (Haering et al. 2004). This model was thought to be debunked when a subsequent crystal structure of Smc3p-Mcd1p showed that the Mcd1p N-terminal domain bound to the coiled coil of Smc3p (see below). However, the position of the R1199 RID opens up the possibility that cohesin might exist in two distinct states in which Mcd1p binds to Smc3p at either the coiled coil or the winged-helix binding domain. Further characterization of these three RIDs to test these models may provide significant new insight into cohesin structure and function.

Head-proximal coiled coil insertions reveal an Mcd1p binding site

A large number of RIDs clustered to a region of the Smc3p coiled coil that was immediately adjacent to the Smc3p head domain. Most of these RIDs were introduced into an *smc3*Δ strain harboring the *SMC3 URA3 CEN* plasmid and replica plated to 5-FOA plates to assess function. This includes fifteen spanning Smc3's N-terminal coiled coil from amino acids G171 to T233 and six within its C-terminal coiled coil from A1013 to V1041 (Table 1 and Table 2). A crystal structure containing this region of Smc3p revealed that it bound to the N-terminal helices of Mcd1p forming a tetrameric coil bundle (Gligoris et al. 2014). Strikingly RID mutations were obtained that mapped along the entire interface and suggested that the whole interface may be critical for cohesin function (Figure 2).

The distribution of RIDs in the head-proximal coiled coil could reflect that the whole domain is required for the stable interaction of Mcd1p with Smc3p. However, this interpretation seemed unlikely given the extensive number of contacts between Mcd1p and Smc3p along the interface. In principle, assessing the binding of Mcd1p to Smc3p by coimmunoprecipitation is complicated because even if this interface is perturbed, Mcd1p and Smc3p still coimmunoprecipitate through their independent binding to Smc1p. However, it has been observed that when Mcd1p fails to bind to Smc3p, it is degraded in M-phase-arrested cells. Thus the presence of Mcd1p in M phase serves as a proxy for Mcd1p association with Smc3p. To perform this test, I constructed strains that express *SMC3*, *smc3-I196*, *smc3-K1023* or *smc3-L1029R* alleles from the *LEU2* locus. These strains also have an auxin-inducible-degron-tagged (AID) *SMC3-AID* allele

at the native *SMC3* locus. This tag allows proteolysis of Smc3-AIDp in the presence of the drug auxin. The *smc3-L1029R* allele was identified previously as a mutant in the Smc3p/Mcd1p interface that blocked Smc3p binding to Mcd1p (Gligoris et al. 2014). Early log phase cultures of these strains were arrested in G1 using alpha factor. Auxin was added to deplete Smc3-AIDp. Alpha factor was then washed out of the cultures and cells were resuspended in fresh YPD containing auxin and nocodazole to allow them to proceed through the cell cycle and arrest in mid-M phase. Samples were collected and Mcd1p levels assessed by Western blot.

As expected, abundant Mcd1p was detected in the strain with Smc3p. Similarly, in strains where Mcd1p binding to Smc3p was abrogated (*SMC3-AID* or *smc3-L1029R SMC3-AID*), Mcd1p was almost undetectable (Figure 3B). Note the absence of Mcd1p in the *smc3-L1029R SMC3-AID* strain showed that the auxin regimen successfully removed all the Smc3-AIDp. In contrast, *smc3-I196 SMC3-AID* and *smc3-K1023 SMC3-AID* cells supported much greater Mcd1p in M phase than the *smc3-L1029R* mutant but somewhat less than is supported by wild-type (Figure 3B). These results suggest that the two *SMC3* RID alleles in the Smc3p-Mcd1p interface nonetheless allow substantial interaction between Smc3p and Mcd1p.

While reduced, the level of protected Mcd1p in *smc3-I196* and *smc3-K1023* mutants suggested sufficient cohesin was assembled to promote binding to chromosomes and cohesion. To assess the function of cohesin supported by these mutants, I used the same strains and regimen (Figure 3A) but instead assessed cohesion by scoring nuclear GFP-LacIp foci at the *LYS4* locus, and binding of cohesin to chromosomes by immunofluorescence against Mcd1p on chromosome spreads. Compared to wild-type, no Mcd1p binding was observed in chromosome spreads from *smc3-I196 SMC3-AID* or *smc3-K1023 SMC3-AID* cells, similar to that seen for *smc3-L1029R SMC3-AID* (Figure 3C). Also, both RID alleles exhibited the same nearly complete loss of sister-chromatid cohesion as the *SMC3-AID* and *smc3-L1029R SMC3-AID* strains at the *LYS4* locus on chromosome IV (Figure 3D). These defects, despite apparent formation of significant amounts of binding of Mcd1p to Smc3p, suggest that the Smc3p-Mcd1p interface likely has functions in cohesin binding to DNA beyond simply ensuring cohesin trimer formation.

Discussion

The prevailing model for how Smc proteins contribute to cohesin function is simple. Smcs form a ring that topologically encircles one or two DNA duplexes, and the joining together of Smc head domains by Mcd1p modulates opening and closing of the ring. I hypothesized that a more complex mechanism of cohesin function would be revealed through a RID screen of the key subunit Smc3p. This and subsequent chapters will show that the RID screen I undertook has generated mutants that reveal new aspects of cohesin's Smc architecture and regulation.

Since cohesin Smc head domains serve as a platform for the recruitment and activity of regulatory factors, analysis of RIDs in this domain are of immense interest. Two such RIDs, following D84 and D127 flank the conserved acetylated lysines K112 and K113. One simple possibility is that these two flanking regions constitute part of a binding site for Eco1p that allows it to acetylate K112 and K113. Alternatively, these

flanking regions may be important structures that are altered by the acetylation state to regulate cohesin functions. The acetylation of K112 and K113 is thought in part to inhibit Wpl1p. Since the D127 RID is a loss-of-function allele, it may prevent Eco1p-dependent acetylation or render Smc3p's interface with Mcd1p susceptible to the action of Wpl1p even with acetylation intact. Whether *smc3-D127* inviability can be suppressed by *wpl1*Δ will be an important test of this model. Genetic and biochemical evidence support a role for Wpl1p at the interface of Smc3p and Mcd1p near the acetylated lysines (Rowland et al. 2009; Beckouet et al. 2016). Multiple mutations near lysines 112 and 113 confer viability to the *eco1* temperature-sensitive mutant in a manner thought to imitate loss of Wpl1p activity. These include *SMC3* point mutants S75R and R107I (Rowland et al. 2009). Acetylation of K112 and K113 is also thought to regulate the cohesin ATPase. This regulation likely involves a change in head conformation, given the distance between these lysines and the ATPase active site. The flanking regions defined by D84 and D127 may help to transduce the signal from the acetylated lysines to promote this conformation change. If so the RID mutations at D127 and D84 would be expected to allow acetylation but block cohesion establishment, a novel phenotype.

Multiple lines of evidence suggest that the interface between Smc3p and Mcd1p is an important nexus controlling cohesin function. The difference between the ability of *smc3-I196*, *K1023* and *L1029R* alleles to support Mcd1p levels suggests that not all mutations near this interface have the same effect on cohesin function. Considering the size of RID insertions, it was surprising that Smc3-I196p and Smc3-K1023p preserve enough Mcd1p binding to allow cohesin assembly and detection of Mcd1p in M phase while Smc3-L1029Rp does not. One explanation is that L1029R completely abolishes Mcd1p binding leading to its degradation while I196 and K1023 alleles merely reduce it. Despite the ability of Smc3-I196p and Smc3-K1023p to bind Mcd1p, they must be impaired at either loading or stable association of cohesin with chromosomes because Mcd1p cannot be detected on chromosome spreads. Consistent with these findings, strength of biochemical interaction between Smc3p and Mcd1p's N-terminus is poorly correlated with cohesin function and viability (Arumugam et al. 2006; Gligoris et al. 2014). These results suggest the existence of a second mode of interaction between Smc3p and Mcd1p. Interestingly, my discovery of an inviable insertion at R1199 in Smc3p's putative winged-helix binding domain supports the possibility that Mcd1p may toggle to a second binding site at this location. Further investigation into the dynamic interface between Smc3p and Mcd1p will be necessary to address the requirements for stable Mcd1p binding and to define its role in cohesin assembly and loading.

My inviable RID mutant collection further extends the region of the Smc3p coiled coil near the head that is important for cohesin function. Incorporation of a UV-activatable amino acid at residues 181 and 185 but not 206 of Smc3p allowed crosslinking to Mcd1p (Gligoris et al. 2014). My RID screen identified mutations as far up the coiled coil as T233 some 10's of amino acids beyond the known Mcd1p-Smc3p interface. If the interface between Mcd1p and Smc3p only extends up to amino acid 206 of Smc3's coiled coil then why are RIDs at positions 211, 216, 217, 231, and 233 not viable? The region of coiled coil defined by these positions displays strong conservation beyond the portion bound by Mcd1p (Figure 2A of Gligoris et al. 2014). An interesting possibility comes from crosslinking studies of purified human cohesin and Pds5Bp. Pds5Bp crosslinks just beyond Mcd1p's binding site on Smc3p's coiled coil (Huis in 't

Veld et al. 2014). Future experiments should shed light on whether the RID mutants identified here define a Pds5p interaction site.

I found two clusters of inviable RIDs that do not obviously disrupt cohesin assembly interfaces or ATPase function. The first cluster is in the middle of Smc3p's coiled coil near S343. The prevailing model of coiled-coil function is that it serves to link the head and hinge domains and prevent DNA from escaping after entrapment. My discovery of inviable insertions at a very narrowly defined region of Smc3p's coiled coil is inconsistent with topological entrapment being its sole function. In Chapter 4 of this dissertation I will discuss experiments that demonstrate a new role of the Smc3p coiled coil in loading or stable binding of cohesin to chromosomes.

Finally, a cluster of inviable RIDs were discovered in Smc3p's hinge domain. Originally thought merely to mediate dimerization between Smcs, recent studies suggest that the function of this domain is more nuanced (Mishra et al. 2010; Kurze et al. 2011; Murayama et al. 2015). In the next chapter of this dissertation I examine a RID at D667, and demonstrate that the hinge plays an essential role in maintaining cohesion from its establishment during replication until mitosis.

Acknowledgements

I thank Vincent Guacci, Thomas Eng and the entire Koshland lab for helpful discussions, reagents, and constructive feedback.

Materials and Methods

Random insertion screen

Plasmid pBR25 containing *pGAL-SMC3 URA3 ARS/CEN* was subject to *in vitro* transposition according to the protocol recommended by the MuA transposase MGS Kit (ThermoFisher Cat. F701). After transforming into TOP10 cells (Thermo), 5,756 AmpR KanR colonies were pooled and plasmids harvested by Midi Prep (Qiagen). The pooled library was digested with NotI to excise the KanR marker, gel extracted, and religated. Ligation products were transformed once again into TOP10 cells and confirmed to have lost KanR by replica plating. >30,000 colonies were pooled, and plasmids harvested by Midi Prep to obtain a library of *pGAL-SMC3* plasmids with fifteen extra nucleotides randomly inserted. Library complexity was calculated making the following assumptions: 1) all clones from AmpR KanR colonies were represented in the AmpR KanS clones and 2) 100% efficiency for *in vitro* transposition, NotI excision, and religation steps 3) unbiased transposition insertion location within pBR25. Library depth was calculated by multiplying the fraction of pBR25 coding for *SMC3* (3,693 bp / 10,083 bp = 0.368) by the number of AmpR KanR colonies (5,756) to obtain 2,118 plasmids expected to have an insertion in *SMC3*. The length of the ORF in base pairs divided by the number of plasmids with insertions in the ORF yields a complexity of one insertion plasmid for every 1.7 base pairs of *SMC3*. The library, therefore, is expected to contain an insertion following every single amino acid in *SMC3*. The library was transformed into wild-type (3349-1B) and *smc3-42* (3358-3B) strains and transformants selected on synthetic complete 2% dextrose media lacking uracil (SC –URA Dex). 3,382 wild-type colonies and 1,811 *smc-42* colonies were screened. Transformation plates were replica plated onto SC –URA 2% galactose plates and SC –URA Dex again and grown overnight for comparison. Colonies exhibiting reduced or absent growth on galactose compared to dextrose media were pulled off of dextrose plates, grown overnight in liquid YPD media, and dilution plated onto SC –URA Dex, Gal to confirm slow growth and 5-FOA Gal plates to confirm linkage of slow growth to the plasmid. Insertion mutations were identified by colony PCR and Sanger sequencing across *SMC3*.

Yeast strains, media, and growth

All strains used are in the A364A background and their genotypes can be found in the Strain List. Yeast extract/peptone/dextrose media and synthetic dropout media was prepared as previously described (Guacci et al. 1997). Conditional AID degron strains were grown in YPD and 3-indoleacetic acid (IAA, Sigma Aldrich Cat I3750) dissolved in DMSO added to cultures to a final concentration of 750 μM. YPD + auxin plates were made by cooling molten YPD 2% agar to 55˚C prior to addition of auxin to a final concentration of 750 μM.

Cohesion assays

Sister chromatid cohesion was assessed at either the centromere-distal *LYS4* locus or centromere-proximal *TRP1* locus on Chr IV in which *LacO* arrays have been integrated.

An allele expressing the *GFP-LacI* fusion integrated at *HIS3* allows fluorescence microscopic visualization of *LacO* arrays. Cohesion was scored by growing cells to mid-log phase (OD600 ~0.3) and arresting them in G1 using alpha factor at 10^{-8} M (Sigma Aldrich). After arresting for 3 hours, auxin was added to a final concentration of 750 μM to deplete Smc3-AIDp for one hour. Cells were released from G1 arrest by washing in YPD containing auxin and 0.1 mg/mL Pronase E (Sigma Aldrich) five times and resuspending in fresh YPD containing auxin and 15 μg/mL nocodazole (Sigma Aldrich). Cultures were incubated at 23˚C and samples fixed either 1) every 15 minutes for assessing S-phase cohesion establishment or 2) after three hours to allow arrest in mid-M phase. In addition to fixation for microscopy, samples were taken in parallel to assess DNA content by flow cytometry. Cohesion was scored by counting the number of GFP-LacIp foci in the nucleus by fluorescence microscopy of fixed cells.

Chromosome spreads and microscopy

Cells were grown as if for assessing cohesion by arresting in YPD containing auxin and nocodazole. Chromosome spreads were prepared as previously described (Wahba et al. 2013). Slides were incubated with 1:5,000 rabbit polyclonal anti-Mcd1p and 1:5,000 mouse anti-V5 antibody (Life Technologies). Antibodies were diluted in spreads blocking buffer (5% BSA, 0.2% milk, 1X PBS, 0.2% Triton X-100). Secondary Alexa Fluor 488-congugated chicken anti-mouse and Alexa Fluor 568-congugated donkey anti-rabbit (ThermoFisher Cats. A21200 and A10042) antibodies were diluted 1:5,000 in blocking buffer. Indirect immunofluorescence was detected on an Axioplan2 microscope (Zeiss, Thornwood, NY) using the 100X objective (numerical aperture 1.40) which is equipped with a Quantix charge-coupled camera (Photometrics).

Strain List

Strain	Genotype	Reference
BRY474	*MAT**a** SMC3-LEU2:leu2-3,112 SMC3-3V5-AID^{608} trp1∆::OsTIR1-CaTRP1 lys4::LacO(DK)-NAT pHIS3-GFPLacI-HIS3:his3-11,15 ura3-52 bar1*	this study
BRY476	*MAT**a** smc3-I196-LEU2:leu2-3,112 SMC3-3V5-AID^{608} trp1∆::OsTIR1-CaTRP1 lys4::LacO(DK)-NAT pHIS3-GFPLacI-HIS3:his3-11,15 ura3-52 bar1*	this study
BRY486	*MAT**a** smc3-K1023-LEU2:leu2-3,112 SMC3-3V5-AID^{608} trp1∆::OsTIR1-CaTRP1 lys4::LacO(DK)-NAT pHIS3-GFPLacI-HIS3:his3-11,15 ura3-52 bar1*	this study
BRY492	*MAT**a** SMC3(L1029R)-LEU2:leu2-3,112 SMC3-3V5-AID^{608} trp1∆::OsTIR1-CaTRP1 lys4::LacO(DK)-NAT pHIS3-GFPLacI-HIS3:his3-11,15 ura3-52 bar1*	this study
VG3349-1B	*MAT**a** lys4::LacO(DK)-NAT trp1-1 GFPLacI-HIS3:his3-11,15 bar1 leu2-3,112 ura3-52*	Guacci and Koshland 2012
VG3358-3B	*MAT**a** smc3-42 lys4::LacO(DK)-NAT trp1-1 pHIS3-GFP-LACI-HIS3:his3-11,15 bar1 leu2-3,112 ura3-52*	Guacci and Koshland 2012
VG3464-16C	*MAT**a** smc3∆::HPH lys4::LacO(DK)-NAT bar1 pHIS3-GFPLacI-TRP1:his3-11,15 trp1-1 leu2-3,112 ura3-52* +pEU42 (*SMC3 CEN URA3*)	Guacci and Koshland 2012
VG3651-3D	*MAT**a** SMC3-3V5-AID^{608} trp1∆::pGPD1-TIR1-CaTRP1 lys4::LacO(DK)-NAT pHIS3-GFPLacI-HIS3:his3-11,15 leu2-3,112 ura3-52 bar1*	Çamdere et al. 2015

References

Arumugam, P., Gruber, S., Tanaka, K., Haering, C. H., Mechtler, K., & Nasmyth, K. (2003). ATP hydrolysis is required for cohesin's association with chromosomes. *Current Biology : CB*, *13*(22), 1941–1953.

Arumugam, P., Nishino, T., Haering, C. H., Gruber, S., & Nasmyth, K. (2006). Cohesin's ATPase activity is stimulated by the C-terminal Winged-Helix domain of its kleisin subunit. Current Biology : CB, 16(20), 1998–2008.

Bürmann, F., Basfeld, A., Vazquez Nunez, R., Diebold-Durand, M.-L., Wilhelm, L., & Gruber, S. (2017). Tuned SMC Arms Drive Chromosomal Loading of Prokaryotic Condensin. *Molecular Cell*, *65*(5), 861–872.e9.

Eng, T., Guacci, V., & Koshland, D. (2014). ROCC, a conserved region in cohesin's Mcd1 subunit, is essential for the proper regulation of the maintenance of cohesion and establishment of condensation. Molecular Biology of the Cell, 25(16), 2351–2364.

Gligoris, T. G., Scheinost, J. C., Bürmann, F., Petela, N., Chan, K.-L., Uluocak, P., et al. (2014). Closing the cohesin ring: structure and function of its Smc3-kleisin interface. *Science*, *346*(6212), 963–967.

Gruber, S., Haering, C. H., & Nasmyth, K. (2003). Chromosomal Cohesin Forms a Ring. Cell, 112(6), 765–777.

Guacci, V., & Koshland, D. (2012). Cohesin-independent segregation of sister chromatids in budding yeast. *Molecular Biology of the Cell*, *23*(4), 729–739.

Haering, C. H., Farcas, A.-M., Arumugam, P., Metson, J., & Nasmyth, K. (2008). The cohesin ring concatenates sister DNA molecules. Nature, 454(7202), 297–301.

Haering, C. H., Schoffnegger, D., Nishino, T., Helmhart, W., Nasmyth, K., & Löwe, J. (2004). Structure and stability of cohesin's Smc1-kleisin interaction. Molecular Cell, 15(6), 951–964.

Huis in t Veld, P. J., Herzog, F., Ladurner, R., Davidson, I. F., Piric, S., Kreidl, E., et al. (2014). Characterization of a DNA exit gate in the human cohesin ring. *Science*, *346*(6212), 968–972.

Kurze, A., Michie, K. A., Dixon, S. E., Mishra, A., Itoh, T., Khalid, S., et al. (2011). A positively charged channel within the Smc1/Smc3 hinge required for sister chromatid cohesion. The EMBO Journal, 30(2), 364–378.

Milutinovich, M., Ünal, E., Ward, C., Skibbens, R. V., & Koshland, D. (2007). A Multi-Step Pathway for the Establishment of Sister Chromatid Cohesion. *PLoS Genet*, *3*(1), e12.

Mishra, A., Hu, B., Kurze, A., Beckouët, F., Farcas, A.-M., Dixon, S. E., et al. (2010). Both interaction surfaces within cohesin's hinge domain are essential for its stable chromosomal association. *Current Biology : CB*, *20*(4), 279–289.

Murayama, Y., & Uhlmann, F. (2015). DNA Entry into and Exit out of the Cohesin Ring by an Interlocking Gate Mechanism. Cell, 163(7), 1628–1640.

Noble, D., Kenna, M. A., Dix, M., Skibbens, R. V., Ünal, E., & Guacci, V. (2006). Intersection between the regulators of sister chromatid cohesion establishment and maintenance in budding yeast indicates a multi-step mechanism. *Cell Cycle (Georgetown, Tex.)*, *5*(21), 2528–2536.

Soh, Y.-M., Bürmann, F., Shin, H.-C., Oda, T., Jin, K. S., Toseland, C. P., et al. (2015). Molecular Basis for SMC Rod Formation and Its Dissolution upon DNA Binding. *Molecular Cell*, *57*(2), 290–303.

Stigler, J., Çamdere, G. Ö., Koshland, D. E., & Greene, E. C. (2016). Single-molecule imaging reveals a collapsed conformational state for DNA-bound cohesin. *Cell Reports* 15:988–998.

Ünal, E., Heidinger-Pauli, J. M., Kim, W., Guacci, V., Onn, I., Gygi, S. P., & Koshland, D. E. (2008). A molecular determinant for the establishment of sister chromatid cohesion. *Science*, *321*(5888), 566–569.

Zhang, J., Shi, X., Li, Y., Kim, B.-J., Jia, J., Huang, Z., et al. (2008). Acetylation of Smc3 by Eco1 Is Required for S Phase Sister Chromatid Cohesion in Both Human and Yeast. *Molecular Cell*, *31*(1), 143–151.

Figure Legends

Table 1: List of RIDs identified in wild type screen

The Location column specifies the amino acid and its position within Smc3 that is immediately followed by the five amino acid sequence in the Insertion column. Viability indicates whether the RID allele under its native promoter is viable as the sole copy of *SMC3*. Integrating *SMC3-RID LEU2* plasmids were transformed into an *smc3*Δ strain containing the *SMC3 URA3 CEN* plasmid and dilution plated to 5-FOA plates to assess growth in the absence of wild-type *SMC3*. Growth is defined as (+) wild-type growth and viability, (-) no growth and (NT) not tested.

Table 2: List of RIDs identified in the sensitized *smc3-42* screen

The Location column specifies the amino acid and its position within Smc3 that is immediately followed by the five amino acid sequence in the Insertion column. Viability indicates whether the RID allele under its native promoter is viable as the sole copy of *SMC3*. Integrating *SMC3-RID LEU2* plasmids were transformed into an *smc3*Δ strain containing the *SMC3 URA3 CEN* plasmid and dilution plated to 5-FOA plates to assess growth in the absence of wild-type *SMC3*. Growth is defined as (+) wild-type growth and viability, (-) no growth and (NT) not tested.

Figure 1: *SMC3* RID mutations cluster in globular head, hinge, and coiled-coil domains

A) *SMC3* RID screen workflow. A *pGAL-SMC3* URA3 CEN/ARS plasmid, pBR25, was subject to *in vitro* transposase mutagenesis to generate the RID library which consists of plasmids with fifteen additional nucleotides randomly inserted (see Materials and Methods). Haploid yeast were transformed with the SMC3 RID library and selected under uninducing conditions on dextrose plates. Transformants were replica plated to galactose plates to induce expression by *pGAL*. Mutants that had decreased viability when grown on galactose were selected for further analysis. Slow growth in mutant strains were confirmed to be caused by the RID plasmid, and the plasmids were sequenced to determine insertion location.

B) Smc3p, left, and Smc1p, right, are drawn approximately to scale with coiled-coils separating the globular head and hinge domains. Location of RID mutations are indicated by arrows, and arrow color denotes ability to support viability. Blue arrows indicate RIDs that are viable as the sole copy of *SMC3,* while red arrows indicate inviable mutations.

C) Ribbon structure of the Smc3p head domain, blue, bound to the N-terminus of Mcd1p, green, and ATPγS (Gligoris et al. 2014). Amino acids within the ATPase Walker A, Walker B, D-loop and Signature motifs are highlighted in cyan. Amino acids Smc3-D127 and R1199 are represented as red spheres to highlight the location of RIDs. The approximate location of the RID following D84 is represented

by the dashed box since it is within an unstructured loop. Lysines K112 and K113 of Smc3p are depicted in magenta.

D) Ribbon structure of the Smc1p head domain, purple, C-terminus of Mcd1p, green, and two molecules of ATPγS represented in the same orientation as (B) (Haering et al. 2004). Amino acids within the ATPase Walker A, Walker B, D-loop and Signature motifs are highlighted in cyan.

Figure 2: RIDs within the head-proximal Smc3p coiled coil define an Mcd1p binding site

Crystal structure of inset region highlighted on cohesin at right showing the physical interaction between Smc3p, blue, and Mcd1p's N-terminus, green (Gligoris et al. 2014). RID insertion locations are indicated by red highlights on Smc3p.

Figure 3: Smc3p coiled-coil RID mutants Smc3-I196p, K1023p fail to load cohesin on DNA

A) Regimen for preparing cells to assess M phase cohesion and Mcd1p binding to chromosomes. Logarithmically growing cells were arrested in G1 by the addition of alpha factor. Once arrested, auxin was added to deplete Smc3-AIDp. Cells were washed and released into fresh media containing nocodazole and auxin, which allowed cells to progress through the cell cycle and arrest in mid-M phase. Once 95% cells were arrested, samples were then collected to assess DNA content, cohesion, protein levels, and Mcd1p binding to spread chromosomes.

B) Mcd1p protein levels detected by western blot. Strains containing *SMC3-AID* along with an additional copy of either *SMC3*, *smc3-I196*, *smc3-K1023, smc3-L1029R*, or no additional *SMC3* (BRY474, BRY476, BRY486, BRY492, 3651-3D) were treated as described in (A). Cells were collected after G1 arrest, after auxin incubation, and following mid-M phase arrest. Tub1p was blotted as a loading control.

C) Smc3p mutant DNA masses probed to detect Mcd1p by immunofluorescence, as a measure of cohesin binding to chromosomes. Strains analyzed in (B) were prepared according to the regimen in (A) and then processed for chromosomes spreads (see Materials and Methods). Polyclonal rabbit anti-Mcd1p antibody was used to detect Mcd1p and DAPI used for DNA.

D) Percentage of mid-M arrested cells displaying sister chromatid cohesion loss at the CEN-distal *LYS4* locus. *SMC3* mutants tested in (B) and (C) were prepared in accordance to the regimen described in (A). Cells were then fixed and scored as having a single GFP focus or two GFP foci (separated sisters) (see Materials and Methods).

Figure 1

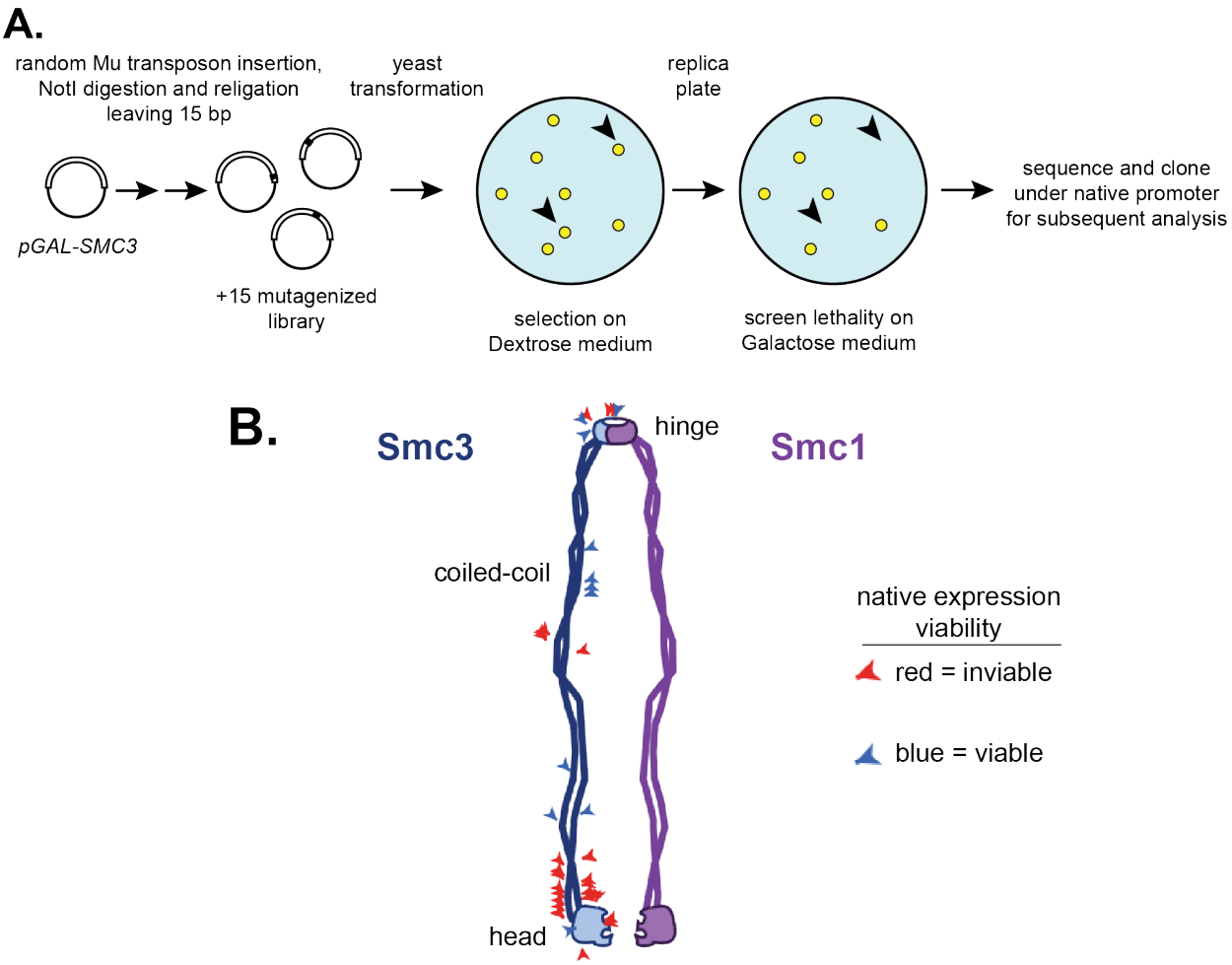
A.
random Mu transposon insertion,
NotI digestion and religation
leaving 15 bp
yeast
transformation
replica
plate
pGAL-SMC3
+15 mutagenized
library
selection on
Dextrose medium
screen lethality on
Galactose medium
sequence and clone
under native promoter
for subsequent analysis
B.
Smc3
hinge
Smc1
coiled-coil
head
native expression
viability
red = inviable
blue = viable
C.
Mcd1
Smc3
D127
K112, K113
D84
R1199
D-loop
Signature
Walker B
Walker A
D.
Smc1
Mcd1
D-loop
Signature
Walker B
Walker A

Figure 2

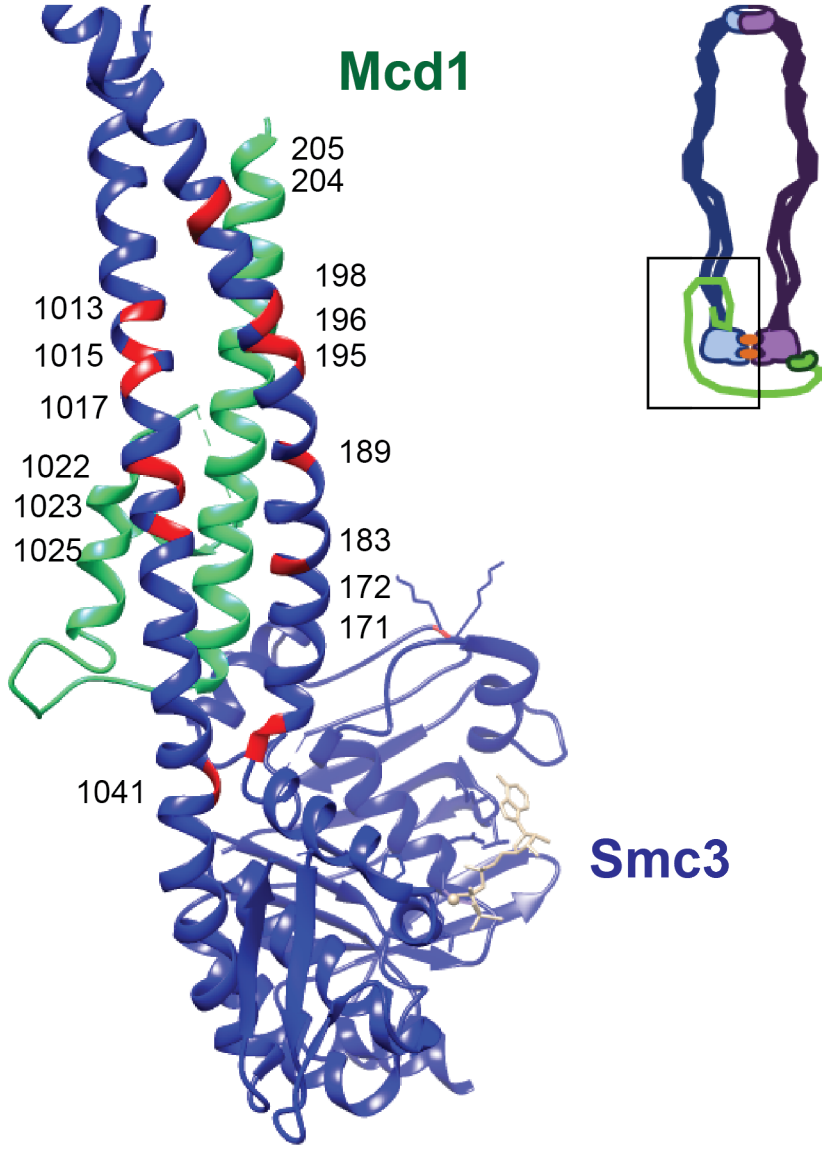
Mcd1
205
204
198
196
195
189
183
172
171
1013
1015
1017
1022
1023
1025
1041
Smc3

Figure 3

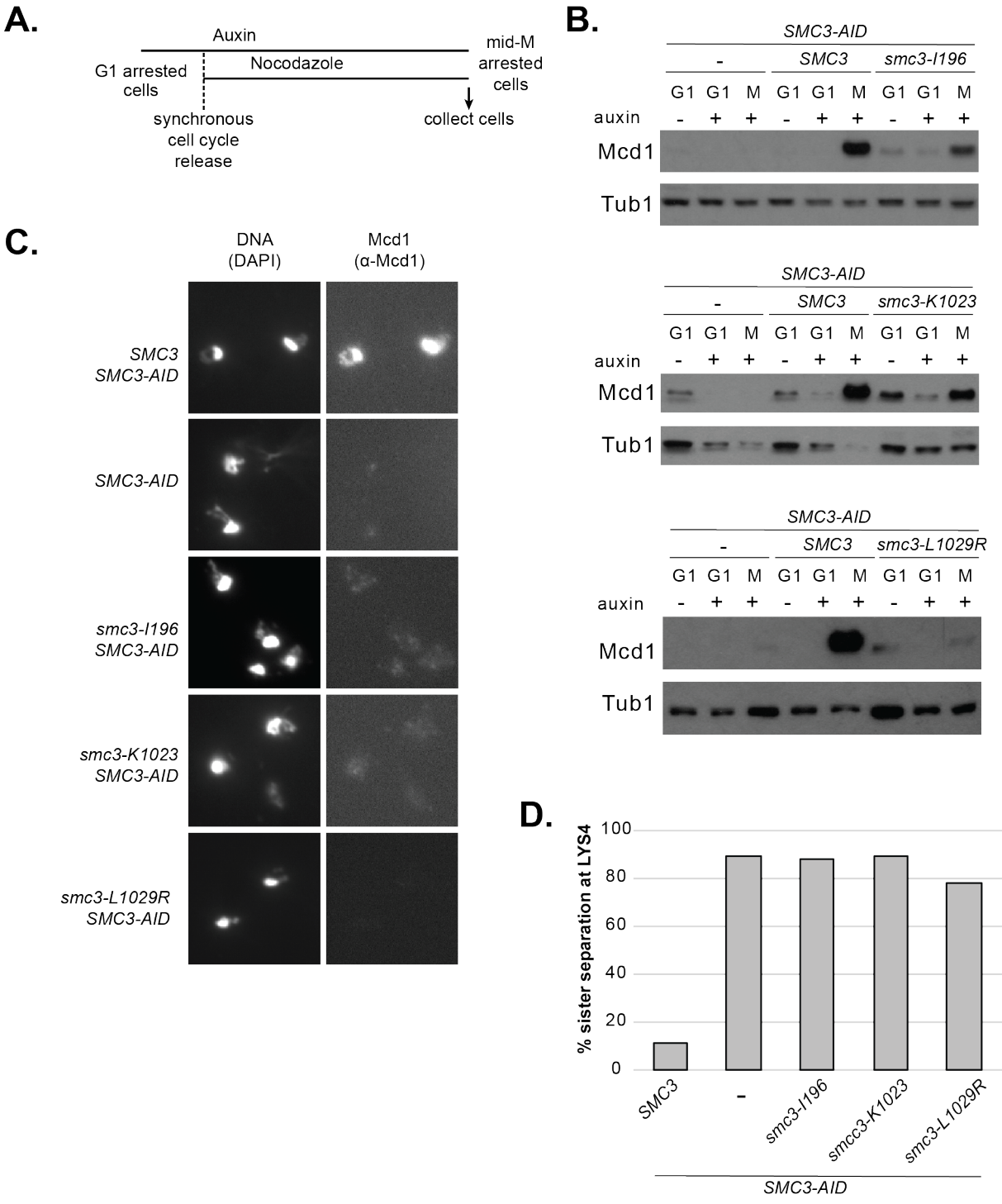
A.
Auxin
Nocodazole
G1 arrested cells
mid-M arrested cells
synchronous cell cycle release
collect cells
B.
SMC3-AID
-
SMC3
smc3-I196
G1 G1 M G1 G1 M G1 G1 M
auxin - + + - + + - + +
Mcd1
Tub1
SMC3-AID
-
SMC3
smc3-K1023
G1 G1 M G1 G1 M G1 G1 M
auxin - + + - + + - + +
Mcd1
Tub1
SMC3-AID
-
SMC3
smc3-L1029R
G1 G1 M G1 G1 M G1 G1 M
auxin - + + - + + - + +
Mcd1
Tub1
C.
DNA (DAPI)
Mcd1 (α-Mcd1)
SMC3 SMC3-AID
SMC3-AID
smc3-I196 SMC3-AID
smc3-K1023 SMC3-AID
smc3-L1029R SMC3-AID
D.
% sister separation at LYS4
100
80
60
40
20
0
SMC3
-
smc3-I196
smcc3-K1023
smc3-L1029R
SMC3-AID

Chapter Three: A role of Smc3p's hinge domain in cohesion maintenance

Introduction

Cohesin is a conserved protein complex required for multiple aspects of chromosome function in eukaryotic cells. Cohesin tethers sister chromatids together from their replication in S phase through metaphase. This ensures that sister chromatids form bipolar attachment to the mitotic spindle and segregate to opposite poles during mitosis. In addition to sister chromatid cohesion, cohesin is also involved in chromosome condensation, DNA damage repair, and transcription. Understanding the mechanisms by which cohesin is regulated and how regulation manifests in different activities of cohesin on DNA are critical subjects to investigate.

In the budding yeast *Saccharomyces cerevisiae*, core cohesin subunits include Smc1p, Smc3p, Mcd1p (also called Scc1p), and Scc3p. The Smc subunits comprise a V-shaped heterodimer connected by binding of the Mcd1p N-terminus to Smc3p and the Mcd1p C-terminus to Smc1p. Between these two Smc binding domains of Mcd1p is a flexible linker bound by Scc3p. Cohesin assembles and is loaded onto DNA by the Scc2p/Scc4p complex in late G1 phase (Ciosk et al. 2000). Cohesin is loaded at centromeres and along chromosome arms at cohesin-associated regions or CARs (Laloraya et al. 2000). During DNA replication, cohesion establishment occurs when chromosome-bound cohesin is converted to a form capable of tethering sister chromatids by Eco1p, an essential regulator that acetylates Smc3p at lysines 112 and 113 (K112, K113) (Ünal et al. 2008, Ben-Shahar et al. 2008, Zhang et al. 2008). Though multiple mechanistic consequences of acetylation have been proposed, the ways by which these mechanisms promote cohesion establishment are still under investigation (Rowland et al. 2009). One role of Smc3p acetylation is to disrupt the activity of Wpl1p, a factor thought to release the N-terminus of Mcd1p from Smc3p (Chan et al. 2013, Beckouet et al. 2016). The fact that *wpl1*Δ restores viability to *eco1*Δ cells seems to support this model. However, *eco1*Δ *wpl1*Δ cells appear to survive because cohesin function in condensation, but not cohesion, is restored (Guacci and Koshland 2012). Additional factors beyond inhibition of Wpl1p must therefore be responsible for promoting cohesion establishment.

Recent studies have revealed an additional role for Eco1p in regulating the cohesin ATPase (Çamdere et al. 2015, Elbatsh et al. 2016). The head domains of Smc1p and Smc3p form a composite ATPase that is bridged by Mcd1p. A mutation that reduces the rate of ATP hydrolysis, *SMC1-D1164E*, restores viability and cohesion to *eco1*Δ cells. Therefore, a second role of Eco1p may be to promote cohesion through regulating the ATPase of cohesin. It has been proposed that ATP hydrolysis is coupled to conformational changes necessary for cohesin function (Arumugam et al. 2006). Therefore, a regulated ATPase-dependent conformational change may accompany the process of cohesion establishment.

Once cohesion is established in S phase, the regulator Pds5p is recruited to cohesin and acts to maintain cohesion through mitosis. How Pds5p functions to maintain cohesion is not well understood. Two major models have been proposed for the essential function of Pds5p in cohesion maintenance. The first model is based on observations that Mcd1p is degraded by a polySUMO-dependent pathway in *pds5* cells,

suggesting that Pds5p functions to protect Mcd1p until anaphase onset (Noble et al. 2006; D'Ambriosio et al. 2014). However, the temperature-sensitive *pds5-1* mutant but not *pds5*Δ can be partially suppressed by deleting the factors responsible for Mcd1p polySUMOylation and degradation (D'Ambrosio et al. 2014). This observation suggests an additional essential function of Pds5p exists beyond protecting Mcd1p. A second model for Pds5p function emerged from the observation that *pds5* mutants are defective in the Eco1p-dependent acetylation of Smc3p at K112 and K113, a phenotype that can be rescued by deletion of the Hos1p deacetylase (Chan et al. 2013). However, *hos1*Δ cannot restore viability to a *pds5* temperature-sensitive mutant despite restoring K112, K113 acetylation. Since neither restoring Mcd1p stability nor Smc3p-K112, K113 acetylation compensates for *pds5*, an additional role of Pds5p in cohesion maintenance may exist. Interestingly, crosslinking has shown human Pds5p interacts with all cohesin subunits, implying that its association with cohesin is extensive and/or dynamic (Huis in t Veld et al. 2014). The effects of Pds5p-cohesin interaction on cohesion maintenance remain poorly understood.

The architecture of cohesin is complex. At its core are Smc1p and Smc3p, which share features common to all SMC proteins. The primary sequences of Smc proteins fold back on themselves to form large dumbbell shaped structures with two globular domains, referred to as the head and hinge, separated by a long coiled coil. The hinge is where the polypeptide folds back on itself while the head forms where the N and C termini come together. The head domains of Smc1p and Smc3p heterodimerize to form a compound ATPase with two active sites. ATPase activity has been shown to be important for both DNA binding and tethering. The hinge domains of Smc1p and Smc3p heterodimerize to form a toroidal structure with two interfaces termed "North" and "South" (Mishra et al. 2010). The hinge dimers of multiple SMC complexes can bind DNA, and may serve regulatory functions (Kurze et al. 2011; Murayama and Uhlmann 2015; Soh et al. 2015).

Cohesin exhibits multiple conformations when observed under an electron microscope. Heterodimers of Smc1p and Smc3p have been observed with coiled coil arms in multiple conformations, including V or Y shapes by electron microcopy or as compact rod by scanning force microcopy (Haering et al. 2002; Kulemzina et al. 2016). Cohesin holocomplex also exhibits both ring-like and rod-like structures by electron microscopy (Kulemzina et al. 2016). Like cohesin, the bacterial BsSMC dimer and holocomplex can appear as rods by electron microscopy (Soh et al. 2015). A truncated BsSMC hinge containing a short 100 amino acid stretch of coiled coil can be crosslinked as dimers, implying that hinge-proximal coiled coils are closely juxtaposed. Interestingly, crosslinking is reduced in the presence of DNA, implying that DNA binding near the hinge-arm junction may promote a structural transition of the coiled-coil arms. It is possible that information can be communicated from Smc hinge to head domains (or vice versa). Interaction has between detected between the cohesin hinge and head domains, as well as between hinge and head-proximal subunits (Mc Intyre et al. 2007, Murayama and Uhlmann 2015). Additionally, the status of the hinge may be communicated to the head domains through the coiled-coils, as has been observed for BsSMC (Hirano and Hirano 2006). Although the significance of communication from the hinge to head domains of Smcs remains poorly understood, it may be that structural transitions modify the function of Smc complexes upon DNA binding.

Results

The D667 region of the Smc3p hinge is required to maintain cohesion

In the course of mapping RID mutations (see Chapter 2 of this dissertation), I found ten within the hinge domain of Smc3p (Figure 1A). Three RIDs mapped to the North hinge interface area while seven mapped near the South interface. Five of the seven South interface RIDs mapped to the bottom of the hinge where the coiled coil exits. The other South interface RIDs at locations D667, and G670 are expected to cause insertions at the top of the hinge, possibly occluding entrance to its channel. I chose to focus my attention on the RID at D667 because of the possibility it occluded the channel. D667 lies within a somewhat conserved loop (Figure 1B). To test whether cells expressing only *smc3-D667* were inviable I introduced this allele or *SMC3* into an *SMC3-3V5-AID* background (henceforth abbreviated *SMC3-AID*) and examined the growth of these strains in the presence of auxin. The cells expressing only smc3-D667p exhibited no growth, resembling cells lacking Smc3p. Thus smc3-D667p was unable to support one or more cohesin functions. The ability of *smc3-D667 SMC3-AID* cells to grow in the absence of auxin indicated that *smc3-D667* must be recessive and therefore the cohesin defect must have resulted from loss of one or more of Smc3p functions.

I began by testing whether cohesin with smc3-D667p could support cohesion. Strains carrying either *smc3-D667 SMC3-AID, SMC3 SMC3-AID,* or just *SMC3-AID* were constructed in backgrounds that allowed me to monitor cohesion at either a centromere-proximal locus (*TRP1)* or centromere-distal arm locus (*LYS4*). These strains were arrested in G1 and treated with auxin to remove Smc3-AIDp. Cells were released into media containing auxin and nocodazole to allow progression through S phase and arrest in M phase (Figure 2A). Nearly all G1 cells in all strains contained a single GFP focus, indicating no preexisting aneuploidy (Figure 2B). As expected, when I examined the cells arrested in mid-M phase, a very small fraction of cells with Smc3p (*SMC3 SMC3-AID*) lost cohesion at *TRP1* or *LYS4*, while strains lacking Smc3p (*SMC3-AID*) had almost complete loss of cohesion. Nearly two thirds of cells expressing only *smc3-D667* (*smc3-D667 SMC3-AID)* also had lost cohesion at these two loci. This result suggested that the D667 region of the hinge was required for either robust establishment and/or maintenance of cohesion.

These two possibilities can be distinguished by kinetic analysis of cohesion in populations of cells synchronously progressing through the cell cycle. Mutants that compromise cohesion establishment like those defective in core subunits of cohesin *MCD1*, *SMC3,* and *SMC1* exhibit sister chromatid separation immediately after DNA replication (Eng et al. 2014). Mutants that compromise cohesion maintenance like those defective in the cohesin regulator *PDS5* also lose cohesion but significantly later in the cell cycle than establishment mutants (Eng et al. 2014). Using the same strains as described above along with a *PDS5-AID* strain, I asked which mode of cohesion loss was perturbed by *smc3-D667*. These strains were arrested in G1 and treated with auxin to degrade Smc3-AIDp. Then they were released from G1 in the presence of auxin and nocodazole to allow cells to progress through S phase and arrest in mid-M. After release from G1, aliquots of cells were removed every fifteen minutes to assess DNA content and cohesion at *TRP1* and *LYS4* (Figure 2C,D).

From analysis of the DNA content, all strains exhibited nearly identical kinetics of progression through S phase and subsequent arrest in mid-M. As expected, separated sisters did not appear in cells expressing Smc3p (*SMC3 SMC3-AID*). Sister chromatids were paired during S phase and remained paired through mid-M arrest. In contrast, both strains lacking Smc3p (*SMC3-AID*) and Pds5p (*PDS5*-AID) lost cohesion; however, the cohesion loss in the latter strain was delayed by about 20 minutes, as published previously. Cells expressing only smc3-D667p (*smc3-D667 SMC3-AID*) exhibited delayed cohesion loss at the *LYS4* locus closely resembling cells lacking Pds5p function (*PDS5-AID*) and were even further delayed for cohesion loss at the *TRP1* locus. This delay in cohesion loss in cells with smc3-D667p demonstrated that *smc3-D667* cells, like Pds5p-deficient cells, could establish but not maintain cohesion. Thus, the D667 hinge region of Smc3p is important specifically for efficient maintenance of cohesion at both the centromere and arm of chromosome IV.

In the previous analyses, I arrested cells using nocodazole, a microtubule poison that prevents spindle assembly, thereby eliminating the forces normally resisted by sister chromatid cohesion. In budding yeast the spindle is assembled in S phase and becomes attached to kinetochores during S phase. If *smc3-D667* cells support robust cohesion establishment, then they should display a delay in cohesion loss even in the presence of active spindle forces. To test this prediction, I exploited *CDC20-AID*. Auxin induced destruction of Cdc20-AIDp inactivates the anaphase promoting complex, inducing a mid-M arrest with microtubules intact. My *SMC3-AID* strains with *CDC20-AID* were arrested in G1 and auxin was added to degrade Cdc20-AIDp along with Smc3-AIDp. Cells were released from G1 arrest in medium with auxin. At 15 minute intervals cells were removed to assess DNA content and cohesion (Supplementary Figure 1). Again, the similarity of DNA content of all strains at equivalent times revealed that all strains progressed through S phase and arrested in mid-M with nearly identical kinetics. Cells expressing only smc3-D667p (*smc3-D667 SMC3-AID CDC20-AID*) exhibited a delayed loss of *LYS4* cohesion relative to those lacking Smc3p function (*SMC3-AID CDC20-AID*). Thus, cohesin with smc3-D667p was capable of establishing robust cohesion that could resist spindle forces but was unable to maintain this cohesion. These results further corroborate the conclusion that the D667 region of the hinge is required specifically for the maintenance of cohesion.

The D667 region of the Smc3p hinge is required for condensation

In addition to sister chromatid cohesion, cohesin is also required for the proper mitotic condensation of chromatids in budding yeast. I addressed whether *smc3-D667* cells supported condensation by examining the morphology of the rDNA locus on chromosome XII. In chromosome spreads the rDNA is located on the periphery of the primary chromosome mass. In interphase the rDNA can be seen as a diffuse puff while in M phase it condenses into a loop. Chromosome spreads of the *SMC3-AID* and *PDS5-AID* strains were prepared from cells arrested in mid-M phase (see Materials and Methods). The rDNA morphology was scored as either 1) tight, fully-condensed loop 2) wide, decondensed loop or 3) diffuse, with no apparent loop. In cells with wild-type Smc3p, the rDNA formed tight loops in almost all chromosome masses, as expected for fully functional cohesin. Among chromosome masses from cells lacking Smc3p (*SMC3-*

AID), the rDNA was almost always present as diffuse, recapitulating the established role of Smc3p and cohesin in condensation. Cells expressing only smc3-D667p or depleted for Pds5p (*PDS5-AID*) exhibited very similar condensation defects. Tight loops were barely observed. They also displayed similar proportions of diffuse rDNA and wide loops. Although *smc3-D667* cells lacked tight rDNA loops in M phase arrested cells, it remained possible that condensation was established and then lost. My efforts to assess condensation in cells progressing through the cell cycle have not been successful. Thus, the D667 region of the Smc3p hinge was needed for condensation; dissection of this function in establishment and maintenance of condensation awaits further experimentation.

The D667 region of the Smc3p hinge enhances but is not essential for cohesin binding at CARs and centromeres

My observation that smc3-D667p promoted cohesion establishment suggested that cohesin with smc3-D667p must be able to bind DNA. To assess qualitatively whether *smc3-D667* supported binding of cohesin to chromosomes, I processed mid-M phase arrested cells for chromosome spreads and observed binding of the cohesin subunit Mcd1p by immunofluorescence (Figure 3A). Mcd1p binding to chromosomes is known to require Smc3p. Robust Mcd1p signal was observed on chromosome spreads from cells with Smc3p (*SMC3 SMC3-AID*) but not from cells without it (*SMC3-AID*), as expected. Mcd1p was detected on chromosome spreads from cells expressing smc3-D667p (*smc3-D667 Smc3-AID*) and appeared similar to that seen from cells with wild-type Smc3p, suggesting that cohesin with smc3-D667p can bind DNA.

To assess whether the chromosome binding of smc3-D667p observed in spreads reflected specific binding to CARs, I turned to chromatin immunoprecipitation (ChIP). I generated strains encoding Smc3p and smc3-D667p with a 6HA epitope tag in the *SMC3-AID* background. I chose to insert 6HA following Asn607 since fusion of the 3V5-AID epitope at this position does not impact growth (Eng et al. 2015). I verified expression of Mcd1p, Smc3-6HAp or smc3-6HA-D667p and Smc3-3V5-AIDp in cells at each stage of the regimen in Figure 2A to ensure that I could perform ChIP in M phase. Smc3-3V5-AIDp levels dropped considerably in auxin, and remained low after cells entered M phase arrest (Figure 3B). Importantly, both Mcd1p and smc3-6HA-D667p were detected in M-phase at levels comparable to cells expressing wild-type Smc3-6HAp. I then proceeded to assess chromosome binding in mid-M phase arrested cells by ChIP-qPCR. Robust Smc3-6HAp ChIP signal was observed at two CARs, one near *TRM1* on chromosome IV and *CARL1* on chromosome XII, as well as in the immediate vicinity of two centromeres (Figure 3C). ChIP signal was robust in cells with Smc3-6HAp (*SMC3-6HA SMC3-AID*) and absent in those without it (*SMC3-AID*). The ChIP signal in cells with smc3-6HA-D667p (*smc3-D667-6HA SMC3-AID*) was between 25% and 50% of wild-type at the apex of *TRM1* and *CARL1* peaks, respectively, and 50% wild-type levels near centromeres. Therefore, smc3-6HA-D667p localized specifically to CARs and centromeres, albeit at levels below Smc3-6HAp. To corroborate whether smc3-D667p binding reflected cohesin binding, I performed ChIP-qPCR using an Mcd1p antibody. Like smc3-6HA-D667p, Mcd1p bound less to CARs in cells with smc3-D667p (*smc3-D667 SMC3*-AID) than in cells with wild-type Smc3p (Figure 3D). Near the

centromeres, Mcd1p binding was similar between cells with smc3-D667p and Smc3p. Collectively, these data suggest that smc3-D667p bound to CARs and centromeres as part of the cohesin complex with possibly better binding of cohesin binding near centromeres than at CARs. Thus, the D667 region of the Smc3p hinge may play a more important role in modulating the level of cohesin binding on chromosome arms.

Since the cohesion maintenance defect of the *smc3-D667* mutant resembled the *pds5* mutant, I wondered whether cohesin with smc3-D667p might be unable to recruit Pds5p to chromosomes. To test this idea, I performed ChIP using antibody against native Pds5p. Cells expressing only smc3-D667p (*smc3-D667 SMC3-AID*) supported as much recruitment of Pds5p to CARs and centromeres as was observed for Mcd1p (Figure 3E). This result suggested that smc3-D667p supports Pds5p binding to cohesin. To test this idea further, I introduced the *SCC3-3FLAG* allele into the strains used for ChIP. The Scc3-3FLAGp was immunoprecipitated and the presence of cohesin subunits Pds5p, Smc3-6HAp or smc3-6HA-D667p were assessed by Western blot. In the control cells lacking Smc3p (*SMC3-AID*), immunoprecipitation of Scc3-3FLAGp failed to co-immunoprecipitate Pds5p (Supplementary Figure 2). Robust co-IP of Pds5p and Smc3-6HAp could be detected in cells expressing Smc3-6HAp (*SMC3-6HA SMC3-AID SCC3-3FLAG*) or smc3-6HA-D667p (*smc3-6HA-D667 SMC3-AID SCC3-3FLAG*). This result demonstrated that smc3-D667p supported Pds5p interaction with cohesin. Therefore, the role of the D667 region of the Smc3p hinge in cohesion maintenance was distinct from recruitment of Pds5p to cohesin in solution or on chromosomes.

The D667 region of the Smc3p hinge is not required for its stable binding to chromosomes

A simple hypothesis for the cohesion maintenance defect of *smc3-D667* is that this mutant increased the dissociation of cohesin from DNA, possibly by increasing dissociation of the hinge dimer. This model predicted that the rate of smc3-D667p dissociation from chromosomes should be greater than wild-type Smc3p. To test this prediction, I chose a system that allowed me to examine the stability of smc3-6HA-D667p binding under conditions in which additional loading was prevented by co-depletion of a cohesin loader subunit (Eng et al. 2014). In the absence of Scc2p in mid-M, cohesin that dissociated from chromosomes could not be reloaded, so any loss in ChIP signal had to result from cohesin dissociation from chromosomes. To be able to deplete Scc2p and to follow its depletion I replaced *SCC2* in my strains with *SCC2-3FLAG-AID*. Cultures of these strains were split and auxin was added to one to co-deplete Scc2-3FLAG-AIDp and Smc3-3V5-AIDp. Depletion of Scc2-3FLAG-AIDp and Smc3-3V5-AIDp was verified by Western blot (Figure 4B). After an hour of auxin treatment, the cultures were prepared for ChIP.

Smc3-6HAp showed no difference in binding to CAR sites *TRM1* and *CARL1* after Scc2-3FLAG-AIDp depletion (Figure 4C, left). The persistence of high ChIP levels after an hour indicated that cohesin remained very stably bound to DNA. Smc3-6HAp showed somewhat reduced binding to centromeres XIV and IV after Scc2-3FLAG-AIDp depletion indicating that cohesin is less stably bound at centromeres. My observation of reduced stability of Smc3-6HAp binding at centromeres corroborates the reduced stability of Mcd1p binding at centromeres observed previously (Eng et al. 2014).

Similarly, binding of smc3-6HA-D667p to CAR sites *TRM1* and *CARL1* was not lost in cells depleted of Scc2-3FLAG-AIDp, but was somewhat reduced at centromeres (Figure 4C, right). These results demonstrated that smc3-6HA-D667p was as stably bound to chromosomes as Smc3-6HAp. Thus, the D667 region of the Smc3p hinge was not required for its stable binding to DNA and an explanation other than unstable binding of cohesin to chromosomes must account for the cohesion maintenance defect of *smc3-D667* cells.

The D667 region of the hinge is required for efficient Eco1p acetylation of Smc3p at lysine 113

Eco1p is necessary for establishing cohesion during S phase through its acetylation of Smc3p at lysines K112 and K113. Although cohesion establishment occurs during S phase, Smc3p acetylation remains until anaphase onset, suggesting it may function in cohesion maintenance (Beckouet et al. 2010). Since smc3-D667p supported cohesion establishment, I suspected that it would be acetylated by Eco1p. Therefore, I used an antibody that specifically recognizes acetylated Smc3p-K113 to test the acetylation of smc3-D667p in cells arrested in mid-M. Cells were arrested in mid-M after auxin depletion (Figure 5A). As expected, in cells depleted of Eco1-AIDp or Smc3-AIDp, no acetylated Smc3p was detected (Figure 5B). While wild-type Smc3p showed strong acetylation signal, acetylation of smc3-D667p was remarkably low. Reduced smc3-D667p acetylation in mid-M may have resulted from a defect in Eco1p activity in S phase. Alternatively, the modification may have been lost as cells progressed into mid-M phase arrest. To determine whether smc3-D667p acetylation is established and then lost, I immunoprecipitated smc3-6HA-D667p from cells progressing synchronously through S phase following release from G1 (Figure 5C). As expected, wild-type Smc3-6HAp acetylation began to appear during S phase and remained high through M phase arrest (Figure 5D). In contrast, acetylation of smc3-6HA-D667p appeared at low levels in S phase and remained low as cells progressed to mid-M. Therefore, smc3-D667p exhibited a defect in K113 acetylation by Eco1p during S phase, rather than a failure to maintain this modification as cells progressed to mitosis. It remained unclear whether this acetylation defect was responsible for the failure of *smc3-D667* to maintain cohesion.

The D667 region of the Smc3p hinge likely modulates cohesion maintenance, condensation and viability by a mechanism independent of Eco1p-dependent acetylation

Reduced Smc3p-K113 acetylation is seen in *pds5* mutants, which, like *smc3-D667* can establish S phase cohesion but not sustain it through mitosis (Chan et al. 2013). This correlation suggested that a defect in K113 acetylation might underlie the cohesion maintenance and condensation defects observed in *smc3-D667* cells. To test this model, I further examined the correlation between Smc3p acetylation levels and cohesin function. *mcd1-Q226* cells exhibit defects in both condensation and cohesion maintenance (Eng et al. 2014). Cohesin with mcd1-Q266p, like I have observed for smc3-D667p, binds stably to chromosomes. Given this similarity, I examined Smc3p

acetylation from cohesin assembled with mcd1-Q266p. Log cultures of *mcd1-Q266 MCD1-AID, SMC3 SMC3-AID*, or *smc3-D667 SMC3-AID* cells were treated with auxin (Figure 5A), and Smc3p acetylation levels were compared by Western blot. *mcd1-Q266* supported at least as much Smc3p acetylation as *MCD1* cells (Figure 5E). This result suggested that cohesion maintenance defects occurred independent of Smc3p-K113 acetylation levels. I next asked whether low levels of Smc3p acetylation always led to loss of essential cohesin function. The temperature-sensitive *eco1-1* mutant retains essential cohesin functions at its permissive temperature despite showing a dramatic defect in Smc3p acetylation (Rowland et al. 2009). I therefore compared Smc3p acetylation supported by the temperature-sensitive *eco1-203* mutant to the *smc3-D667* mutant when grown at the permissive temperature 23˚C. The level of Smc3p acetylation in *eco1-203* cells was very similar to *smc3-D667* cells (Figure 5F). This result suggested that the level of smc3-D667p acetylation was sufficient to support essential cohesin functions in condensation, cohesion and viability. Moreover, it suggested that the critical defect in *smc3-D667* cells, like *mcd1-Q226* cells, was independent of Smc3p acetylation.

To further test the importance of low levels of smc3-D667p acetylation for its phenotype, I combined it with mutations in other proteins that reduce the stringency for Smc3p acetylation for viability, cohesion and condensation. Characterization of *eco1*Δ suppressors suggests that Eco1p regulates chromosome-bound cohesin to function in cohesion and condensation through two pathways shown in Figure 6A (Guacci et al. 2015; Çamdere et al. 2015). Deletion of *WPL1* (*wpl1*Δ) restores condensation and viability, but not cohesion, to *eco1*Δ cells (Guacci and Koshland 2012). Thus *wpl1*Δ bypasses the need for any Eco1p-dependent acetylation, including of Smc3p, for condensation and viability. If the failure of smc3-D667p to support viability and condensation was due to its low level of acetylation, then introducing *wpl1*Δ into *smc3-D667 SMC3-AID* cells should restore viability and condensation in media containing auxin. In the presence of auxin, the *smc3-D667 SMC3-AID* and *wpl1*Δ *smc3-D667 SMC3-AID* cells were both inviable (Supplementary Figure 3A) and exhibited the same severe condensation defect (Figure 6B). This result suggested that *smc3-D667* cells were defective at condensation independent of Eco1p-dependent acetylation. The *SMC1-D1164E* allele restores cohesion, condensation and viability to *eco1*Δ cells (Çamdere et al. 2015; Elbatsh et al. 2016). Thus *SMC1-D1164E* bypasses the need for any Eco1p-dependent acetylation, including of Smc3p, for cohesion as well as condensation and viability. In the presence of auxin, *smc3-D667 SMC3-AID* and *SMC1-D1164E smc3-D667 SMC3-AID* cells were inviable (Supplementary Figure 3B) and exhibited high levels of cohesion loss (Figure 6C). Together, these results demonstrated that *smc3-D667* cells are defective at cohesion maintenance, condensation, and viability independent of any function of Eco1p.

The D667 region is necessary for interallelic complementation

Interallelic complementation between alleles of *SMC3* or *MCD1* revealed the ability of two separate cohesin complexes to share activities to restore cohesin functions. Additional evidence suggests that this communication between cohesins might reflect direct cohesin-cohesin interaction (Eng et al. 2015). I wondered whether

the D667 region of the hinge was needed for cohesin-cohesin communication. To test this idea, I asked whether *smc3-D667* could partner with the temperature sensitive *smc3-42* allele to exhibit interallelic complementation. The temperature sensitive *smc3-42* strain cannot grow at its restrictive temperature of 34˚C. Previously it had been shown that the *smc3-K113R* allele cannot support viability as the sole copy of *SMC3*. However, a strain in which both *smc3-K113R* and *smc3-42* alleles are present exhibits robust growth at 34˚C, a condition in which neither single mutant can grow. With this knowledge, I asked whether *smc3-D667* could substitute for *smc3-K113R* and complement *smc3-42*. As a metric for the extent of interallelic complementation, I repeated the previous experiment with *smc3-42* and *smc3-K113*. As expected, at 34˚C neither *smc3-42* nor *smc3-K113R* single mutants were viable, while the *smc3-42 smc3-K113R* double mutant showed robust growth similar to wild-type (Figure 7). As expected, the *smc3-D667* single mutant failed to grow. The double *smc3-42 smc3-D667* mutant resembled the growth of *smc3-42* alone. Thus, the property of interallelic complementation observed between *smc3-42* and *smc3-K113R* was not observed between *smc3-42* and *smc3-D667*. Therefore, *smc3-D667* lacks the activity necessary for interallelic complementation. This result suggested that the D667 region of the hinge was necessary for cohesin-cohesin communication.

Discussion

Cohesin has a complex structural architecture with a heterodimeric ATPase domain and a hinge domain connected by a long coiled coil. The roles of these domains in cohesin's complicated functions are poorly understood. Here, I identified and characterized *smc3-D667*, a mutant in the Smc3p hinge domain that blocks cohesin function in M phase. Kinetic analyses of cohesion during the cell cycle reveal that this mutation allows cohesion establishment but impairs subsequent maintenance of cohesion. I also show that this mutation impairs mitotic chromosome condensation of the rDNA. However this mutation does not perturb the stable association of cohesin with chromosomes as measured by the persistence of this association even after loader inactivation. Together, my results support a function of cohesin's hinge domain in cohesion maintenance and condensation independent of cohesin's stable binding to chromosomes.

The functions of the hinge domain revealed by *smc3-D667* have not been reported previously. One mutation in the Smc1p hinge, *smc1-F584R*, disrupts cohesin loading on chromosomes, while a second, *smc1-M665R*, causes rapid turnover of bound cohesin by FRAP. Thus, the previous study of these two hinge mutants had revealed a role of the hinge in establishing and maintaining cohesin binding to chromosomes. These mutations impact the two interfaces between Smc1p and Smc3p hinges, termed "North" and "South", that mediate dimerization (Mishra et al. 2010). The phenotypic differences between these mutations and *smc3-D667* suggests that the D667 insertion does not impair these interfaces, consistent with my localization by homology of D667 within a loop outside the interface.

Another study designed a cluster of mutations in *SMC1* and *SMC3* that neutralize the positive charges in a central channel formed by hinge dimerization (Kurze et al. 2011). This cluster of mutations (charge neutralization alleles) caused a cohesion defect

but did not impair stable binding of cohesin to chromosomes similar to the smc3-*D667* allele. These charge neutralization mutants also reduced Smc3p acetylation similar to *smc3-D667*. Thus, the charge neutralization and *smc3-D667* alleles had very similar phenotypes. However, the previous study of the charge neutralization alleles did not perform the kinetic analysis of cohesion to distinguish an establishment or maintenance defect in cohesion. This study also did not analyze chromosome condensation. Because of the acetylation defect, the authors assumed the channel neutralization alleles revealed a function for the hinge in cohesion establishment. It would be very interesting to analyze the charge neutralization alleles for cohesion establishment and maintenance as well as condensation. If these alleles had the same cohesion and condensation defects as the *smc3-D667* allele, as I predict, these results would imply that changes to two distinct regions of the hinge dimer contribute to a common function needed for cohesion maintenance and condensation. The potential cooperation of the D667 region of the Smc3p hinge and the hinge channel could reflect a previously unrecognized conformational change of the hinge dimer needed for cohesin function.

The phenotypes of *smc3-D667* are strikingly similar to previously described phenotypes of the ROCC mutant in *MCD1,* Pds5p depletion, and *mcd1-V137K,* an allele that impairs Pds5p binding (Eng et al. 2014). These common phenotypes suggest that the hinge, Mcd1p, and Pds5p perform a common molecular function. This common function cannot be explained by a model in which, by some indirect mechanism, the hinge allows recruitment of Mcd1p and Pds5p to the Smc heterodimer. smc3-D667p perturbs this common function despite binding Pds5p and Mcd1p and assembling with them on chromosomes at CARs and centromeres (this study). Indeed, this common function provides a biological explanation for a number of biochemical studies that suggest the formation of a potential complex of the head, hinge, Mcd1p and Pds5p. Biochemical and structural data have revealed Mcd1p and Pds5p binding to each other and the head domain. Strong fluorescence resonance energy transfer (FRET) has been observed between fluorophore-tagged Pds5p and a fluorophore fused to the Smc1p hinge (Mc Intyre et al. 2007), suggesting close juxtaposition *in vivo*. Recent biochemical experiments failed to detect an *in vitro* interaction between purified *S. pombe* Pds5p and a minimal hinge dimer (Murayama and Uhlmann 2015). However, a supramolecular complex between *S. pombe* hinge dimer, Psc3p (Scc3p), and Mis4p (Scc2p) subunits has been observed (Murayama and Uhlmann 2015). Scc3p is known to bind to Pds5p and Mcd1p. Altogether these biochemical results and my study support the formation of a complex that includes the hinge, Mcd1p, and Pds5p that is required for cohesion maintenance and condensation.

The formation of this complex might also help to explain another intriguing property of the D667 region of the Smc3p hinge, its importance in promoting Smc3p acetylation during S phase. This conclusion was supported by my observation that the *smc3-D667* allele dramatically impaired the accumulation of smc3-K113 acetylation during S phase (this study). Intriguingly, this same phenotype was observed upon Pds5p depletion (Chan et al. 2013). In addition, the channel neutralization alleles also impaired this acetylation. The study with Pds5p depletion suggested that the reduction in K113 acetylation resulted at least in part because of the activity of the Hos1p deacetylase. It is possible that Hos1p access to Smc3-K113 may be inhibited by the putative formation of a hinge, Mcd1p, Pds5p complex.

The requirement for the hinge and Pds5p to ensure normal levels of Smc3p acetylation is not sufficient to explain their common function in cohesion maintenance and condensation. Here, I show that the level of acetylation, although low, in *smc3-D667* is equal to that which supports viability of the *eco1-203* mutant. Furthermore, I show that two different mutations, *wpl1*Δ and *SMC1-D1164E,* that bypass the need for any Eco1p acetylation (including Smc3-K113) for cohesion, condensation, and viability are unable to restore these functions to *smc3-D667.* Thus, the hinge and Pds5p must perform a function in cohesion maintenance and condensation that is independent of acetylation.

Potential insight into this common function of the hinge, Mcd1p and Pds5p in condensation and cohesion maintenance may come from another shared phenotype of mutations perturbing this function. They all perturb condensation and cohesion maintenance without altering cohesin's stable binding to DNA. To account for this phenotype, I have suggested that cohesion must result from a handcuff model with two distinct DNA binding activities. These DNA binding activities could either occur within a single cohesin (intramolecular handcuff) or in two cohesins that oligomerize (intermolecular handcuff). In the intramolecular handcuff model, the D667 region of the hinge would control the function of one of the DNA binding events within cohesin. The D667 allele would inactivate one of these DNA activities, disrupting cohesion but allowing cohesin to remain bound to DNA through the other activity. In the intermolecular handcuff model, the D667 region of the hinge could modulate oligomerization. In this case, the *smc3-D667* allele might impair the oligomerization. In support of the latter I show that the *smc3-D667* allele cannot complement the *smc3-42* mutant in *trans*. We previously showed that interallelic complementation occurs between *smc3* alleles and *mcd1* alleles (Eng et al. 2015), suggesting functional communication between cohesins likely by their physical interaction. The inability of *smc3-D667* to complement *smc3-42* is consistent with the idea that the D667 region of the hinge is necessary for this physical interaction. Confirmation of this idea awaits direct biochemical assays for cohesin oligomerization.

Acknowledgements

I thank Vincent Guacci, Thomas Eng, and the entire Koshland lab for helpful discussions and reagents. The yeast Smc3-K113 acetylation antibody was a kind gift of Katsuhiko Shirahige. I also thank Benjamin Rowland and Ahmed Elbatsh for advice using the Smc3-K113 acetylation antibody.

Materials and Methods

Yeast strains, media, and growth

All strains used are in the A364A background and their genotypes can be found in the Strain List. Yeast extract/peptone/dextrose media and synthetic dropout media was prepared as previously described (Guacci et al. 1997). Conditional AID degron strains were grown in YPD and 3-indoleacetic acid (IAA, Sigma Aldrich Cat I3750) dissolved in DMSO added to cultures to a final concentration of 750 μM. YPD + auxin plates were made by cooling molten YPD 2% agar to 55˚C prior to addition of auxin to a final concentration of 750 μM.

Cohesion assays

Sister chromatid cohesion was assessed at either the centromere-distal *LYS4* locus or centromere-proximal *TRP1* locus on Chr IV in which *LacO* arrays have been integrated. An allele expressing the *GFP-LacI* fusion integrated at *HIS3* allows fluorescence microscopic visualization of *LacO* arrays. Cohesion was scored by growing cells to mid-log phase (OD600 ~0.3) and arresting them in G1 using alpha factor at 10^{-8} M (Sigma Aldrich). After arresting for 3 hours, auxin was added to a final concentration of 750 μM to deplete Smc3-AID for one hour. Cells were released from G1 arrest by washing in YPD containing auxin and 0.1 mg/mL Pronase E (Sigma Aldrich) five times and resuspending in YPD containing auxin and 15 μg/mL nocodozole (Sigma Aldrich). Cultures were incubated at 23˚C and samples fixed either 1) periodically for assessing S-phase cohesion establishment or 2) after >95% of cells had arrested in G2/M after three hours. In addition to fixation for microscopy, samples were taken in parallel to assess DNA content by flow cytometry. Cohesion was scored by counting the number of GFP-LacI foci in the nucleus by fluorescence microscopy of fixed cells.

rDNA locus morphology

Cells were grown as if for assessing cohesion by arresting in YPD containing auxin and nocodazole following release from G1. Cells were processed and chromosomes bound to slides as described previously (Guacci et al. 1994). Briefly, 1 mL of cells were fixed two hours in 100 uL of 37% formaldehyde, washed twice in water, and spheroplasted for one hour. Triton X-100 was added to 0.5% for 5 minutes, cells spun and resuspended in water before 10 uL dropped onto slides for ten minutes. 0.5% SDS was added to cells on slides for 10 minutes, removed, then slides fixed in 3:1 methanol:acetic acid for five minutes and allowed to dry. Cells on slides were treated with RNase A and Proteinase K and dried through a series of 70%, 80%, 90%, and 100% ethanol washes. After drying, chromosomes were visualized with DAPI and rDNA morphology scored.

Chromatin immunoprecipitation (ChIP)

Cells were grown as if for assessing cohesion by arresting in YPD containing auxin and nocodazole following release from G1. ChIP was performed as described previously (Eng et al. 2014; Wahba et al. 2013) except that chromatin shearing was performed on a Bioruptor Pico machine (Diagenode, Denville, NJ) for 5 minutes (30 sec on/off cycling). Immunoprecipitation was performed using monoclonal Mouse anti-HA (Roche), monoclonal Mouse anti-V5 (ThermoFisher), polyclonal Rabbit anti-Pds5p (Covance Biosciences, Princeton, NJ), or polyclonal Rabbit anti-Mcd1p (Covance) antibodies. A no antibody control was always included to assess specificity of chromatin recovery.

Detection of Smc3-K113 acetylation by Western blotting

Cells were grown to OD_{600}=0.5 in YPD at 23˚C before addition of auxin to 0.75 mM for 1 hour, followed by nocodazole addition to 15 µg/mL to arrest cells in mid-M phase. Cells were pelleted and resuspended in lysis buffer consisting of 25 mM HEPES pH 8.0, 2 mM $MgCl_2$, 100 µM EDTA, 500 µM EGTA, 1% NP-40, 150 mM KCl, 15% glycerol, Complete-Mini EDTA-free protease inhibitor cocktail (Roche), 10 mM sodium butyrate, 20 mM beta-glycerophosphate. Cells were incubated in buffer for 30 minutes, then glass beads were added at a 1:1 volume ratio before bead-beating three times for one minute with one minute breaks on ice. Lysates were pelleted at 14K for 10 minutes, 4˚C, and protein concentrations measured by Coomassie Brilliant Blue. Lysates were boiled in 120 mM HEPES pH 7.0 containing 1% SDS at 95˚C for five minutes, then diluted 1:1 in Laemmli sample buffer. Smc3-K113 acetylation was detected by blotting with monoclonal Mouse antibody (a gift from K. Shirahige) at a concentration of 1:1,000 in PBST with 5% milk.

Chromosome spreads and microscopy

Cells were grown as if for assessing cohesion by arresting in YPD containing auxin and nocodazole following release from G1. Chromosome spreads were prepared as previously described (Wahba et al. 2013). Slides were incubated with 1:5,000 rabbit polyclonal anti-Mcd1p and 1:5,000 mouse anti-V5 antibody (Life Technologies). Antibodies were diluted in spreads blocking buffer (5% BSA, 0.2% milk, 1X PBS, 0.2% Triton X-100). Secondary Alexa Fluor 488-congugated chicken anti-mouse and Alexa Fluor 568-congugated donkey anti-rabbit (ThermoFisher Cats. A21200 and A10042) antibodies were diluted 1:5,000 in blocking buffer. Indirect immunofluorescence was detected on an Axioplan2 microscope (Zeiss, Thornwood, NY) using the 100X objective (numerical aperture 1.40) which is equipped with a Quantix charge-coupled camera (Photometrics).

Strain List

Strain	Genotype	Reference
BRY467	*MAT**a** smc3-D667-LEU2:leu2-3,112 smc3Δ::HPH lys4::LacO(DK)-NAT bar1 pHIS3-GFPLacI-TRP1:his3-11,15 trp1-1 ura3-52* + pEU42 (*SMC3 CEN URA3*)	this study
BRY474	*MAT**a** SMC3-LEU2:leu2-3,112 SMC3-3V5-AID^{608} trp1Δ::OsTIR1-CaTRP1 lys4::LacO(DK)-NAT pHIS3-GFPLacI-HIS3:his3-11,15 ura3-52 bar1*	this study
BRY482	*MAT**a** smc3-D667-LEU2:leu2-3,112 SMC3-3V5-AID^{608} trp1Δ::OsTIR1-CaTRP1 lys4::LacO(DK)-NAT pHIS3-GFPLacI-HIS3:his3-11,15 ura3-52 bar1*	this study
BRY602	*MAT**a** smc3-6HA^{608}-D667-URA3:ura3-52 SMC3-3V5-AID^{608} trp1Δ::OsTIR1-CaTRP1 lys4::LacO(DK)-NAT leu2-3,112 pHIS3-GFPLacI-HIS3:his3-11,15 bar1*	this study
BRY604	*MAT**a** SMC3-6HA^{608}-URA3:ura3-52 SMC3-3V5-AID^{608} trp1Δ::OsTIR1-CaTRP1 lys4::LacO(DK)-NAT leu2-3,112 pHIS3-GFPLacI-HIS3:his3-11,15 bar1*	this study
BRY607	*MAT**a** SCC3-3FLAG^{1089}-LEU2:leu2-3,112 SMC3-3V5-AID^{608} trp1Δ::OsTIR1-CaTRP1 lys4::LacO(DK)-NAT pHIS3-GFPLacI-HIS3:his3-11,15 leu2-3,112 ura3-52 bar1*	this study
BRY621	*MAT**a** SCC3-3FLAG^{1089}-LEU2:leu2-3,112 SMC3-6HA^{608}-URA3:ura3-52 SMC3-3V5-AID^{608} trp1Δ::OsTIR1-CaTRP1 lys4::LacO(DK)-NAT pHIS3-GFPLacI-HIS3:his3-11,15 bar1*	this study
BRY625	*MAT**a** SCC3-3FLAG^{1089}-LEU2:leu2-3,112 smc3-6HA^{608}-D667-URA3:ura3-52 SMC3-3V5-AID^{608} trp1Δ::OsTIR1-CaTRP1 lys4::LacO(DK)-NAT pHIS3-GFPLacI-HIS3:his3-11,15 bar1*	this study

BRY647	*MAT**a** SMC3-LEU2:leu2-3,112 smc3Δ::HPH rad61Δ::G418 lys4::LacO(DK)-NAT ura3-52 bar1 pHIS3-GFPLacI-TRP1:his3-11,15 trp1-1* + pEU42 (*SMC3 CEN URA3*)	this study
BRY648	*MAT**a** SMC3(D1189H)-LEU2:leu2-3,112 smc3Δ::HPH rad61Δ::G418 lys4::LacO(DK)-NAT ura3-52 bar1 pHIS3-GFPLacI-TRP1:his3-11,15 trp1-1* + pEU42 (*SMC3 CEN URA3*)	Guacci et al. 2015
BRY649	*MAT**a** smc3-D667-LEU2:leu2-3,112 smc3Δ::HPH rad61Δ::G418 lys4::LacO(DK)-NAT ura3-52 bar1 pHIS3-GFPLacI-TRP1:his3-11,15 trp1-1* + pEU42 (*SMC3 CEN URA3*)	this study
BRY650	*MAT**a** smc3-D667-D1189H-LEU2:leu2-3,112 smc3Δ::HPH rad61Δ::G418 lys4::LacO(DK)-NAT ura3-52 bar1 pHIS3-GFPLacI-TRP1:his3-11,15 trp1-1* + pEU42 (*SMC3 CEN URA3*)	this study
BRY676	*MAT**a** SMC3-3V5-AID^{608} trp1Δ::OsTIR1-CaTRP1 LacO(DK)-NAT:10kb-CEN4 pHIS3-GFPLacI-HIS3:his3-11,15 ura3-52 leu2-3,112 bar1*	this study
BRY678	*MAT**a** SMC3-LEU2:leu2-3,112 SMC3-3V5-AID^{608} trp1Δ::OsTIR1-CaTRP1 LacO(DK)-NAT:10kb-CEN4 pHIS3-GFPLacI-HIS3:his3-11,15 ura3-52 bar1*	this study
BRY680	*MAT**a** smc3-D667-LEU2:leu2-3,112 SMC3-3V5-AID^{608} trp1Δ::OsTIR1-CaTRP1 LacO(DK)-NAT:10kb-CEN4 pHIS3-GFPLacI-HIS3:his3-11,15 ura3-52 bar1*	this study
BRY714	*MAT**a** rad61Δ::HPHMX SMC3-3V5-AID^{608} trp1Δ::OsTIR1-CaTRP1 lys4::LacO(DK)-NAT leu2-3,112 pHIS3-GFPLacI-HIS3:his3-11,15 ura3-52 bar1*	this study
BRY716	*MAT**a** rad61Δ::HPHMX SMC3-LEU2:leu2-3,112 SMC3-3V5-AID^{608} trp1Δ::OsTIR1-CaTRP1 lys4::LacO(DK)-NAT pHIS3-GFPLacI-HIS3:his3-11,15 ura3-52 bar1*	this study

BRY718	*MAT**a** rad61Δ::HPHMX smc3-D667-LEU2:leu2-3,112 SMC3-3V5-AID^{608} trp1Δ::OsTIR1-CaTRP1 lys4::LacO(DK)-NAT pHIS3-GFPLacI-HIS3:his3-11,15 ura3-52 bar1*	this study
BRY720	*MAT**a** smc1-D1164E SMC3-3V5-AID^{608} trp1Δ::OsTIR1-CaTRP1 lys4::LacO(DK)-NAT leu2-3,112 pHIS3-GFPLacI-HIS3:his3-11,15 ura3-52 bar1*	this study
BRY721	*MAT**a** CDC20-3V5-AID2-KANMX smc3-D667-LEU2:leu2-3,112 SMC3-3V5-AID^{608} trp1Δ::OsTIR1-CaTRP1 lys4::LacO(DK)-NAT pHIS3-GFPLacI-HIS3:his3-11,15 ura3-52 bar1*	this study
BRY723	MAT**a** *CDC20-3V5-AID2-KANMX SMC3-3V5-AID^{608} trp1Δ::OsTIR1-CaTRP1 lys4::LacO(DK)-NAT leu2-3,112 pHIS3-GFPLacI-HIS3:his3-11,15 ura3-52 bar1*	this study
BRY724	MAT**a** *CDC20-3V5-AID2-KANMX SMC3-LEU2:leu2-3,112 SMC3-3V5-AID^{608} trp1Δ::OsTIR1-CaTRP1 lys4::LacO(DK)-NAT pHIS3-GFPLacI-HIS3:his3-11,15 ura3-52 bar1*	this study
BRY756	*MAT**a** smc3-D667-LEU2:leu2-3,112 smc3-42 lys4::LacO(DK)-NAT trp1-1 pHIS3-GFPLacI-HIS3:his3-11,15 bar1 ura3-52* + pEU42 (*SMC3 CEN URA3*)	this study
BRY815	*MAT**a** PDS5-3V5-AID2:KanMx6 LacO(DK)-NAT:10kb-CEN4 pHIS3-GFP-LacI-HIS3::his3-11,15 trp1-1 leu2-3,112 bar1 GAL+ ADH1-OsTIR1-URA3::ura3-52*	this study
BRY832	*MAT**a** smc1-D1164E SMC3-LEU2::leu2-3,112 SMC3-3V5-AID^{608} trp1Δ::OsTIR1-CaTRP1 lys4::LacO(DK)-NAT pHIS3-GFPLacI-HIS3:his3-11,15 ura3-52 bar1*	this study
BRY833	*MAT**a** SMC1-D1164E smc3-D667-LEU2::leu2-3,112 SMC3-3V5-AID^{608} trp1Δ::OsTIR1-CaTRP1 lys4::LacO(DK)-NAT pHIS3-GFPLacI-*	this study

	HIS3:his3-11,15 *ura3-52 bar1*	
BRY840	*MAT**a** SCC2-3FLAG-AID2-HPHMX SMC3-N607-6HA-URA3:ura3-52 SMC3-3V5-AID^{608} trp1∆::OsTIR1-CaTRP1 lys4::LacO(DK)-NAT leu2-3,112* *pHIS3-GFPLacI-HIS3:his3-11,15 bar1*	this study
BRY842	*MAT**a** SCC2-3FLAG-AID2-HPHMX smc3-6HA^{608}-D667-URA3:ura3-52 SMC3-3V5-AID^{608} trp1∆::OsTIR1-CaTRP1* *lys4::LacO(DK)-NAT leu2-3,112* *pHIS3-GFPLacI-HIS3:his3-11,15 bar1*	this study
DK5535	*MAT**a** mcd1-Q266-3FLAG-URA3::ura3-52 MCD1-AID-KANMX pGPD1-OsTIR1-LEU2::leu2-3,112 lys4::LacO(DK)-NAT trp1-1 GFPLacI-HIS3:his3-11,15 bar1*	Eng et al. 2014
DK5542	*MAT**a** MCD1-AID-KANMX6 ADH1-OsTIR1-URA3::ura3-52 lys4::LacO(DK)-NAT trp1-1 GFPLacI-HIS3:his3-11,15 bar1 leu2-3,112*	Eng et al. 2014
DK5561	*MAT**a** rad61∆::HPHMX pADH1-TIR1-URA3::ura3-42 lys4::LacO(DK)-NAT trp1-1 GFPLacI-HIS3:his3-11,15 bar1 leu2-3,112*	Eng et al. 2014
TE228	*MAT**a** PDS5-3V5-AID2-KANMX6 lys4::LacO(DK)-NAT pHIS3-GFP-LacI-HIS3::his3-11,15 trp1-1 ura3-52*	Eng et al. 2014
TE576	*MAT**a** smc3-42 lys4::LacO(DK)-NAT pHIS3-GFP-LacI-HIS3:his3-11,15 leu2-3,112 bar1 trp1-1* + pEU42 (*SMC3 CEN URA3*)	Eng et al. 2015
TE578	*MAT**a** smc3-42 smc3-K113R-LEU2::leu2-3,112 lys4::LacO(DK)-NAT pHIS3-GFP-LacI-HIS3:his3-11,15 leu2-3,112 bar1 trp1-1* + pEU42 (*SMC3 CEN URA3*)	Eng et al. 2015
VG3349-1B	*MAT**a** lys4::LacO(DK)-NAT trp1-1 GFPLacI-HIS3:his3-11,15 bar1 leu2-3,112 ura3-52*	Guacci and Koshland 2012

VG3358-3B	*MAT**a** smc3-42 lys4::LacO(DK)-NAT trp1-1 pHIS3-GFP-LACI-HIS3:his3-11,15 bar1 leu2-3,112 ura3-52*	Guacci and Koshland 2012
VG3464-16C	*MAT**a** smc3Δ::HPH lys4::LacO(DK)-NAT bar1 pHIS3-GFPLacI-TRP1:his3-11,15 trp1-1 leu2-3,112 ura3-52* +pEU42 (*SMC3 CEN URA3*)	Guacci and Koshland 2012
VG3486	*MAT**a** smc3Δ::HPH lys4::LacO(DK)-NAT bar1 pHIS3-GFPLacI-TRP1:his3-11,15 trp1-1 leu2-3,112 ura3-52* +pEU42 (*SMC3 CEN URA3*) + pEU41 (*SMC3 CEN LEU2*)	Eng et al. 2015
VG3486-K113R	*MAT**a** smc3Δ::HPH lys4::LacO(DK)-NAT bar1 pHIS3-GFPLacI-TRP1:his3-11,15 trp1-1 leu2-3,112 ura3-52* + pEU42 (*SMC3 URA3 CEN*) + *pEU41-K113R* (*smc3-K113R LEU2 CEN*)	Eng et al. 2015
VG3503-4A	*MAT**a** rad61Δ::HPHMX eco1Δ::KANMX trp1-1 lys4::LacO(DK)-NAT leu2-3,112 pHIS3-GFPLacI-HIS3:his3-11,15 ura3-52 bar1*	Çamdere et al. 2015
VG3506-5D	*MAT**a** eco1-203 LacO-NAT:10kb-CEN4 trp1-1 pHIS3-GFPLacI-HIS3:his3-11,15 leu2-3,112 ura3-52 bar1*	this study
VG3575-2C	*MAT**a** smc1-D1164E rad61Δ::HPHMX eco1Δ::G418 lys4::LacO(DK)-NAT GFPLacI-HIS3:his3-11,15 trp1-1 leu2-3,112 ura3-52 bar1*	Çamdere et al. 2015
VG3578-1A	*MAT**a** smc3Δ::HPHMX rad61Δ::KANMX leu2-3,112 lys4::LacO(DK)-NAT ura3-52 bar1 pHIS3-GFPLacI-TRP1:his3-11,15 trp1-1* + pEU42 (*SMC3 CEN URA3*)	Guacci et al. 2015
VG3620-4C	*MAT**a** trp1Δ::pGPD1-TIR1-CaTRP1 lys4::LacO(DK)-NAT leu2-3,112 pHIS3-GFPLacI-HIS3:his3-11,15 ura3-52 bar1*	Çamdere et al. 2015
VG3633-2D	*MAT**a** ECO1-3V5-AID2-KANMX trp1Δ::pGPD1-TIR1-CaTRP1 lys4::LacO(DK)-NAT leu2-3,112 pHIS3-GFPLacI-HIS3:his3-11,15 bar1 ura3-52*	this study

VG3651-3D	*MAT**a** SMC3-3V5-AID^{608} trp1∆::pGPD1-TIR1-CaTRP1 lys4::LacO(DK)-NAT pHIS3-GFPLacI-HIS3:his3-11,15 leu2-3,112 ura3-52 bar1*	Çamdere et al. 2015

References

Anderson, D. E., Losada, A., Erickson, H. P., & Hirano, T. (2002). Condensin and cohesin display different arm conformations with characteristic hinge angles. The Journal of Cell Biology, 156(3), 419–424.

Arumugam, P., Nishino, T., Haering, C. H., Gruber, S., & Nasmyth, K. (2006). Cohesin's ATPase activity is stimulated by the C-terminal Winged-Helix domain of its kleisin subunit. *Current Biology : CB*, *16*(20), 1998–2008.

Beckouët, F., Hu, B., Roig, M. B., Sutani, T., Komata, M., Uluocak, P., et al. (2010). An Smc3p acetylation cycle is essential for establishment of sister chromatid cohesion. *Molecular Cell*, *39*(5), 689–699.

Beckouët, F., Srinivasan, M., Roig, M. B., Chan, K.-L., Scheinost, J. C., Batty, P., et al. (2016). Releasing Activity Disengages Cohesin's Smc3/Scc1 Interface in a Process Blocked by Acetylation. *Molecular Cell*, *61*(4), 563–574.

Çamdere, G., Guacci, V., Stricklin, J., & Koshland, D. (2015). The ATPases of cohesin interface with regulators to modulate cohesin-mediated DNA tethering. *eLife*, *4*, 13115.

Chan, K.-L., Gligoris, T., Upcher, W., Kato, Y., Shirahige, K., Nasmyth, K., & Beckouët, F. (2013). Pds5p promotes and protects cohesin acetylation. *Proceedings of the National Academy of Sciences of the United States of America*, *110*(32), 13020–13025.

Ciosk, R., Shirayama, M., Shevchenko, A., Tanaka, T., Tóth, A., Shevchenko, A., & Nasmyth, K. (2000). Cohesin's Binding to Chromosomes Depends on a Separate Complex Consisting of Scc3p and Scc4p Proteins. *Molecular Cell*, *5*(2), 243–254.

D'Ambrosio, L. M., & Lavoie, B. D. (2014). Pds5p Prevents the PolySUMO-Dependent Separation of Sister Chromatids. *Current Biology*, *24*(4), 361–371.

Elbatsh, A. M. O., Haarhuis, J. H. I., Petela, N., Chapard, C., Fish, A., Celie, P. H., et al. (2016). Cohesin Releases DNA through Asymmetric ATPase-Driven Ring Opening. *Molecular Cell*, *61*(4), 575–588.

Eng, T., Guacci, V., & Koshland, D. (2014). ROCC, a conserved region in cohesin's Mcd1p subunit, is essential for the proper regulation of the maintenance of cohesion and establishment of condensation. *Molecular Biology of the Cell*, *25*(16), 2351–2364.

Eng, T., Guacci, V., & Koshland, D. (2015). Interallelic complementation provides functional evidence for cohesin-cohesin interactions on DNA. *Molecular Biology of the Cell*, *26*(23), 4224–4235.

Guacci, V., & Koshland, D. (2012). Cohesin-independent segregation of sister chromatids in budding yeast. *Molecular Biology of the Cell*, *23*(4), 729–739.

Guacci, V., Koshland, D., & Strunnikov, A. (1997). A Direct Link between Sister Chromatid Cohesion and Chromosome Condensation Revealed through the Analysis of MCD1 in S. cerevisiae. *Cell*, *91*(1), 47–57.

Guacci, V., Hogan, E., & Koshland, D. (1994). Chromosome condensation and sister chromatid pairing in budding yeast. *The Journal of Cell Biology*, *125*(3), 517–530.

Haering, C. H., Löwe, J., Hochwagen, A., & Nasmyth, K. (2002). Molecular architecture of SMC proteins and the yeast cohesin complex. *Molecular Cell*, *9*(4), 773–788.
Hons, M. T., Veld, P. J. H. I. T., Kaesler, J., Rombaut, P., Schleiffer, A., Herzog, F., et al. (2016). Topology and structure of an engineered human cohesin complex bound to Pds5B. Nature Communications, 7, 12523.

Huis in t Veld, P. J., Herzog, F., Ladurner, R., Davidson, I. F., Piric, S., Kreidl, E., et al. (2014). Characterization of a DNA exit gate in the human cohesin ring. Science, 346(6212), 968–972.

Kulemzina, I., Ang, K., Zhao, X., Teh, J.-T., Verma, V., Suranthran, S., et al. (2016). A Reversible Association between Smc Coiled Coils Is Regulated by Lysine Acetylation and Is Required for Cohesin Association with the DNA. *Molecular Cell*, *63*(6), 1044–1054.

Kurze, A., Michie, K. A., Dixon, S. E., Mishra, A., Itoh, T., Khalid, S., et al. (2011). A positively charged channel within the Smc1/Smc3p hinge required for sister chromatid cohesion. *The EMBO Journal*, *30*(2), 364–378.

Laloraya, S., Guacci, V., & Koshland, D. (2000). Chromosomal addresses of the cohesin component Mcd1p. *The Journal of Cell Biology*, *151*(5), 1047–1056.

Mc Intyre, J. M., Muller, E. G., Weitzer, S., Snydsman, B. E., Davis, T. N., & Uhlmann, F. (2007). In vivo analysis of cohesin architecture using FRET in the budding yeast Saccharomyces cerevisiae. *The EMBO Journal*, *26*(16), 3783–3793.

Milutinovich, M., Ünal, E., Ward, C., Skibbens, R. V., & Koshland, D. (2007). A Multi-Step Pathway for the Establishment of Sister Chromatid Cohesion. *PLoS Genet*, *3*(1), e12.

Minnen, A., Bürmann, F., Wilhelm, L., Anchimiuk, A., Diebold-Durand, M.-L., & Gruber, S. (2016). Control of Smc Coiled Coil Architecture by the ATPase Heads Facilitates Targeting to Chromosomal ParB/parS and Release onto Flanking DNA. *Cell Reports*, *14*(8), 2003–2016.

Mishra, A., Hu, B., Kurze, A., Beckouët, F., Farcas, A.-M., Dixon, S. E., et al. (2010). Both interaction surfaces within cohesin's hinge domain are essential for its stable chromosomal association. *Current Biology : CB*, *20*(4), 279–289.

Murayama, Y., & Uhlmann, F. (2015). DNA Entry into and Exit out of the Cohesin Ring by an Interlocking Gate Mechanism. *Cell*, *163*(7), 1628–1640.

Noble, D., Kenna, M. A., Dix, M., Skibbens, R. V., Ünal, E., & Guacci, V. (2006). Intersection between the regulators of sister chromatid cohesion establishment and maintenance in budding yeast indicates a multi-step mechanism. *Cell Cycle (Georgetown, Tex.)*, *5*(21), 2528–2536.

Rolef Ben-Shahar, T., Heeger, S., Lehane, C., East, P., Flynn, H., Skehel, M., & Uhlmann, F. (2008). Eco1-dependent cohesin acetylation during establishment of sister chromatid cohesion. Science, 321(5888), 563–566.

Rowland, B. D., Roig, M. B., Nishino, T., Kurze, A., Uluocak, P., Mishra, A., et al. (2009). Building sister chromatid cohesion: smc3 acetylation counteracts an antiestablishment activity. *Molecular Cell*, *33*(6), 763–774.

Soh, Y.-M., Bürmann, F., Shin, H.-C., Oda, T., Jin, K. S., Toseland, C. P., et al. (2015). Molecular Basis for SMC Rod Formation and Its Dissolution upon DNA Binding. *Molecular Cell*, *57*(2), 290–303.

Ünal, E., Heidinger-Pauli, J. M., Kim, W., Guacci, V., Onn, I., Gygi, S. P., & Koshland, D. E. (2008). A molecular determinant for the establishment of sister chromatid cohesion. *Science*, *321*(5888), 566–569.

Ünal, E., Heidinger-Pauli, J. M., Kim, W., Guacci, V., Onn, I., Gygi, S. P., & Koshland, D. E. (2008). A molecular determinant for the establishment of sister chromatid cohesion. *Science*, *321*(5888), 566–569.

Wahba, L., Gore, S. K., Koshland, D., & Proudfoot, N. (2013). The homologous recombination machinery modulates the formation of RNA–DNA hybrids and associated chromosome instability. *eLife*, *2*, e00505.

Zhang, J., Shi, X., Li, Y., Kim, B.-J., Jia, J., Huang, Z., et al. (2008). Acetylation of Smc3p by Eco1p Is Required for S Phase Sister Chromatid Cohesion in Both Human and Yeast. *Molecular Cell*, *31*(1), 143–151.

Figure Legends

Figure 1: The *smc3-D667* RID mutation maps near the channel entrance and lies atop the Smc3p hinge South interface

A) Diagram of cohesin highlighting location of the *smc3-D667* RID insertion. The homologous residue of *smc3*-D667 in mice was predicted by sequence alignment using ClustalW, and highlighted in orange in the mice Smc1/Smc3p crystal structure (PDB: 2WD5, Kurze et al. 2011). The amino acid location of other RIDs isolated in this screen were approximated by sequence alignment represented as green spheres.
B) Sequence alignment of Smc3p homologues showing conserved region around D667. The position of Asp667 is highlighted in yellow and the sequence of the five amino acid insertion, AAAAD, that follows Asp667 in the *smc3-D667* RID is depicted above in red.
C) Growth supported by *smc3-D667* under the native *SMC3* promoter. Saturated BRY474 (*SMC3 SMC3-AID*), VG3651-3D (*SMC3-AID)*, and BRY482 (*smc3-D667 SMC3-AID*) liquid cultures were serially diluted and plated onto YPD plates with and without 0.75 mM auxin and grown for two days at 23˚C.

Figure 2: *smc3-D667* exhibits a cohesion maintenance defect

A) Regimen used to prepare cells for mid-M phase cohesion assay in (B). Cultures were grown to mid-log phase at 23˚C and treated with alpha factor for three hours to arrest them G1 phase. Auxin was added to deplete Smc3-3V5-AIDp for one hour and G1 samples collected and fixed for microscopy before alpha factor was washed out to release them from arrest. Following washes, cells were resuspended in YPD containing auxin and nocodazole and incubated an additional three hours to arrest them in mid-M phase, after which they were fixed to assess cohesion by microscopy.
B) Percentage of G1 and mid-M phase arrested cells displaying cohesion loss at CEN-proximal *TRP1* and CEN-distal *LYS4* loci. Haploid *SMC3-AID* yeast with wild-type *SMC3,* no additional *SMC3,* or *smc3-D667* (BRY678, BRY676, BRY680 respectively) with LacO arrays integrated at *TRP1*, left, or *LYS4*, right (BRY474, VG3651-3D, BRY482) were treated as in (A). Samples were collected after one hour of auxin in G1 and following mid-M phase arrest to score cohesion. The average percentage of separated sister chromatids from two independent experiments are plotted in which 100-200 cells were scored per sample. Error bars represent SD.
C) Percentage of cells displaying cohesion loss at the CEN-proximal *TRP1* locus as a function of time following release from G1 arrest. Haploid strains BRY678 (*SMC3 SMC3-AID*). BRY676 (*SMC3-AID)*, BRY680 (*smc3-D667 SMC3-AID*) and BRY815 (*PDS5-AID)* were arrested in G1 with alpha factor, treated with auxin, and released from arrest into fresh YPD containing auxin and nocodazole. Samples were collected every fifteen minutes starting thirty minutes after G1 release to score separated sisters (left) and assess DNA replication by flow cytometry (right). 100 to 200 cells were scored for cohesion for each time point.

D) Percetage of cells displaying cohesion loss at the CEN-distal *LYS4* locus as a function of time after release from G1 arrest. Haploid strains BRY474 (*SMC3 SMC3-AID*), VG3651-3D (*SMC3-AID*), BRY482 (*smc3-D667 SMC3-AID*) and TE228 (*PDS5-AID*) were treated as described in (C) and samples collected every fifteen minutes starting thirty minutes after G1 release to score separated sisters (left) and assess DNA replication by flow cytometry (right). 100 to 200 cells were scored for cohesion for each time point.
E) Percentage of chromosome masses displaying tight loop, wide loop, or diffuse rDNA morphologies. BRY474 (*SMC3 SMC3-AID*), VG3651-3D (*SMC3-AID*), BRY482 (*smc3-D667 SMC3-AID*), and TE228 (*PDS5-AID*) cells were treated as in (A) and processed as if for *in situ* hybridization (see Materials and Methods). Chromosome masses were scored for chromosome morphology after staining with DAPI. Shown are averages from two independent experiments in which 100 chromosome masses were scored. Error bars depict SD.

Figure 3: Chromosomes binding and localization supported by *smc3-D667*

A) Cells treated according to the regimen in Figure 2A were processed for chromosome spreads after arresting in mid-M phase. Immunofluorescence was used to detect global Mcd1p binding to chromosomes from BRY474 (*SMC3 SMC3-AID*), VG3651-3D (*SMC3-AID*), and BRY482 (*smc3-D667 SMC3-AID*) cells.
B) Protein levels supported by internally 6HA epitope tagged Smc3p alleles. *SMC3-3V5-AID* strains expressing *SMC3-6HA^{607}-D667* (BRY602), *SMC3-6HA^{607}* (BRY604), or no additional *SMC3* allele (VG3561-3D) were grown according to the regimen in Figure 2A. Samples were collected in G1 before and after auxin addition and after arrest in mid-M phase.
C) Chromosome binding of HA-epitope tagged WT Smc3-6HA^{607}p (BRY604), dashed line or white bar, and Smc3-6HA^{607}-D667p (BRY602), solid line or black bar, to cohesin associated regions *TRM1* and *CARL1* (left), and centromeres I and XIV (right) by ChIP-qPCR. Cells were prepared according to the regimen in Figure 2A and fixed after arresting in mid-M phase. Chromatin was sheared and immunoprecipitated with anti-HA antibody (see Materials and Methods). Depicted is the HA ChIP sample qPCR signal relative to total chromatin sample qPCR signal from multiple primer pairs spanning each site expressed as a percentage.
D) Chromosome binding of Mcd1p in haploid strains BRY474 (*SMC3 SMC3-AID*), VG3651-3D (*SMC3-AID*), and BRY482 (*smc3-D667 SMC3-AID*) arrested in mid-M phase according to the regimen in Figure 2A. Binding was assessed at cohesin associated regions *CARC1* and *CARL1* (left), and centromeres I and XIV (right) by ChIP-qPCR. Chromatin was sheared and immunoprecipitated with polyclonal anti-Mcd1p antibody.
E) Chromosome binding of Pds5p in haploid strains BRY474 (*SMC3 SMC3-AID*), VG3651-3D (*SMC3-AID*), and BRY482 (*smc3-D667 SMC3-AID*) arrested in mid-M phase according to the regimen in Figure 2A. Binding was assessed at cohesin associated regions *TRM1* and *CARL1* (left), and centromeres I and XIV (right) by ChIP-qPCR. Chromatin was sheared and immunoprecipitated with polyclonal anti-Pds5p antibody.

Figure 4: *smc3-D667* supports stable cohesin binding to chromosomes

A) Regimen used to assess stability of cohesin binding to DNA upon depletion of the loader subunit Scc2p. Haploid *SMC3-3V5-AID SCC2-3FLAG-AID2* strains expressing either *SMC3-6HA* (BRY839) or *smc3-6HA-D667* (BRY841) were grown to mid-log phase and arrested in mid-M phase by incubation with nocodazole for three hours. Cultures were split and auxin added to one to a final concentration of 0.75 mM and incubated for sixty minutes. After collecting samples for protein levels, 30 ODs of cells from each culture were fixed and processed for ChIP (see Materials and Methods).
B) Protein levels in cells processed for ChIP to determine cohesin binding stability. *SMC3-6HA* and *smc3-6HA-D667* cultures were treated as described in Figure 4A and protein extracted by glass bead lysis in TCA. Protein samples were separated by SDS-PAGE and subject to Western blotting with the indicated antibodies. Tubbs1 was probed as a loading control.
C) Smc3-6HAp and smc3-6HA-D667p binding at CARs and centromeres in the presence (solid lines and filled columns) and absence (dashed lines and open columns) of Scc2-3FLAG-AID2p and Smc3-3V5-AIDp. Left column: Cells expressing Smc3-6HAp were fixed after treating as in (A). Chromatin was sheared, clarified, and subject to ChIP with anti-HA antibody. From top to bottom: binding to CARs *TRP1* and *CARL1*, and centromeres XIV and IV was determined using qPCR primer pairs spanning each region. Right column: Binding of smc3-6HA-D667p was determined by ChIP-qPCR for cells treated with or without auxin.

Figure 5: Reduced acetylation of smc3-D667p at K113 by Eco1p

A) Regimen used to assess Smc3-K113 acetylation in mid-M phase arrested cells. Early log phase cultures were treated with 0.75 mM auxin for one hour to deplete Smc3-3V5-AIDp prior to addition of nocodazole and incubated for three hours to arrest cells in mid-M phase. Arrest was confirmed by monitoring bud morphology
B) Reduced K113 acetylation of smc3-D667p. Haploid VG3633-2D (*ECO1-AID*), VG3651-3D (*SMC3-AID*), BRY474 (*SMC3 SMC3-AID*), and BRY482 (*smc3-D667 SMC3-AID*) cultures grown as described in (A) and protein harvested (see Materials and Methods). Samples were resolved by SDS-PAGE and subject to Western blotting with the indicated antibodies. Short and long film exposures of the anti-Smc3-K113ac (Smc3-ac) blot are shown so that levels can be more easily compared.
C) Regimen used to determine the kinetics of Smc3-K113 acetylation establishment within a single cell cycle. Log phase cultures were arrested in G1 in alpha factor, treated with auxin for one hour, and released into fresh YPD containing auxin and nocodazole. Samples were taken at the indicated
D) Reduced smc3-6HA-D667p acetylation in S phase. Haploid cells expressing Smc3-6HAp (BRY604, left) or smc3-6HA-D667p (BRY602, right) were grown at 23˚C and treated as described in (C). Left: Cells were collected and frozen for each time point and lysed. Total protein samples were collected, then anti-HA antibody was added to

the remaining lysates to immunoprecipitate Smc3-6HAp or smc3-6HA-D667p. Precipitated protein was bound to magnetic beads, which were washed and then boiled in sample buffer. Samples were resolved by SDS-PAGE prior to Western blotting with the indicated antibodies. Tub1pis used as a loading control for the total protein samples. Short and long film exposures of the anti-Smc3-K113ac blots are shown so that levels can be more easily compared. Right: Samples were collected in parallel to those used for immunoprecipitations in order to assess DNA content by flow cytometry.

E) Robust Smc3-K113 acetylation supported by mcd1-Q266p but not smc3-D667p. Haploid strains VG3651-3D (*SMC3-AID*), BRY474 (*SMC3 SMC3-AID*), BRY482 (*smc3-D667 SMC3-AID*), DK5535 (*mcd1-Q266-3FLAG MCD1-AID*), and DK5542 (*MCD1-AID*) were treated as described in (A) prior to SDS-PAGE and Western blotting with indicated antibodies. Tub1pis used as a loading control.

F) Reduced smc3-D667p acetylation at K113 resembles that supported by *eco1-203* at its restrictive temperature. Haploid strains VG3651-3D (*SMC3-AID*), BRY474 (*SMC3 SMC3-AID*), BRY482 (*smc3-D667 SMC3-AID*), and VG3506-5D (*eco1-203*) were treated as described in (A) prior to SDS-PAGE and Western blotting with indicated antibodies. Tub1pis used as a loading control. Short and long film exposures of the anti-Smc3-K113ac blots are shown so that levels can be more easily compared.

Figure 6: *eco1*Δ suppressors fail to restore condensation or cohesion to *smc3-D667*

A) Model of how Eco1p regulates chromosome-bound cohesin. Top: ATP hydrolysis by the Smc3p ATPase antagonizes cohesion, a process thought to be inhibited by Eco1p or Smc1-D1164E (Çamdere et al. 2015; Elbatsh et al. 2016). Bottom: Wpl1p antagonizes cohesin function in condensation, a process inhibited by Eco1p (Guacci and Koshland 2012). Smc1-D1164E can bypass the need for Eco1p activity for cohesion and viability, while *wpl1*Δ can bypass the need for Eco1p activity for condensation and viability.

B) Quantification of condensed rDNA in mid-M phase arrested cells. Haploid strains VG3651-3D (*SMC3-AID*), BRY474 (*SMC3 SMC3-AID*), BRY482 (*smc3-D667 SMC3-AID*), BRY718 (*smc3-D667 SMC3-AID wpl1*Δ), and DK5561 (*wpl1*Δ) were treated as in Figure 2A and fixed as if for *in situ* hybridization (see Materials and Methods). Shown are the percentage of chromosome masses displaying a tight rDNA loop.

C) Percentage of G1 and mid-M phase arrested cells displaying cohesion loss at the CEN-distal *LYS4* locus. Haploid strains VG3503-4A (*eco1*Δ *wpl1*Δ), VG3575-2C (*eco1*Δ *wpl1*Δ *SMC1-D1164E*), BRY720 (*SMC3-AID SMC1-D1164E*), BRY482 (*smc3-D667 SMC3-AID*), BRY833 (*smc3-D667 SMC3-AID SMC1-D1164E*), and BRY832 (*SMC3 SMC3-AID SMC1-D1164E*) cells were grown according the regimen in Figure 2A and samples collected after auxin treatment in G1 or following mid-M phase arrest to score cohesion loss. The average percentage of separated sister chromatids from two independent experiments are plotted, in which 100-200 cells were scored per sample. Error bars represent SD.

Figure 7: The D667 region is necessary for interallelic complementation

Dilution plating for growth in the presence (YPD) or absence (5-FOA) of the *SMC3 URA3 CEN* plasmid. Haploid strains VG3486 (*SMC3*), TE576 (*smc3-42*), BRY467 (*smc3-D667*), BRY756 (*smc3-42 smc3-D667*), VG3486-K113R (*smc3-K113R*), and TE578 (*smc3-42 smc3-K113R*) were grown to saturation in SC – URA Dextrose liquid media. Cells from these cultures were used to inoculate fresh YPD cultures which were again grown to saturation to allow loss of the *SMC3 URA3 CEN* plasmid. These cells were then subject to 10-fold serial dilutions and plated to YPD or 5-FOA plates for growth at the indicated temperatures.

Supplementary Figure 1

Cohesion loss at the CEN-distal *LYS4* locus after release from G1 arrest into Cdc20-3V5-AID2p depletion arrest. Haploid strains BRY724 (*SMC3 SMC3-AID CDC20-AID*), BRY721 (*smc3-D667 SMC3-AID CDC20-AID*), and BRY723 (*SMC3-AID CDC20-AID*) were arrested as in Figure 2A and samples collected every fifteen minutes starting thirty minutes after G1 release into YPD containing auxin to score separated sisters (left) and assess DNA replication by flow cytometry (right). 100 to 200 cells were counted per time point.

Supplementary Figure 2

Smc3-D667p supports assembly of cohesin containing Pds5p and Scc3-3FLAGp. Haploid strains VG3561-3D (*SMC3-AID*), BRY607 (*SCC3-3FLAG SMC3-AID*), BRY604 (*SMC3-6HA SMC3-AID*), BRY621 (*SCC3-3FLAG SMC3-6HA SMC3-AID*), and BRY625 (*SCC3-3FLAG smc3-6HA-D667 SMC3-AID*) cells were grown to mid log phase. Cells were then lysed and clarified lysate subject to immunoprecipitation using anti-FLAG antibody. Precipitated protein was resolved by SDS-PAGE and Western blotting performed with the indicated antibodies. An irrelevant lane was removed.

Supplementary Figure 3

A) Haploid strains featured in Figure 6B with the indicated genotype were grown to saturation in YPD, ten-fold serial diluted and spotted onto YPD or YPD containing 0.75 mM auxin and grown for 2 days at 23˚C. Strains from top to bottom: VG3349-1B, BRY474, BRY716, BRY482, BRY718, VG3651-3D, BRY714.
B) Haploid strains featured in Figure 6C with the indicated genotype were grown to saturation in YPD, ten-fold serial diluted and spotted onto YPD or YPD containing 0.75 mM auxin and grown for 2 days at 23˚C. Strains from top to bottom: VG3349-1B, BRY474, BRY832, VG3651-3D, BRY720, BRY482, BRY833.

Figure 1

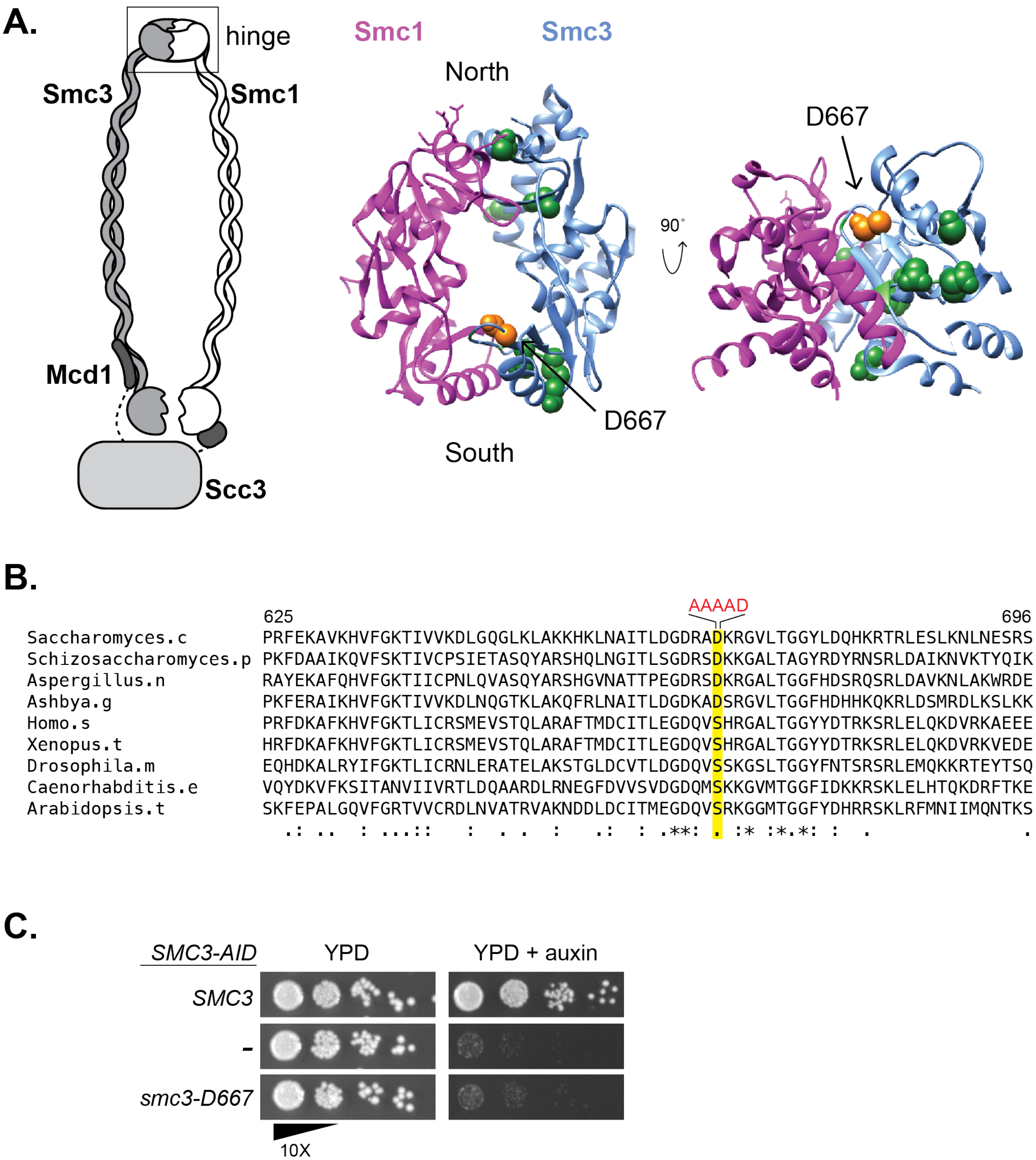
A.
hinge
Smc3
Smc1
Mcd1
Scc3
Smc1
Smc3
North
South
D667
90˚
D667
B.
AAAAD
625
696
Saccharomyces.c PRFEKAVKHVFGKTIVVKDLGQGLKLAKKHKLNAITLDGDRADKRGVLTGGYLDQHKRTRLESLKNLNESRS
Schizosaccharomyces.p PKFDAAIKQVFSKTIVCPSIETASQYARSHQLNGITLSGDRSDKKGALTAGYRDYRNSRLDAIKNVKTYQIK
Aspergillus.n RAYEKAFQHVFGKTIICPNLQVASQYARSHGVNATTPEGDRSDKRGALTGGFHDSRQSRLDAVKNLAKWRDE
Ashbya.g PKFERAIKHVFGKTIVVKDLNQGTKLAKQFRLNAITLDGDKADSRGVLTGGFHDHHKQKRLDSMRDLKSLKK
Homo.s PRFDKAFKHVFGKTLICRSMEVSTQLARAFTMDCITLEGDQVSHRGALTGGYYDTRKSRLELQKDVRKAEEE
Xenopus.t HRFDKAFKHVFGKTLICRSMEVSTQLARAFTMDCITLEGDQVSHRGALTGGYYDTRKSRLELQKDVRKVEDE
Drosophila.m EQHDKALRYIFGKTLICRNLERATELAKSTGLDCVTLDGDQVSSKGSLTGGYFNTSRSRLEMQKKRTEYTSQ
Caenorhabditis.e VQYDKVFKSITANVIIVRTLDQAARDLRNEGFDVVSVDGDQMSKKGVMTGGFIDKKRSKLELHTQKDRFTKE
Arabidopsis.t SKFEPALGQVFGRTVVCRDLNVATRVAKNDDLDCITMEGDQVSRKGGMTGGFYDHRRSKLRFMNIIMQNTKS
.: .. : ...:: : . . : .: : .**: . :* :*.*: : . .
C.
SMC3-AID
YPD
YPD + auxin
SMC3
-
smc3-D667
10X

Figure 2

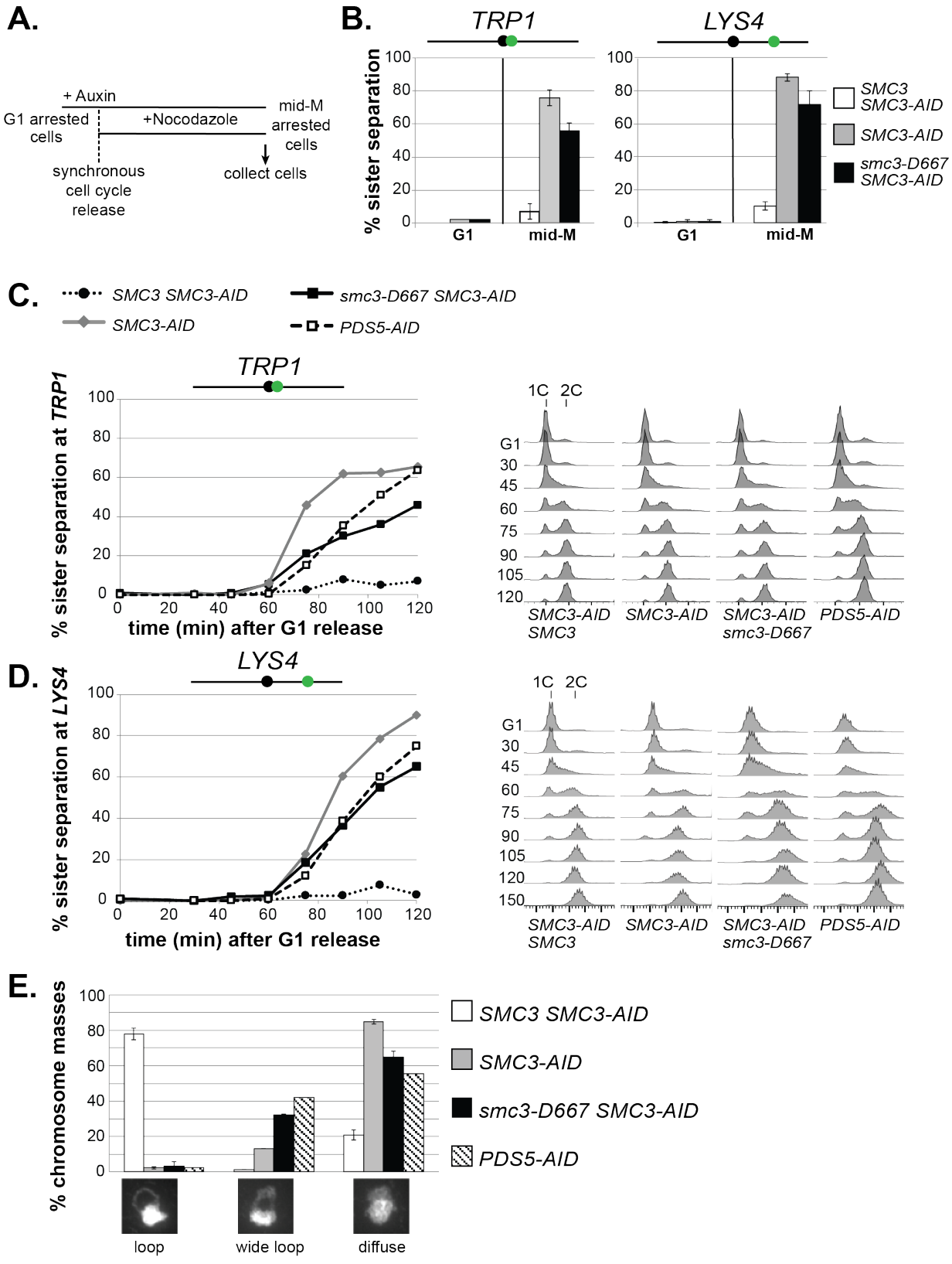
A.
+ Auxin
G1 arrested cells
+Nocodazole
mid-M arrested cells
synchronous cell cycle release
collect cells
B.
TRP1
LYS4
% sister separation
G1
mid-M
SMC3 SMC3-AID
SMC3-AID
smc3-D667 SMC3-AID
C.
SMC3 SMC3-AID
smc3-D667 SMC3-AID
SMC3-AID
PDS5-AID
% sister separation at TRP1
time (min) after G1 release
1C 2C
SMC3-AID SMC3
SMC3-AID
SMC3-AID smc3-D667
PDS5-AID
D.
% sister separation at LYS4
time (min) after G1 release
E.
% chromosome masses
loop
wide loop
diffuse

Figure 3

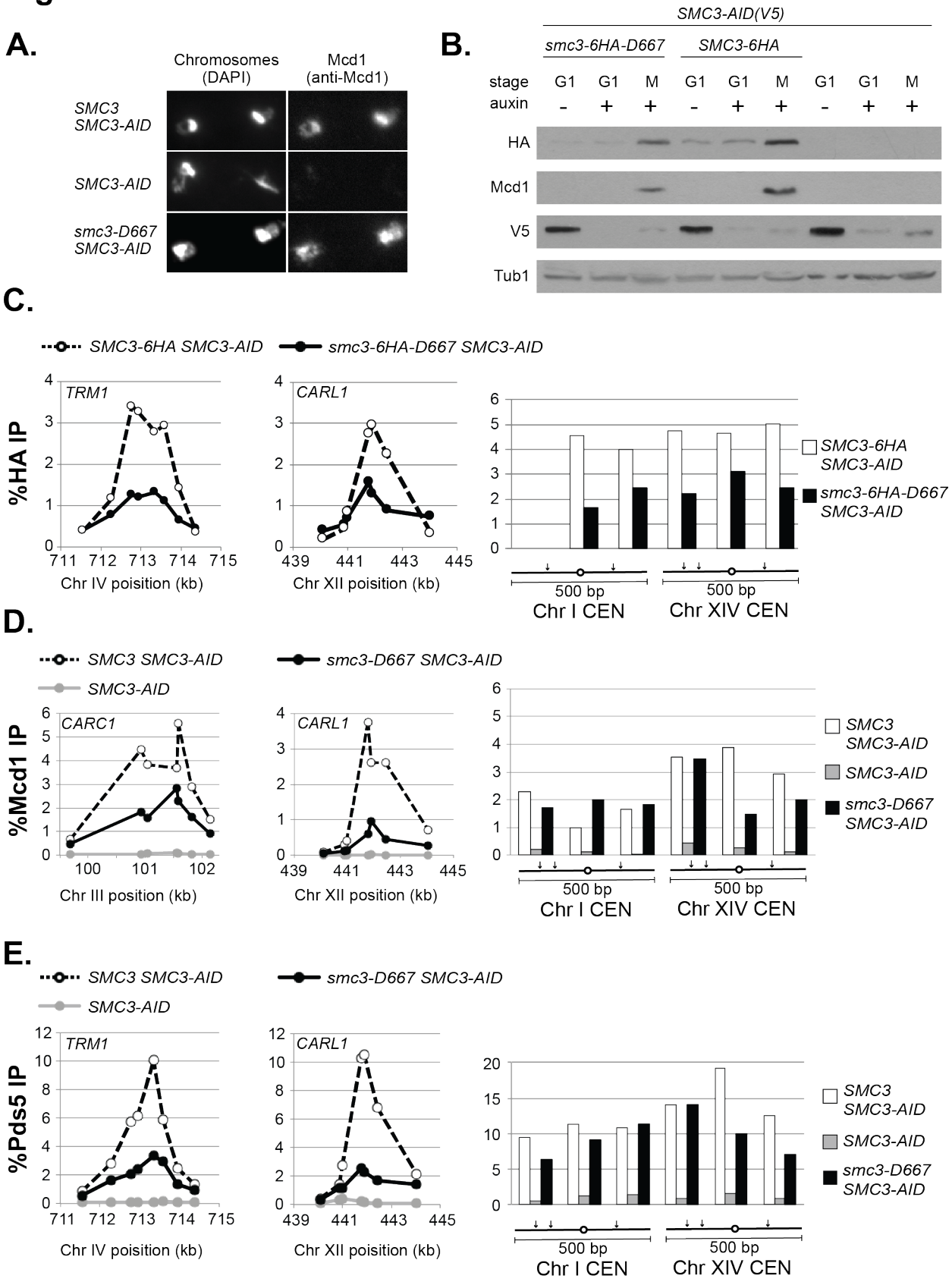
A.
Chromosomes (DAPI)
Mcd1 (anti-Mcd1)
SMC3 SMC3-AID
SMC3-AID
smc3-D667 SMC3-AID
B.
SMC3-AID(V5)
smc3-6HA-D667
SMC3-6HA
stage G1 G1 M G1 G1 M G1 G1 M
auxin - + + - + + - + +
HA
Mcd1
V5
Tub1
C.
SMC3-6HA SMC3-AID
smc3-6HA-D667 SMC3-AID
%HA IP
TRM1
Chr IV position (kb)
CARL1
Chr XII position (kb)
SMC3-6HA SMC3-AID
smc3-6HA-D667 SMC3-AID
500 bp
Chr I CEN
500 bp
Chr XIV CEN
D.
SMC3 SMC3-AID
smc3-D667 SMC3-AID
SMC3-AID
%Mcd1 IP
CARC1
Chr III position (kb)
CARL1
Chr XII position (kb)
SMC3 SMC3-AID
SMC3-AID
smc3-D667 SMC3-AID
500 bp
Chr I CEN
500 bp
Chr XIV CEN
E.
SMC3 SMC3-AID
smc3-D667 SMC3-AID
SMC3-AID
%Pds5 IP
TRM1
Chr IV position (kb)
CARL1
Chr XII position (kb)
SMC3 SMC3-AID
SMC3-AID
smc3-D667 SMC3-AID
500 bp
Chr I CEN
500 bp
Chr XIV CEN

Figure 4

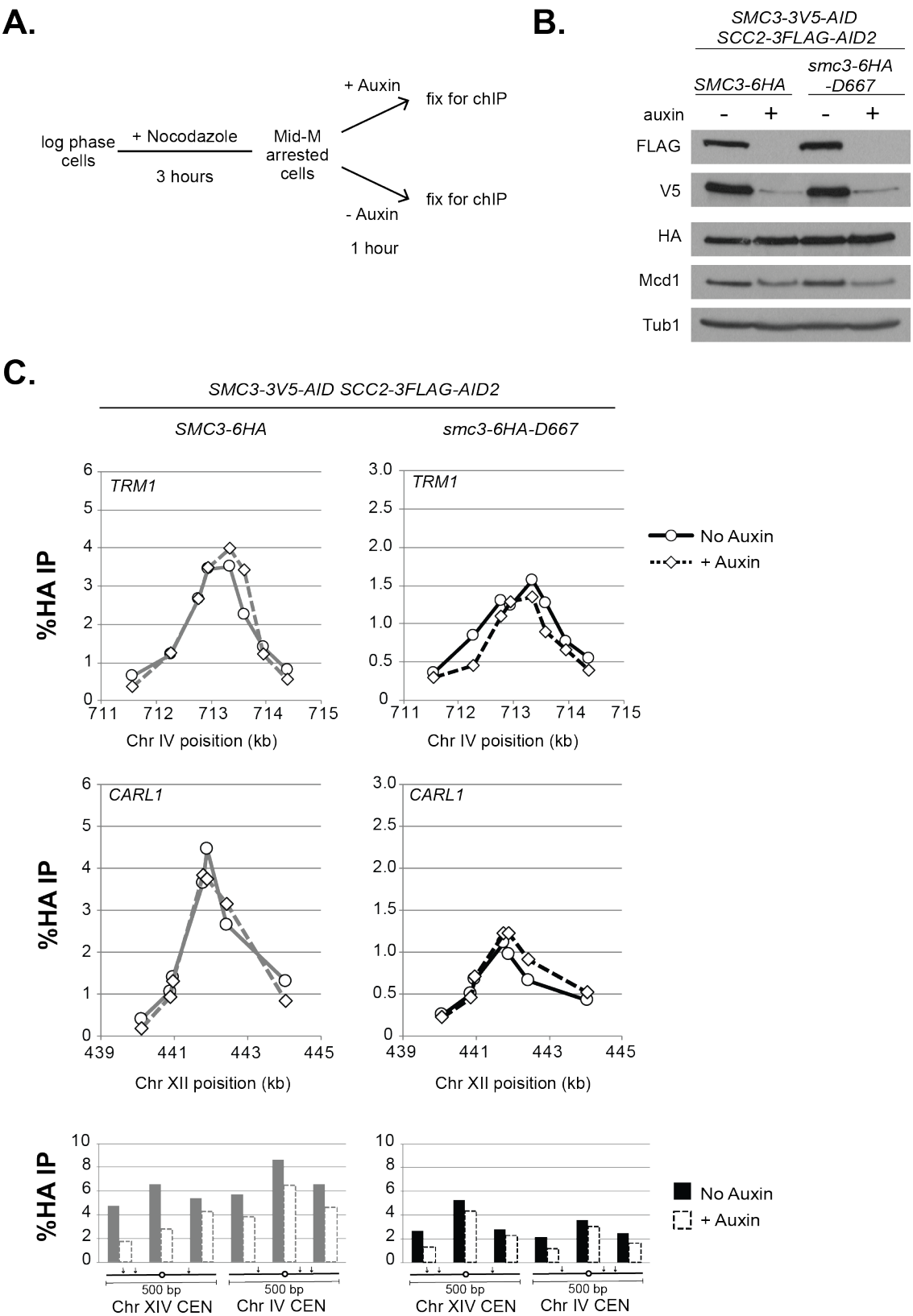
A.
log phase cells
+ Nocodazole
3 hours
Mid-M arrested cells
+ Auxin
fix for chIP
- Auxin
1 hour
fix for chIP
B.
SMC3-3V5-AID
SCC2-3FLAG-AID2
SMC3-6HA
smc3-6HA -D667
auxin - + - +
FLAG
V5
HA
Mcd1
Tub1
C.
SMC3-3V5-AID SCC2-3FLAG-AID2
SMC3-6HA
smc3-6HA-D667
TRM1
%HA IP
Chr IV poisition (kb)
No Auxin
+ Auxin
CARL1
Chr XII poisition (kb)
500 bp
Chr XIV CEN
Chr IV CEN

Figure 5

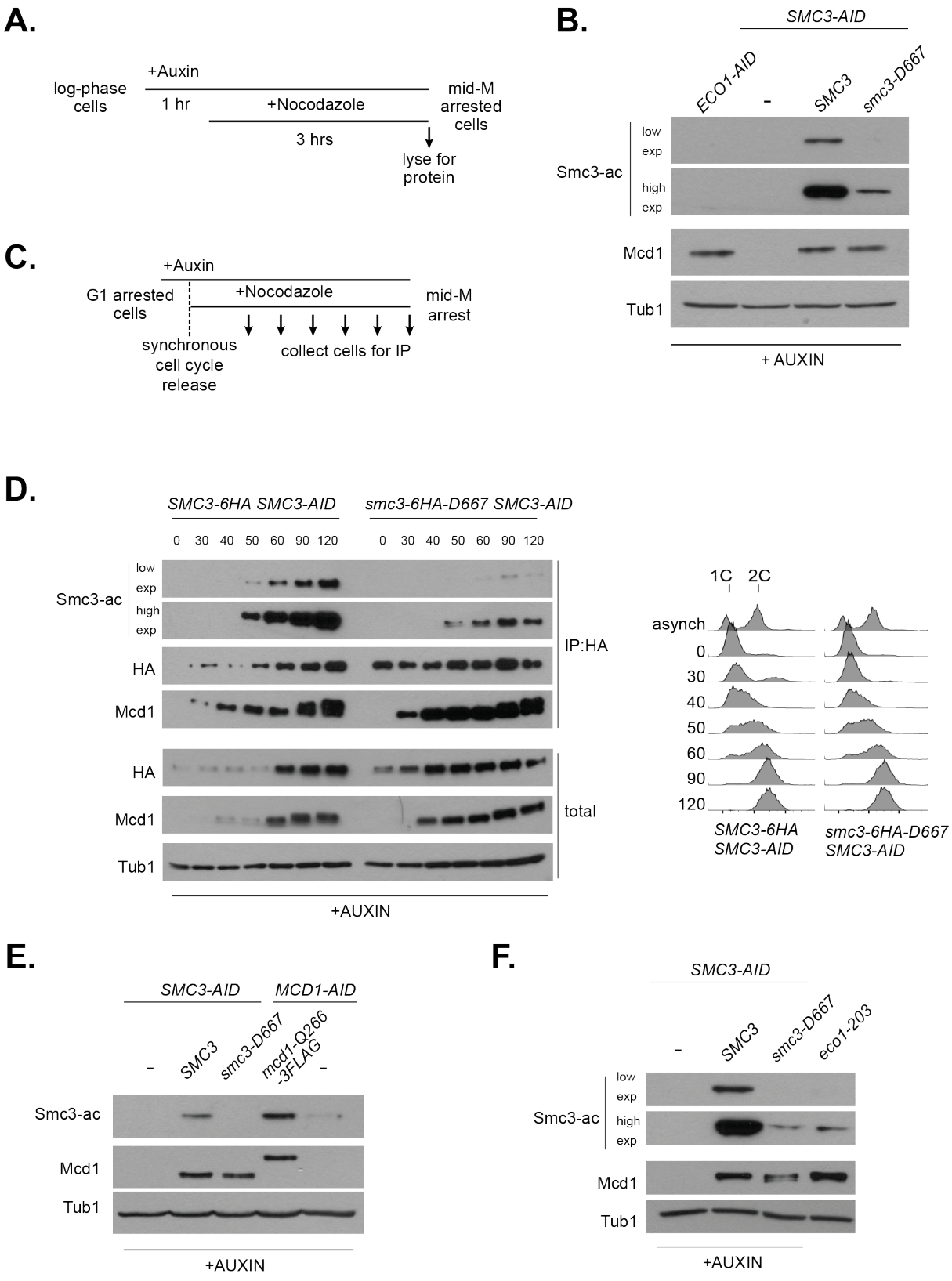
A.
log-phase cells
+Auxin
1 hr
+Nocodazole
3 hrs
mid-M arrested cells
lyse for protein
B.
SMC3-AID
ECO1-AID
-
SMC3
smc3-D667
Smc3-ac
low exp
high exp
Mcd1
Tub1
+ AUXIN
C.
+Auxin
G1 arrested cells
+Nocodazole
mid-M arrest
synchronous cell cycle release
collect cells for IP
D.
SMC3-6HA SMC3-AID
smc3-6HA-D667 SMC3-AID
0 30 40 50 60 90 120
0 30 40 50 60 90 120
Smc3-ac
low exp
high exp
HA
Mcd1
IP:HA
HA
Mcd1
Tub1
total
+AUXIN
1C 2C
asynch
0
30
40
50
60
90
120
SMC3-6HA SMC3-AID
smc3-6HA-D667 SMC3-AID
E.
SMC3-AID
MCD1-AID
-
SMC3
smc3-D667
mcd1-Q266 -3FLAG
-
Smc3-ac
Mcd1
Tub1
+AUXIN
F.
SMC3-AID
-
SMC3
smc3-D667
eco1-203
Smc3-ac
low exp
high exp
Mcd1
Tub1
+AUXIN

Figure 6

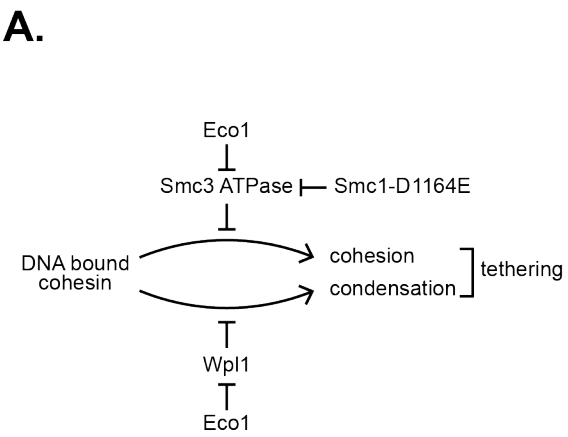
A.
Eco1
Smc3 ATPase
Smc1-D1164E
DNA bound cohesin
cohesion
condensation
tethering
Wpl1
Eco1

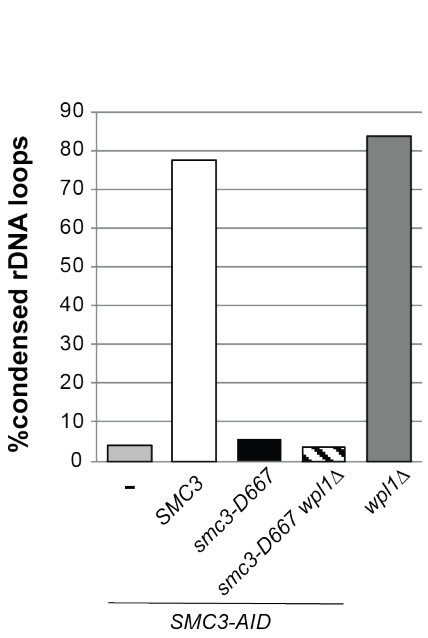
B.
%condensed rDNA loops
90
80
70
60
50
40
30
20
10
0
-
SMC3
smc3-D667
smc3-D667 wpl1Δ
wpl1Δ
SMC3-AID

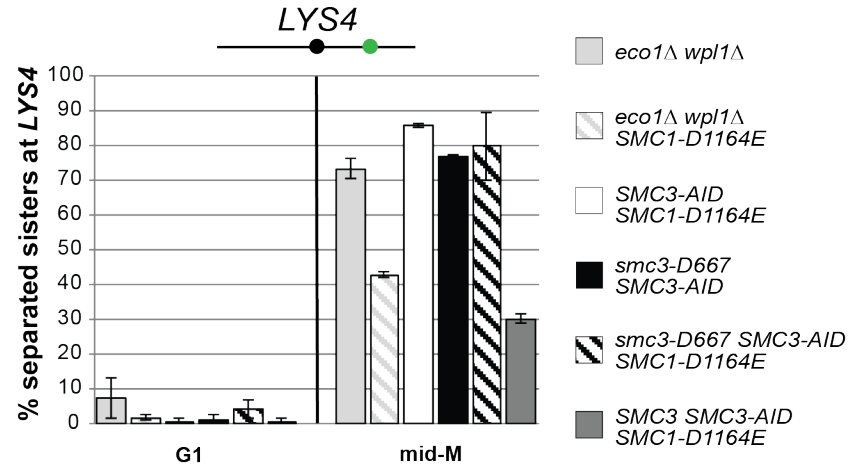
C.
LYS4
% separated sisters at LYS4
100
90
80
70
60
50
40
30
20
10
0
G1
mid-M
eco1Δ wpl1Δ
eco1Δ wpl1Δ SMC1-D1164E
SMC3-AID SMC1-D1164E
smc3-D667 SMC3-AID
smc3-D667 SMC3-AID SMC1-D1164E
SMC3 SMC3-AID SMC1-D1164E

Figure 7

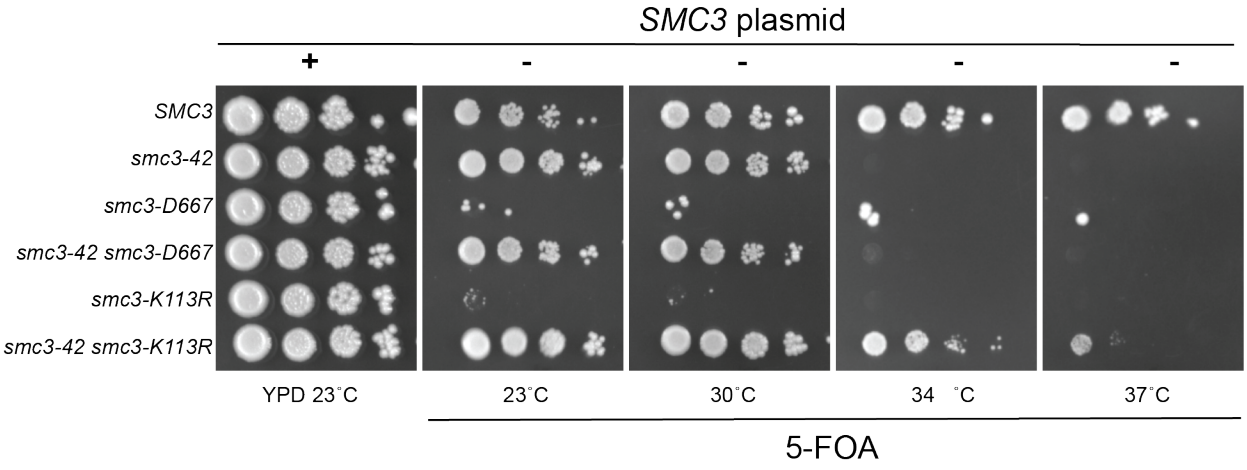
SMC3 plasmid
+
-
-
-
-
SMC3
smc3-42
smc3-D667
smc3-42 smc3-D667
smc3-K113R
smc3-42 smc3-K113R
YPD 23˚C
23˚C
30˚C
34 ˚C
37˚C
5-FOA

Supplementary Figure 1

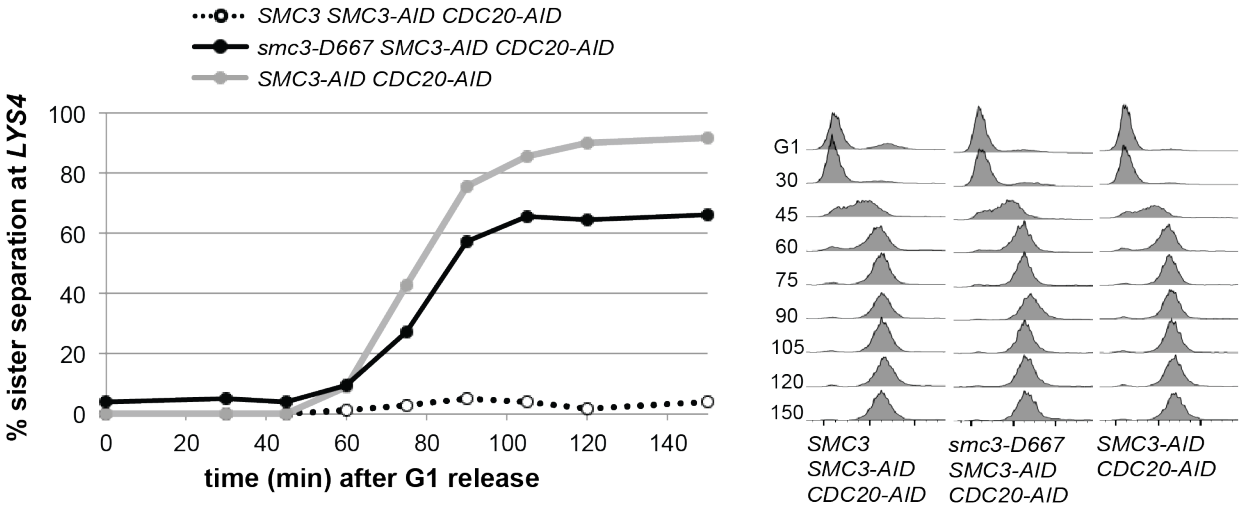

Supplementary Figure 2

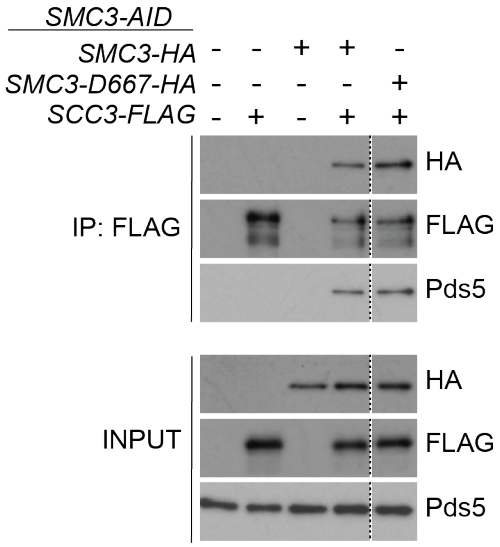

Supplementary Figure 3

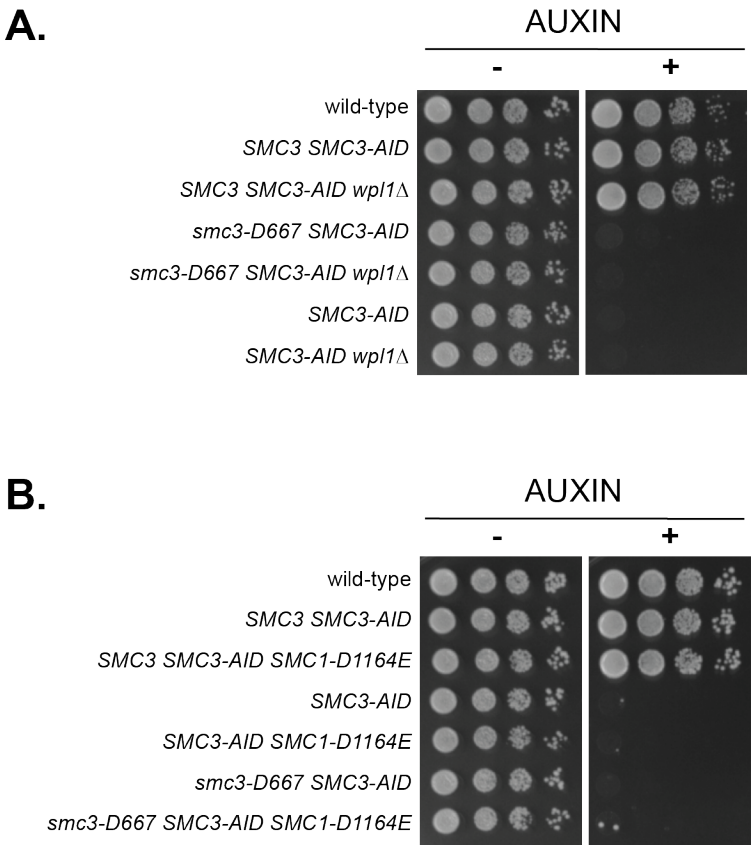

Chapter Four: A role for the Smc3p coiled coil in cohesin binding chromosomes

Introduction

The critical roles of cohesin in shaping and segregating chromosomes have been explained in terms of its curious architecture. Cohesin binding to DNA involves a topological entrapment (Haering et al. 2008; Stigler et al. 2016). Following binding, tethering between sister chromatids results from either co-entrapment within a single cohesin or through cohesin-cohesin interactions (Haering et al. 2002; Eng et al. 2014; Eng et al. 2015). The topological mode of cohesin binding to DNA has led many studies to focus on the interfaces of this complex (Haering et al. 2004; Kurze et al. 2011; Gligoris et al. 2014). However, the ~45 nm long coiled coils of cohesin subunits Smc1p and Smc3p have been largely overlooked as having important structural features necessary for cohesin function. Proteolytic cleavage of the coiled coil revealed that its integrity is necessary to maintain topological binding of cohesin to DNA (Gruber et al. 2003). As a result, coiled coils have been ascribed a simple function- to prevent escape of entrapped DNA molecules. I investigated my panel of Smc3p RID mutants to see if any challenged this simplistic model of coiled coil function.

Results

Identification of a specific region of Smc3p's coiled coil essential for cohesin function

In my screen for RID mutants of *SMC3*, I anticipated many would be found that disrupt interfaces with other cohesin subunits and the ATPase motifs. I was therefore surprised that thirty-seven out of a total of sixty-two RIDs mapped to the coiled coil of Smc3p, which I define as spanning from G171 to T510 and R677 to V1060. 19 of 37 coiled coil RIDs map to the region of Smc3p bound to Mcd1p (Gligoris et al. 2014). This class is discussed in Chapter 2 of this dissertation. Of the remaining eighteen coiled-coil RIDs, seven map to a conserved region immediately adjacent to the Mcd1p binding region (Figure 2A of Gligoris et al. 2014). Six of these seven RID alleles were cloned into plasmids under the native *SMC3* promoter and transformed into an *smc3*Δ supported by a *SMC3 URA3 CEN* plasmid. Serial dilutions of transformants were plated on 5-FOA to select for cells that had lost the *SMC3 URA3 CEN* plasmid to assess the ability of RID alleles to support viability. Five of these six *SMC3* RID alleles (encoding insertions following E211, E216, L217, Q231 and T233) failed to support growth on 5-FOA, while the RID at T986 supported viability. While I have not investigated these mutants further, I note that human Pds5Bp can be crosslinked to this section of the hSmc3p coiled coil. I speculate that this stretch of the Smc3p coiled coil may be involved in an essential function involving Pds5p. The remaining eleven RIDs mapped to a large central region of the Smc3p coiled coil.

Ten of these remaining eleven RID alleles were cloned into plasmids, which were transformed into the *smc3*Δ (*SMC3 URA3 CEN*) strain to assess viability when expressed from the native *SMC3* promoter. I omitted one allele encoding an insertion of SAAAQ following Smc3-Q347 from analysis, instead focusing on an allele encoding

MRPQQ at the same position. Transformants expressing RID alleles that encode insertions following Smc3-Y254, L287, N783, T809, K818, and S823 supported growth on 5-FOA, while RID insertions following Smc3-S343, I345, Q347, and V888 failed to support growth on 5-FOA (Figure 1A, bottom, and Chapter 2 of this dissertation). I chose not to further characterize RIDs within the coiled coil that support viability. However, these results revealed that five amino acid insertions at multiple regions spanning the Smc3p coiled coil do not disrupt the essential functions of cohesin. Instead, I focused my attention on the four RID alleles that were unable to support viability.

To assess the functions of these 4 RID alleles, I introduced them into a *SMC3-AID* strain. Serial dilutions of transformants were plated onto YPD containing auxin, and growth assessed after two days at 23˚C. Robust growth was observed in cells with Smc3p (*SMC3 SMC3-AID*) but not in cells without it (*SMC3-AID*). Cells expressing smc3-S343p (*smc3-S343 SMC3-AID*), smc3-I345p (*smc3-I345 SMC3-AID*), smc3-Q347p (*smc3-Q347 SMC3-AID*), and smc3-V888p (*smc3-V888 SMC3-AID*) were unable to grow in the presence of auxin (Figure 1A and data not shown). This inviability confirmed that these RID alleles encoded Smc3p proteins defective in an essential function. They also were recessive indicating that the defects of these RID mutants resulted from a loss of function.

Three of these RIDs map to amino acids that are remarkably close together on the N-terminal portion of the Smc3p coiled coil (S343, I345, Q347) while the fourth is located on the anti-parallel C-terminal coiled coil. I estimated the location of these RID insertions relative to the junction of the coiled coil with the Smc3p half-hinge. I define the N terminal coiled coil as spanning from G171 to T510 and the C terminal coiled coil as spanning from R677 to V1060. S343 is located 167 amino acids away from T510 and V888 is located 211 amino acids away from R677. From this, I estimate that S343 is somewhat closer to the hinge than V888. Since S343 is 167 amino acids away from the hinge end of the coiled coil and 172 amino acids away from the head, it lies roughly in the middle of the N-terminal coiled coil of Smc3p. The approximate locations of these RID insertions are illustrated on cohesin in Figure 1B.

The region of Smc3p's coiled coil with S343, I345, and Q347 is poorly conserved except for an invariant leucine and proline nearby (Figure 1C), whereas the V888 region is even more poorly conserved (Figure 1D). To further define the region of Smc3p's coiled coil that is susceptible to insertions, I created a panel of Smc3p mutants with insertions of IAAAS residues upstream and downstream of S343, I345, and Q347 (Figure 1C). I chose to insert these five residues because they match the RID at S343 and could therefore conceivably produce inviable mutants when inserted at other regions of the coiled coil. Plasmids were transformed into *SMC3-AID* and transformants were assayed for viability on YPD plates containing auxin. Cells with Smc3p (*SMC3 SMC3*-AID) grew well while those lacking Smc3p failed to grow (*SMC3-AID*). Smc3p mutants with IAAAS resides inserted following E328, L333, L338, L352, P357, and L362 all supported growth on auxin (Figure 1E). Therefore, the region defined by inviable insertions at S343, I345, and Q347 is very specific. Together, I will refer to the region at the middle of Smc3p's coiled coil defined by these RIDs as the S343-V888 region.

The S343-V888 region of Smc3p promotes cohesion establishment

I sought to determine which essential functions of Smc3p are impaired by RIDs in its coiled coil. First, I assessed whether smc3-I345p and smc3-V888p mutants could establish and maintain cohesion at the CEN-distal *LYS4* locus. Mutants that compromise cohesion establishment, like those defective in core subunits of cohesin *MCD1*, *SMC3,* and *SMC1* show sister chromatid separation immediately after replication (Eng et al. 2014). Mutants that compromise cohesion maintenance like those defective in the cohesin regulator *PDS5* (Eng et al. 2014) and *smc3-D667* (Chapter 3) also lose cohesion but at significantly later times after the establishment mutants. Strains were grown to early log phase at 30˚C and arrested in G1 with alpha factor. Auxin was added to the cultures in order to deplete Smc3-AIDp or Pds5-AIDp for one hour, at which point cells were washed and resuspended in YPD containing nocodazole and auxin to release them from G1 and allow them to progress to mid-M.

As expected, cells with wild type Smc3p (*SMC3 SMC3-AID*) established cohesion in S phase and maintained cohesion until mid-M (Figure 2A). Cells lacking Smc3p (*SMC3-AID*) showed a rapid separation of sister chromatids, while those lacking Pds5p (*PDS5-AID*) exhibited a ~15-minute delay in the appearance of separated sister chromatids, as published previously. Cells expressing smc3-I345p (*smc3-I345 SMC3-AID*) lost cohesion quickly, with similar kinetics to cells lacking any Smc3p. Therefore, smc3-I345p displays a cohesion establishment defect. Next, I performed an identical experiment with cells expressing smc3-V888p (*smc3-V888 SMC3*-AID). Like smc3-I345p, smc3-V888p cells exhibited early cohesion loss consistent with a defect in establishment (Figure 2B). Therefore, two mutants in the S343-V888 region exhibit cohesion establishment defects. This implicates the Smc3p coiled coil in an early stage of cohesin function.

Cells can live without strong cohesion as long as cohesin's function in chromosome condensation remains intact (Guacci and Koshland 2012). The lethality of the RID mutations in the coiled coil suggested that they were compromised for condensation. To test this possibility, chromosome spreads were prepared from three of the coiled-coil mutant strains. These mutants were arrested in G1, treated with auxin to remove Smc3-AIDp, released from G1 arrest into nocodazole to allow cells to progress to mid-M. Chromosome spreads of the arrested cells were prepared and rDNA condensation was assessed. As expected, rDNA morphology of almost all cells with wild type Smc3p (*SMC3 SMC3-AID*) displayed the tight rDNA loop morphology of condensed chromosomes (Figure 2C). Almost all cells depleted of Smc3p (*SMC3-AID*) displayed diffuse rDNA, which indicated a severe condensation defect. The rDNA morphology observed in *smc3-S343 SMC3-AID*, *smc3-I345 SMC3-AID*, and *smc3-Q347 SMC3-AID* cells all resembled cells depleted for Smc3p; thus they had a profound defect in condensation. Therefore, these RIDs define a region of the coiled coil critical for cohesin's two key functions in mitotic chromosome structure.

The S343-V888 region of Smc3p is required for a step other than cohesin assembly

A simple explanation for this region of the coiled coil was that it was necessary for proper assembly of cohesin or association with cohesin accessory factors. Therefore, I assessed whether smc3-I345p associates with the cohesin subunit Mcd1p

(as a reporter for cohesin assembly) and Pds5p (Figure 3A, 3C). As expected, Mcd1p was present in the immunoprecipitates of cells expressing Smc3-6HAp but absent in immunoprecipitate from cells lacking HA-tagged Smc3p (Figure 3B). Similarly Pds5p was present in the immunoprecipitates of Scc3-3FLAGp but absent in cells depleted for Smc3p (Figure 3D). These results demonstrated that Mcd1p associated with Smc3p and that Scc3-3FLAG associated with Pds5p only when Smc3p was present. When these same two assays were applied to cells expressing smc3-I345p, similar levels of Mcd1p and Pds5p were present in the immunoprecipitates (Figure 3B, 3D). These results suggested that the coiled-coil mutants were competent to assemble cohesin and bind the Pds5p auxiliary factor. Therefore, the S343-V888 region is required for cohesin function at a step other than cohesin assembly or Pds5p recruitment.

The S343-V888 region is required for cohesin binding to chromosomes in M phase

Cohesin is known to bind at centromeres, pericentromeres and CARs along chromosome arms, in a process requiring the cohesin loader complex Scc2p-Scc4p (Ciosk et al. 2000; Laloryaya et al. 2000). I tested the ability of smc3-I345p to support cohesin binding and localization at these distinct chromosomal sites in cells arrested in mid-M phase by ChIP-qPCR (Figure 4A). Wild-type Smc3p (*SMC3 SMC3-AID*) supported robust Mcd1p ChIP at all four chromosomal loci, while little binding was seen in cells lacking Smc3p (*SMC3-AID*). Importantly, little if any enrichment of Mcd1p binding to CARs or centromeres was evident in ChIP from *smc3-I345 SMC3-AID* cells. Therefore, smc3-I345p had a major defect in the ability to support Mcd1p binding to chromosomes. The S343-V888 region is therefore required for loading or stable association of cohesin with chromosomes.

The failure of smc3-I345p to support Mcd1p ChIP to chromosomes suggests that insertions in the S343-V888 region may disrupt the mechanism by which cohesin is loaded. In fact, the *S. pombe* cohesin loader binds to the middle of the Psm3p (Smc3p) coiled coil (Murayama and Uhlmann 2014). Therefore, I sought to determine whether the failure of smc3-I345p to support Mcd1p loading could be explained by a defect in smc3-I345p interaction with Scc2p, a subunit of the loader complex. I assessed whether cohesin with smc3-I345-6HAp interacted with Scc2-3FLAGp. I chose to arrest cells in S phase because Scc2p is engaged in cohesin loading during replication (Figure 3A). Mcd1p and Scc2-3FLAGp were present in the precipitate of Smc3-6HAp or smc3-I345-6HAp (Figure 3B). No FLAG signal was detected in a control strain lacking HA-tagged Smc3p. These results suggest that the S343-V888 region of Smc3p's coiled coil is required for cohesin association with chromosomes at a step after binding of Scc2p to cohesin.

Discussion

In the course of examining RID alleles of *SMC3*, I have made several observations that provide a new understanding of the Smc3p coiled coil. The primary sequence requirements for coiled coils are well known. A pattern repeated every seven residues referred to as a heptad repeat generates amphipathic alpha helices. Two such

helices can associate through hydrophobic interactions with one another to form a coiled coil. The pairing of helices through hydrophobic interactions creates a proper register between them in the final folded protein. Insertion mutations that disrupt register can abolish the function of coiled coil domains (Pu et al. 1991, Burmann et al. 2017). I identified a class of viable RID alleles distributed throughout the Smc3p coiled coil. This revealed that the Smc3p coiled coil is tolerant to mutations expected to disrupt register.

It has been proposed that the coiled coil arms of BsSMC, condensin and cohesin may transmit information from the hinge to head domains or vice versa (Hirano and Hirano 2006; Minnen et al. 2016; Soh et al. 2015). In support of this model, insertions along the length of the BsSMC coiled coil abolish BsSMC function (Burmann et al. 2017). The authors of this study proposed that information transmission required intact register along the BsSMC coiled coil. My data demonstrated that intact register along the Smc3p coiled coil is not essential for cohesin function. Therefore, if information is transmitted along cohesin's coiled coils, it does so through a mechanism unlike BsSMC.

Although many Smc3p coiled-coil insertions were viable, I was intrigued by the small region susceptible to loss of function by RID insertions centered around Smc3-I345. Smc3-I345 lies approximately in the middle of the Smc3p N-terminal coiled coil. What accounts of the significance of this particular region of the coiled coil? Smc1p/Smc3p dimers have been observed under electron microscopy to assume V or Y shapes when connected at their hinge domains (Haering et al. 2002). The Y shape shows the arms separating half way along the coiled coils, and this position is found kinked in multiple EM images. Significantly, Smc3-I345 is only twelve amino acids away from the only proline present in the N-terminal half of Smc3p's coiled coil since prolines are expected to disrupt coiled coils. Is there any evidence to suggest that a kink in Smc3p near Smc3-I345 could impair a structural requirement of cohesin? Recently, Smc1p/Smc3p coiled coils have been observed to form collapsed "rods" by scanning force microscopy, and this conformation is also suggested by extensive crosslinking between human Smc1p/Smc3p coiled coils (Kulemzina et al. 2016; Huis in t Veld et al. 2014). Mutations that reduce coiled-coil juxtaposition abolish cohesin loading on chromosomes and do not support viability in yeast. It is possible that mid-coiled coil RIDs may also disrupt formation of the cohesin "rod" conformation. However, my observation that smc3-I345p is capable of interacting with Scc2p suggests that, if indeed it cannot form a "rod," it can nevertheless form a loading complex. I consider it more likely that a subsequent step in the loading of cohesin, after interaction with the loader, is impaired in *smc3-I345* cells. Although the mechanism of cohesin loading on DNA is not well understood, it has been proposed to proceed through an intermediate involving the association of the hinge domain with the Smc heads (Murayama and Uhlmann 2015). To achieve this conformation, the coiled coils would have to bend back on themselves. It is possible that the Smc3-I345 region may accommodate this contortion in the process of loading cohesin on chromosomes. My results indicate that mutants in the S343-V888 region could be valuable tools to investigate the role of the cohesin coiled coils in the mechanism of cohesin loading on DNA.

Materials and Methods

Yeast strains, media, and growth

All strains used are in the A364A background and their genotypes can be found in the Strain List. Yeast extract/peptone/dextrose media and synthetic dropout media was prepared as previously described (Guacci et al. 1997). Conditional AID degron strains were grown in YPD and 3-indoleacetic acid (IAA, Sigma Aldrich Cat I3750) dissolved in DMSO added to cultures to a final concentration of 750 μM. YPD + auxin plates were made by cooling molten YPD 2% agar to 55˚C prior to addition of auxin to a final concentration of 750 μM.

Cohesion assays

Sister chromatid cohesion was assessed at either the centromere-distal *LYS4* locus or centromere-proximal *TRP1* locus on Chr IV in which *LacO* arrays have been integrated. An allele expressing the *GFP-LacI* fusion integrated at *HIS3* allows fluorescence microscopic visualization of *LacO* arrays. Cohesion was scored by growing cells to mid-log phase (OD600 ~0.3) and arresting them in G1 using alpha factor at 10^{-8} M (Sigma Aldrich). After arresting for 3 hours, auxin was added to a final concentration of 750 μM to deplete Smc3-AID for one hour. Cells were released from G1 arrest by washing in YPD containing auxin and 0.1 mg/mL Pronase E (Sigma Aldrich) five times and resuspending in YPD containing auxin and 15 μg/mL nocodozole (Sigma Aldrich). Cultures were incubated at 23˚C and samples fixed either 1) periodically for assessing S-phase cohesion establishment or 2) after >95% of cells had arrested in G2/M after three hours. In addition to fixation for microscopy, samples were taken in parallel to assess DNA content by flow cytometry. Cohesion was scored by counting the number of GFP-LacI foci in the nucleus by fluorescence microscopy of fixed cells.

rDNA locus morphology

Cells were grown as if for assessing cohesion by arresting in YPD containing auxin and nocodazole following release from G1. Cells were processed and chromosomes bound to slides as described previously (Guacci et al. 1994). Briefly, 1 mL of cells were fixed two hours in 100 uL of 37% formaldehyde, washed twice in water, and spheroplasted for one hour. Triton X-100 was added to 0.5% for 5 minutes, cells spun and resuspended in water before 10 uL dropped onto slides for ten minutes. 0.5% SDS was added to cells on slides for 10 minutes, removed, then slides fixed in 3:1 methanol:acetic acid for five minutes and allowed to dry. Cells on slides were treated with RNase A and Proteinase K and dried through a series of 70%, 80%, 90%, and 100% ethanol washes. After drying, chromosomes were visualized with DAPI and rDNA morphology scored.

Chromatin immunoprecipitation (ChIP)

Cells were grown as if for assessing cohesion by arresting in YPD containing auxin and nocodazole following release from G1. ChIP was performed as described previously (Eng et al. 2014; Wahba et al. 2013) except that chromatin shearing was performed on a Bioruptor Pico machine (Diagenode, Denville, NJ) for 5 minutes (30 sec on/off cycling). Immunoprecipitation was performed using monoclonal Mouse anti-HA (Roche), monoclonal Mouse anti-V5 (ThermoFisher), polyclonal Rabbit anti-Pds5p (Covance Biosciences, Princeton, NJ), or polyclonal Rabbit anti-Mcd1p (Covance) antibodies. A no antibody control was always included to assess specificity of chromatin recovery.

Chromosome spreads and microscopy

Cells were grown as if for assessing cohesion by arresting in YPD containing auxin and nocodazole following release from G1. Chromosome spreads were prepared as previously described (Wahba et al. 2013). Slides were incubated with 1:5,000 rabbit polyclonal anti-Mcd1p and 1:5,000 mouse anti-V5 antibody (Life Technologies). Antibodies were diluted in spreads blocking buffer (5% BSA, 0.2% milk, 1X PBS, 0.2% Triton X-100). Secondary Alexa Fluor 488-congugated chicken anti-mouse and Alexa Fluor 568-congugated donkey anti-rabbit (ThermoFisher Cats. A21200 and A10042) antibodies were diluted 1:5,000 in blocking buffer. Indirect immunofluorescence was detected on an Axioplan2 microscope (Zeiss, Thornwood, NY) using the 100X objective (numerical aperture 1.40) which is equipped with a Quantix charge-coupled camera (Photometrics).

Strain List

BRY424	*MAT**a** SMC3-LEU2:leu2-3,112 smc3Δ::HPH lys4::LacO(DK)-NAT bar1 pHIS3-GFPLacI-TRP1:his3-11,15 trp1-1 leu2-3,112 ura3-52* +pEU42 (*SMC3 CEN URA3*)	this study
BRY469	*MAT**a** smc3-V888-LEU2:leu2-3,112 smc3Δ::HPH lys4::LacO(DK)-NAT bar1 pHIS3-GFPLacI-TRP1:his3-11,15 trp1-1 leu2-3,112 ura3-52* +pEU42 (*SMC3 CEN URA3*)	this study
BRY474	*MAT**a** SMC3-LEU2:leu2-3,112 SMC3-3V5-AID^{608} trp1Δ::OsTIR1-CaTRP1 lys4::LacO(DK)-NAT pHIS3-GFPLacI-HIS3:his3-11,15 ura3-52 bar1*	this study
BRY562	*MAT**a** smc3-I345-LEU2:leu2-3,112 SMC3-3V5-AID^{608} trp1Δ::OsTIR1-CaTRP1 lys4::LacO(DK)-NAT pHIS3-GFPLacI-HIS3:his3-11,15 ura3-52 bar1*	this study
BRY584	*MAT**a** smc3-S343-LEU2:leu2-3,112 SMC3-3V5-AID^{608} trp1Δ::OsTIR1-CaTRP1 lys4::LacO(DK)-NAT pHIS3-GFPLacI-HIS3:his3-11,15 ura3-52 bar1*	this study
BRY590	*MAT**a** smc3-Q347-LEU2:leu2-3,112 SMC3-3V5-AID^{608} trp1Δ::OsTIR1-CaTRP1 lys4::LacO(DK)-NAT pHIS3-GFPLacI-HIS3:his3-11,15 ura3-52 bar1*	this study
BRY604	*MAT**a** SMC3-6HA^{608}-URA3:ura3-52 SMC3-3V5-AID^{608} trp1Δ::OsTIR1-CaTRP1 lys4::LacO(DK)-NAT leu2-3,112 pHIS3-GFPLacI-HIS3:his3-11,15 bar1*	this study
BRY607	*MAT**a** SCC3-3FLAG^{1089}-LEU2:leu2-3,112 SMC3-3V5-AID^{608} trp1Δ::OsTIR1-CaTRP1 lys4::LacO(DK)-NAT pHIS3-GFPLacI-HIS3:his3-11,15 leu2-3,112 ura3-52 bar1*	this study
BRY613	*MAT**a** SCC2-3FLAG-KANMX SMC3-6HA^{608}-URA3:ura3-52 SMC3-3V5-AID^{608} trp1Δ::OsTIR1-CaTRP1 lys4::LacO(DK)-NAT leu2-3,112 pHIS3-GFPLacI-HIS3:his3-11,15 bar1*	this study

BRY614	*MAT**a** smc3-I345-6HA^{608}-URA3:ura3-52 SCC2-3FLAG-KANMX SMC3-3V5-AID^{608} trp1∆::OsTIR1-CaTRP1 lys4::LacO(DK)-NAT leu2-3,112 pHIS3-GFPLacI-HIS3:his3-11,15 bar1*	this study
BRY621	*MAT**a** SMC3-6HA^{608}-URA3:ura3-52 SCC3-3FLAG^{1089}-LEU2:leu2-3,112 SMC3-3V5-AID^{608} trp1∆::OsTIR1-CaTRP1 lys4::LacO(DK)-NAT pHIS3-GFPLacI-HIS3:his3-11,15 bar1*	this study
BRY623	*MAT**a** smc3-I345-6HA^{608}-URA3:ura3-52 SCC3-3FLAG^{1089}-LEU2:leu2-3,112 SMC3-3V5-AID^{608} trp1∆::OsTIR1-CaTRP1 lys4::LacO(DK)-NAT pHIS3-GFPLacI-HIS3:his3-11,15 bar1*	this study
BRY657	*MAT**a** SCC2-3FLAG-KANMX SMC3-3V5-AID^{608} trp1∆::OsTIR1-CaTRP1 lys4::LacO(DK)-NAT leu2-3,112 pHIS3-GFPLacI-HIS3:his3-11,15 ura3-52 bar1*	this study
BRY664	*MAT**a** smc3-L338-LEU2:leu2-3,112 SMC3-3V5-AID^{608} trp1∆::OsTIR1-CaTRP1 lys4::LacO(DK)-NAT pHIS3-GFPLacI-HIS3:his3-11,15 ura3-52 bar1*	this study
BRY666	*MAT**a** smc3-L333-LEU2:leu2-3,112 SMC3-3V5-AID^{608} trp1∆::OsTIR1-CaTRP1 lys4::LacO(DK)-NAT pHIS3-GFPLacI-HIS3:his3-11,15 ura3-52 bar1*	this study
BRY668	*MAT**a** smc3-E328-LEU2:leu2-3,112 SMC3-3V5-AID^{608} trp1∆::OsTIR1-CaTRP1 lys4::LacO(DK)-NAT pHIS3-GFPLacI-HIS3:his3-11,15 ura3-52 bar1*	this study
BRY670	*MAT**a** smc3-L352-LEU2:leu2-3,112 SMC3-3V5-AID^{608} trp1∆::OsTIR1-CaTRP1 lys4::LacO(DK)-NAT pHIS3-GFPLacI-HIS3:his3-11,15 ura3-52 bar1*	this study
BRY672	*MAT**a** smc3-P357-LEU2:leu2-3,112 SMC3-3V5-AID^{608} trp1∆::OsTIR1-CaTRP1 lys4::LacO(DK)-NAT pHIS3-GFPLacI-HIS3:his3-11,15 ura3-52 bar1*	this study

BRY674	*MAT**a** smc3-L362-LEU2:leu2-3,112 SMC3-3V5-AID^{608} trp1∆::OsTIR1-CaTRP1 lys4::LacO(DK)-NAT pHIS3-GFPLacI-HIS3:his3-11,15 ura3-52 bar1*	this study
TE228	*MAT**a** PDS5-3V5-AID2-KANMX6 lys4::LacO(DK)-NAT pHIS3-GFP-LacI-HIS3::his3-11,15 trp1-1 ura3-52*	Eng et al. 2014
VG3464-16C	*MAT**a** smc3∆::HPH lys4::LacO(DK)-NAT bar1 pHIS3-GFPLacI-TRP1:his3-11,15 trp1-1 leu2-3,112 ura3-52* +pEU42 (*SMC3 CEN URA3*)	Guacci and Koshland 2012
VG3651-3D	*MAT**a** SMC3-3V5-AID^{608} trp1∆::pGPD1-TIR1-CaTRP1 lys4::LacO(DK)-NAT pHIS3-GFPLacI-HIS3:his3-11,15 leu2-3,112 ura3-52 bar1*	Çamdere et al. 2015

References

Bürmann, F., Basfeld, A., Vazquez Nunez, R., Diebold-Durand, M.-L., Wilhelm, L., & Gruber, S. (2017). Tuned SMC Arms Drive Chromosomal Loading of Prokaryotic Condensin. Molecular Cell, 65(5), 861–872.e9.

Ciosk, R., Shirayama, M., Shevchenko, A., Tanaka, T., Tóth, A., Shevchenko, A., & Nasmyth, K. (2000). Cohesin's Binding to Chromosomes Depends on a Separate Complex Consisting of Scc2 and Scc4 Proteins. Molecular Cell, 5(2), 243–254.

Eng, T., Guacci, V., & Koshland, D. (2014). ROCC, a conserved region in cohesin's Mcd1 subunit, is essential for the proper regulation of the maintenance of cohesion and establishment of condensation. Molecular Biology of the Cell, 25(16), 2351–2364.

Gligoris, T. G., Scheinost, J. C., Bürmann, F., Petela, N., Chan, K.-L., Uluocak, P., et al. (2014). Closing the cohesin ring: structure and function of its Smc3-kleisin interface. Science, 346(6212), 963–967.

Gruber, S., Haering, C. H., & Nasmyth, K. (2003). Chromosomal Cohesin Forms a Ring. Cell, 112(6), 765–777.

Guacci, V., & Koshland, D. (2012). Cohesin-independent segregation of sister chromatids in budding yeast. Molecular Biology of the Cell, 23(4), 729–739.

Guacci, V., Koshland, D., & Strunnikov, A. (1997). A Direct Link between Sister Chromatid Cohesion and Chromosome Condensation Revealed through the Analysis of MCD1 in S. cerevisiae. Cell, 91(1), 47–57.

Haering, C. H., Farcas, A.-M., Arumugam, P., Metson, J., & Nasmyth, K. (2008). The cohesin ring concatenates sister DNA molecules. Nature, 454(7202), 297–301.

Haering, C. H., Löwe, J., Hochwagen, A., & Nasmyth, K. (2002). Molecular architecture of SMC proteins and the yeast cohesin complex. Molecular Cell, 9(4), 773–788.

Haering, C. H., Schoffnegger, D., Nishino, T., Helmhart, W., Nasmyth, K., & Löwe, J. (2004). Structure and stability of cohesin's Smc1-kleisin interaction. Molecular Cell, 15(6), 951–964.

Hirano, M., & Hirano, T. (2006). Opening closed arms: long-distance activation of SMC ATPase by hinge-DNA interactions. Molecular Cell, 21(2), 175–186.

Huis in t Veld, P. J., Herzog, F., Ladurner, R., Davidson, I. F., Piric, S., Kreidl, E., et al. (2014). Characterization of a DNA exit gate in the human cohesin ring. Science, 346(6212), 968–972.

Kulemzina, I., Ang, K., Zhao, X., Teh, J.-T., Verma, V., Suranthran, S., et al. (2016). A Reversible Association between Smc Coiled Coils Is Regulated by Lysine Acetylation and Is Required for Cohesin Association with the DNA. Molecular Cell, 63(6), 1044–1054.

Kurze, A., Michie, K. A., Dixon, S. E., Mishra, A., Itoh, T., Khalid, S., et al. (2011). A positively charged channel within the Smc1/Smc3 hinge required for sister chromatid cohesion. The EMBO Journal, 30(2), 364–378.

Laloraya, S., Guacci, V., & Koshland, D. (2000). Chromosomal addresses of the cohesin component Mcd1p. The Journal of Cell Biology, 151(5), 1047–1056.

Minnen, A., Bürmann, F., Wilhelm, L., Anchimiuk, A., Diebold-Durand, M.-L., & Gruber, S. (2016). Control of Smc Coiled Coil Architecture by the ATPase Heads Facilitates Targeting to Chromosomal ParB/parS and Release onto Flanking DNA. Cell Reports, 14(8), 2003–2016.

Murayama, Y., & Uhlmann, F. (2014). Biochemical reconstitution of topological DNA binding by the cohesin ring. Nature, 505(7483), 367–371.

Murayama, Y., & Uhlmann, F. (2015). DNA Entry into and Exit out of the Cohesin Ring by an Interlocking Gate Mechanism. Cell, 163(7), 1628–1640.

Pu, W. T., & Struhl, K. (1991). The leucine zipper symmetrically positions the adjacent basic regions for specific DNA binding. Proceedings of the National Academy of Sciences of the United States of America, 88(16), 6901–6905.

Soh, Y.-M., Bürmann, F., Shin, H.-C., Oda, T., Jin, K. S., Toseland, C. P., et al. (2015). Molecular Basis for SMC Rod Formation and Its Dissolution upon DNA Binding. Molecular Cell, 57(2), 290–303.

Stigler, J., Çamdere, G. Ö., Koshland, D. E., & Greene, E. C. (2016). Single-Molecule Imaging Reveals a Collapsed Conformational State for DNA-Bound Cohesin. Cell Reports, 15(5), 988–998.

Wahba, L., Gore, S. K., Koshland, D., & Proudfoot, N. (2013). The homologous recombination machinery modulates the formation of RNA–DNA hybrids and associated chromosome instability. eLife, 2, e00505.

Figure Legends

Figure 1: Identification mid-coiled coil RID insertions that impair cohesin function

A) Top: Haploid strains BRY474 (*SMC3 SMC3-AID*), BRY423 (*SMC3-AID*), BRY584 (*smc3-S343 SMC3-AID*), BRY562 (*smc3-I345 SMC3-AID*), and BRY590 (*smc3-Q347 SMC3-AID*) were grown to saturation overnight in liquid YPD, then dilution plated onto YPD plates with and without 0.75 mM auxin and grown at 23˚C for 2 days prior to imaging. Bottom: BRY424 *(SMC3*), VG3464-16C (empty vector), and BRY469 (*smc3-V888*) were grown to saturation in SC –URA dextrose media, then these cultures used to start YPD cultures. Upon reaching saturation, these cells were dilution plated onto YPD and 5-FOA and analyzed for growth phenotypes. Only strains that can lose the *SMC URA3 CEN* plasmid grow on FOA plates.
B) Illustration of cohesin depicting the approximate location of inviable RID insertions from (A) in the coiled coil of Smc3p.
C) Smc3p amino acid alignment between indicated species from S326 to D382 residues on the coiled coil. Amino acids S343, I345, and Q347 are highlighted in yellow and the sequence of their RID insertions in red. The location and sequence of engineered insertions -5, -10, and -15 amino acids from *S. cerevisiae* S343 and +5, +10, and +15 amino acids from Q347 are indicated above the alignment.
D) Amino acid sequence alignment of full-length Smc3p homologs from the indicated species centered on *S. cerevisiae* positions Q874 to I902, with the location of V888 highlighted in yellow. The sequence of the V888 insertion is indicated above in red.
E) Haploid strains BRY474 (*SMC3 SMC3-AID*), BRY423 (*SMC3-AID*), BRY664 (*smc3-L338 SMC3-AID*), BRY666 (*smc3-L333 SMC3-AID*), BRY668 (*smc3-E328 SMC3-AID*), BRY670 (*smc3-L352 SMC3-AID*), BRY672 (*smc3-P357 SMC3-AID*), and BRY674 (*smc3-L362 SMC3-AID*) were grown to saturation in YPD, dilution plated to YPD with and without 0.75 mM auxin and grown at 23˚C for 2 days before imaging.

Figure 2: Cohesion and condensation phenotypes of mid-coiled coil Smc3p RID mutants

A) Haploid strains BRY474 (*SMC3 SMC3-AID*), BRY423 (*SMC3-AID*), BRY562 (*smc3-I345 SMC3-AID*) and TE228 (*PDS5-AID*) were grown to early log phase at 30˚C in YPD and arrested in G1 by addition of alpha factor. Auxin was added for one hour, then cells were released from G1 arrest into YPD containing auxin and nocodazole. Samples were collected before G1 release and throughout cell cycle progression to assess sister chromatid separation at the CEN-distal *LYS4* locus. 100 cells were scored per time point.
B) Haploid strains BRY474 (*SMC3 SMC3-AID*), BRY423 (*SMC3-AID*), BRY494 (*smc3-V888 SMC3-AID*) and TE228 (*PDS5-AID*) were grown to early log phase at 30˚C in YPD and arrested in G1 by addition of alpha factor. Auxin was added

for one hour, then cells were released from G1 arrest into YPD containing auxin and nocodazole. Samples were collected throughout cell cycle progression to assess sister chromatid separation at the CEN-distal *LYS4* locus. 100 cells were scored per time point.

C) Haploid strains BRY474 (*SMC3 SMC3-AID*), BRY423 (*SMC3-AID*), BRY584 (*smc3-S343 SMC3*-AID), BRY562 (*smc3-I345 SMC3-AID*) and BRY590 (*smc3-Q347 SMC3-AID*) were grown to early log phase at 23˚C and arrested in G1 with alpha factor. Auxin was added to each culture for one hour, and cells were released from arrest by washing into YPD containing nocodazole and auxin. After arrest in mid-M phase, cells were fixed and processed as if for *in situ* hybridization (see Materials and Methods). Chromosome masses on slides were visualized by staining with DAPI, and rDNA morphology scored as tight loops, wide loops, or diffuse.

Figure 3: Assembly of cohesin and interaction with loader complex subunit Scc2p is supported by smc3-I345-6HAp

A) Regimen used to grow cells prior to immunoprecipitation in (B). Mid log phase cells growing at 23˚C were arrested in S phase with hydroxyurea for three hours. Auxin was added to each culture for sixty minutes, then cells were collected and lysed for immunoprecipitation. All strains are in the *SMC3-AID* background and treated with auxin.

B) Haploid strains BRY657 (*SCC2-3FLAG*, first lane), BRY604 (*SMC3-6HA SMC3-AID*, second lane), BRY613 (*SCC2-3FLAG SMC3-6HA SMC3-AID*, third lane), and BRY614 (*SCC2-3FLAG smc3-I345-6HA SMC3-AID*, fourth lane) were treated according to (A). After collecting totals samples, clarified lysate was immunoprecipitated for three hours with anti-HA antibody, and the presence of Scc2-3FLAGp, Mcd1p and Smc3-6HAp (or smc3-I345-6HAp) detected in the precipitate by Western blot.

C) Regimen used to grow cells prior to immunoprecipitation in (D). Mid log phase cells growing at 30˚C were arrested in G1 with alpha factor for 2 hours. Auxin was added to each culture for 30 minutes, then cells were released from G1 arrest into fresh YPD containing nocodazole and auxin for 2.5 hours. M phase arrested cells were collected and lysed for immunoprecipitation. All strains are in the *SMC3-AID* background and treated with auxin.

D) Haploid strains BRY423 (*SMC3-AID*, first lane), BRY607 (*SCC3-3FLAG SMC3-AID*, second lane), BRY604 (*SMC3-6HA SMC3-AID*, third lane), BRY621 (*SCC3-FLAG SMC3-6HA SMC3-AID*, fourth lane) and BRY623 (*SCC3-3FLAG smc3-I345-6HA SMC3-AID*, fifth lane) were treated according to the regimen in (C). Extracts were prepared from collected cells. FLAG tagged Scc3p was immunoprecipitated, and coimmunoprecipitates Pds5p and Smc3-6HAp were detected by Western blot.

Figure 4: Smc3-I345p does not support cohesin binding to chromosomes

A) Regimen used to prepare cells prior to ChIP. Cells growing at 23˚C to early log phase were arrested in G1 with alpha factor for three hours. Auxin was added to each culture for one hour, then cells were released from G1 arrest by washing into YPD containing nocodazole and auxin. After checking that cells were arrested in mid-M phase, cells were fixed for two hours and collected for lysis and chromatin shearing (see Materials and Methods).
B) Haploid strains BRY474 (*SMC3 SMC3-AID*, black), BRY423 (*SMC3-AID*, grey), and BRY562 (*smc3-I345 SMC3-AID*, red) were treated as in (A). Cells were lysed, chromatin sheared and subjected to ChIP using polyclonal antibody recognizing Mcd1p. From left: Percent Mcd1p immunoprecipitation at CEN-proximal *CARC1,* CEN-distal *CARL1,* and near centromeres I and XIV by ChIP-qPCR. Controls lacking antibody were also processed to ensure specificity of Mcd1p ChIP.

Figure 1

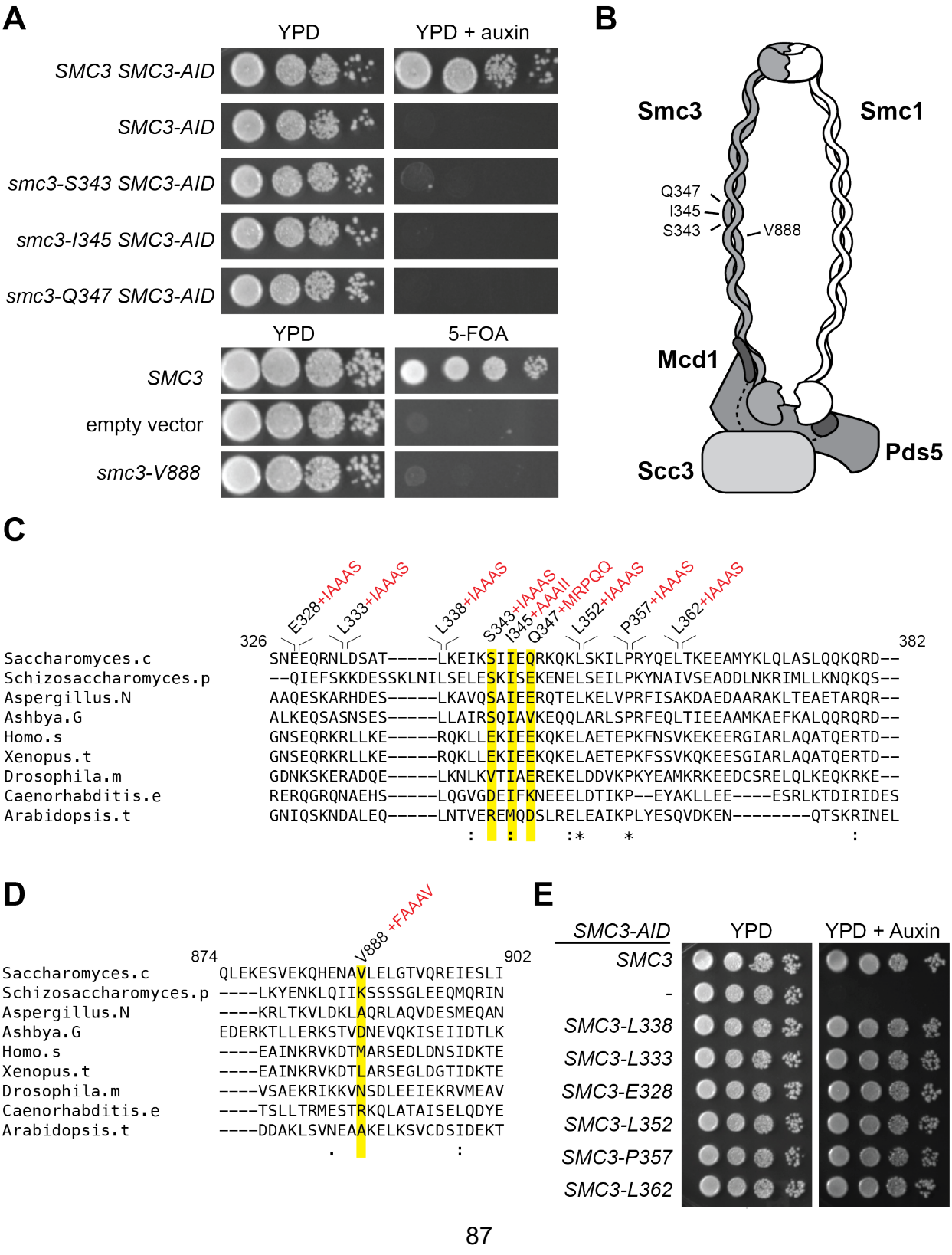
A
YPD
YPD + auxin
SMC3 SMC3-AID
SMC3-AID
smc3-S343 SMC3-AID
smc3-I345 SMC3-AID
smc3-Q347 SMC3-AID
YPD
5-FOA
SMC3
empty vector
smc3-V888
B
Smc3
Smc1
Q347
I345
S343
V888
Mcd1
Scc3
Pds5
C
E328+IAAAS
L333+IAAAS
L338+IAAAS
S343+IAAAS
I345+AAAII
Q347+MRPQQ
L352+IAAAS
P357+IAAAS
L362+IAAAS
326
382
Saccharomyces.c SNEEQRNLDSAT-----LKEIKSIIEQRKQKLSKILPRYQELTKEEAMYKLQLASLQQKQRD--
Schizosaccharomyces.p --QIEFSKKDESSKLNILSELESKISEKENELSEILPKYNAIVSEADDLNKRIMLLKNQKQS--
Aspergillus.N AAQESKARHDES-----LKAVQSAIEERQTELKELVPRFISAKDAEDAARAKLTEAETARQR--
Ashbya.G ALKEQSASNSES-----LLAIRSQIAVKEQQLARLSPRFEQLTIEEAAMKAEFKALQQRQRD--
Homo.s GNSEQRKRLLKE-----RQKLLEKIEEKQKELAETEPKFNSVKEKEERGIARLAQATQERTD--
Xenopus.t GNSEQRKRLLKE-----RQKLLEKIEEKQKELAETEPKFSSVKQKEESGIARLAQATQERTD--
Drosophila.m GDNKSKERADQE-----LKNLKVTIAEREKELDDVKPKYEAMKRKEEDCSRELQLKEQKRKE--
Caenorhabditis.e RERQGRQNAEHS-----LQGVGDEIFKNEEELDTIKP--EYAKLLEE----ESRLKTDIRIDES
Arabidopsis.t GNIQSKNDALEQ-----LNTVEREMQDSLRELEAIKPLYESQVDKEN--------QTSKRINEL
D
V888 +FAAAV
874
902
Saccharomyces.c QLEKESVEKQHENAVLELGTVQREIESLI
Schizosaccharomyces.p ----LKYENKLQIIKSSSSGLEEQMQRIN
Aspergillus.N ----KRLTKVLDKLAQRLAQVDESMEQAN
Ashbya.G EDERKTLLERKSTVDNEVQKISEIIDTLK
Homo.s ----EAINKRVKDTMARSEDLDNSIDKTE
Xenopus.t ----EAINKRVKDTLARSEGLDGTIDKTE
Drosophila.m ----VSAEKRIKKVNSDLEEIEKRVMEAV
Caenorhabditis.e ----TSLLTRMESTRKQLATAISELQDYE
Arabidopsis.t ----DDAKLSVNEAAKELKSVCDSIDEKT
E
SMC3-AID
YPD
YPD + Auxin
SMC3
-
SMC3-L338
SMC3-L333
SMC3-E328
SMC3-L352
SMC3-P357
SMC3-L362

Figure 2

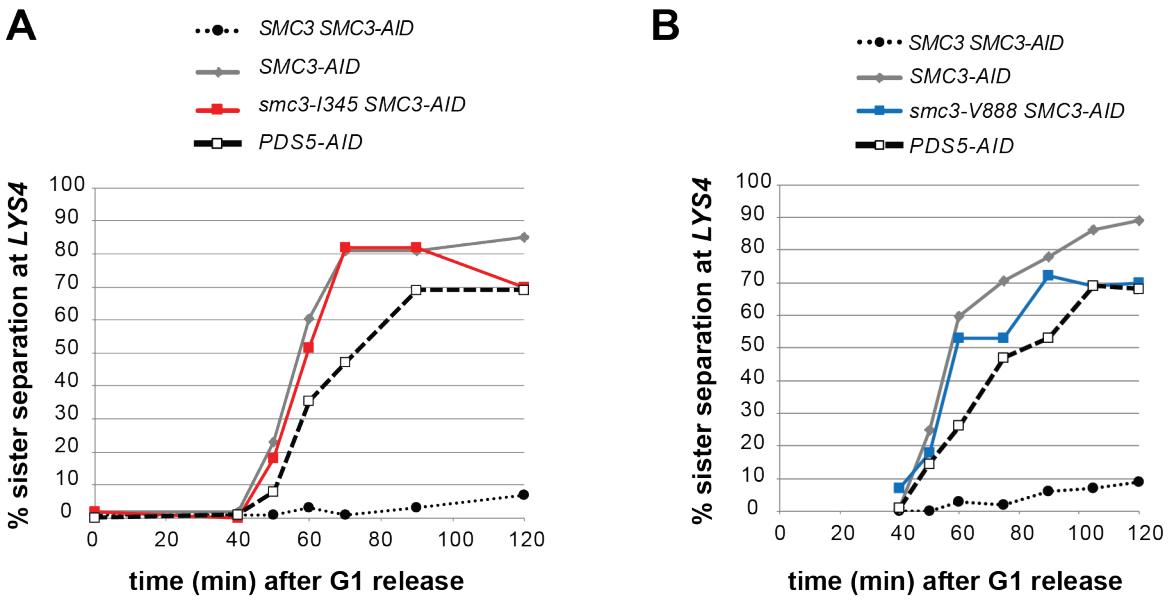
A
SMC3 SMC3-AID
SMC3-AID
smc3-I345 SMC3-AID
PDS5-AID
% sister separation at LYS4
time (min) after G1 release
B
SMC3 SMC3-AID
SMC3-AID
smc3-V888 SMC3-AID
PDS5-AID
% sister separation at LYS4
time (min) after G1 release

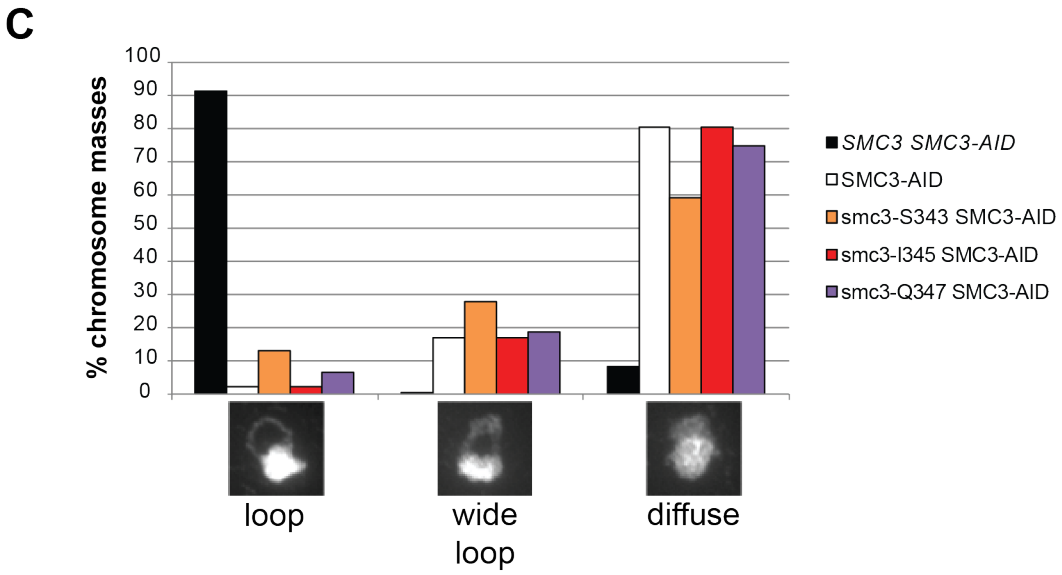
C
% chromosome masses
SMC3 SMC3-AID
SMC3-AID
smc3-S343 SMC3-AID
smc3-I345 SMC3-AID
smc3-Q347 SMC3-AID
loop
wide loop
diffuse

Figure 3

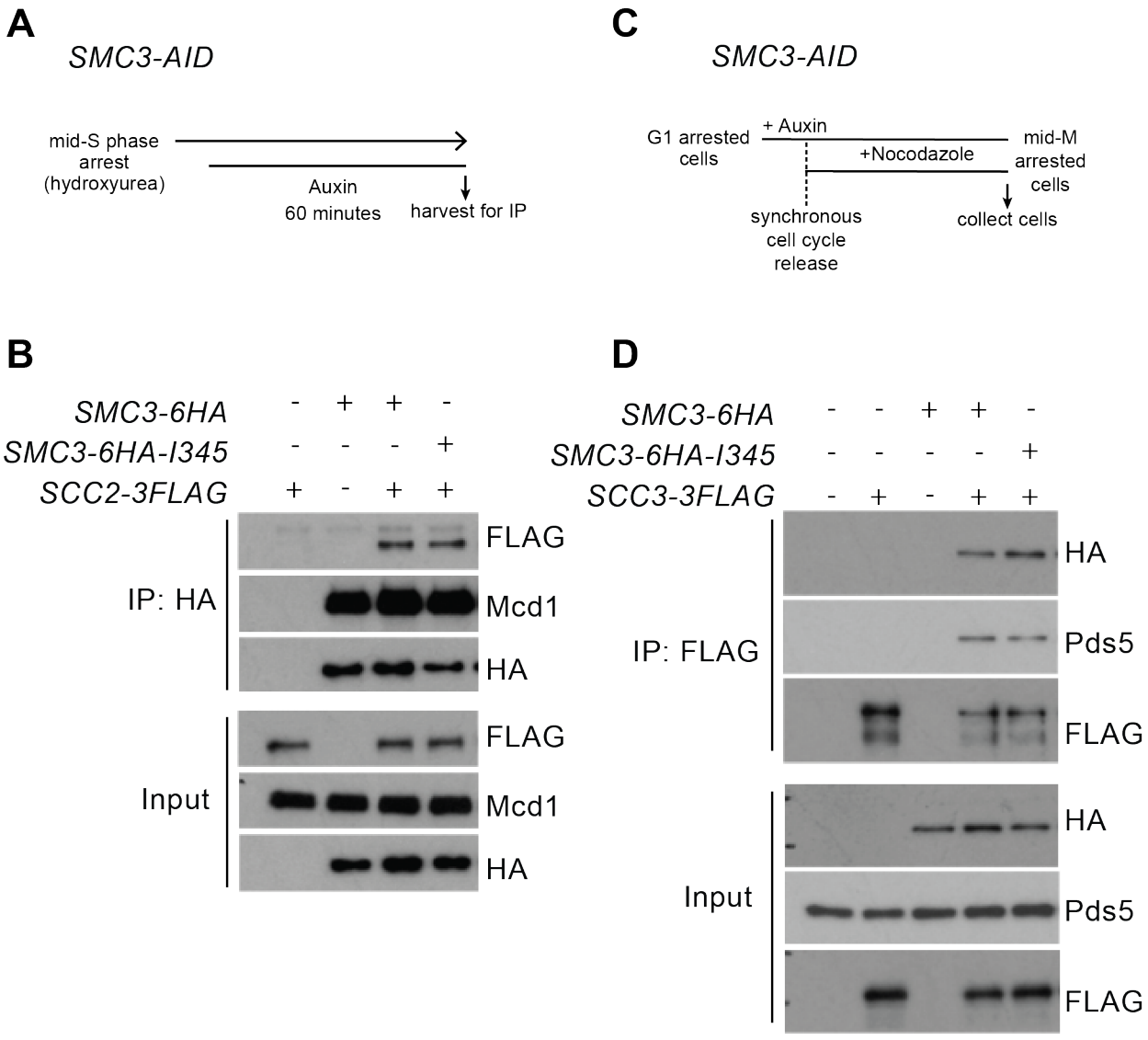
A
SMC3-AID
mid-S phase arrest (hydroxyurea)
Auxin 60 minutes
harvest for IP
C
SMC3-AID
G1 arrested cells
+ Auxin
+Nocodazole
mid-M arrested cells
synchronous cell cycle release
collect cells
B
SMC3-6HA
SMC3-6HA-I345
SCC2-3FLAG
IP: HA
FLAG
Mcd1
HA
Input
FLAG
Mcd1
HA
D
SMC3-6HA
SMC3-6HA-I345
SCC3-3FLAG
IP: FLAG
HA
Pds5
FLAG
Input
HA
Pds5
FLAG

Figure 4

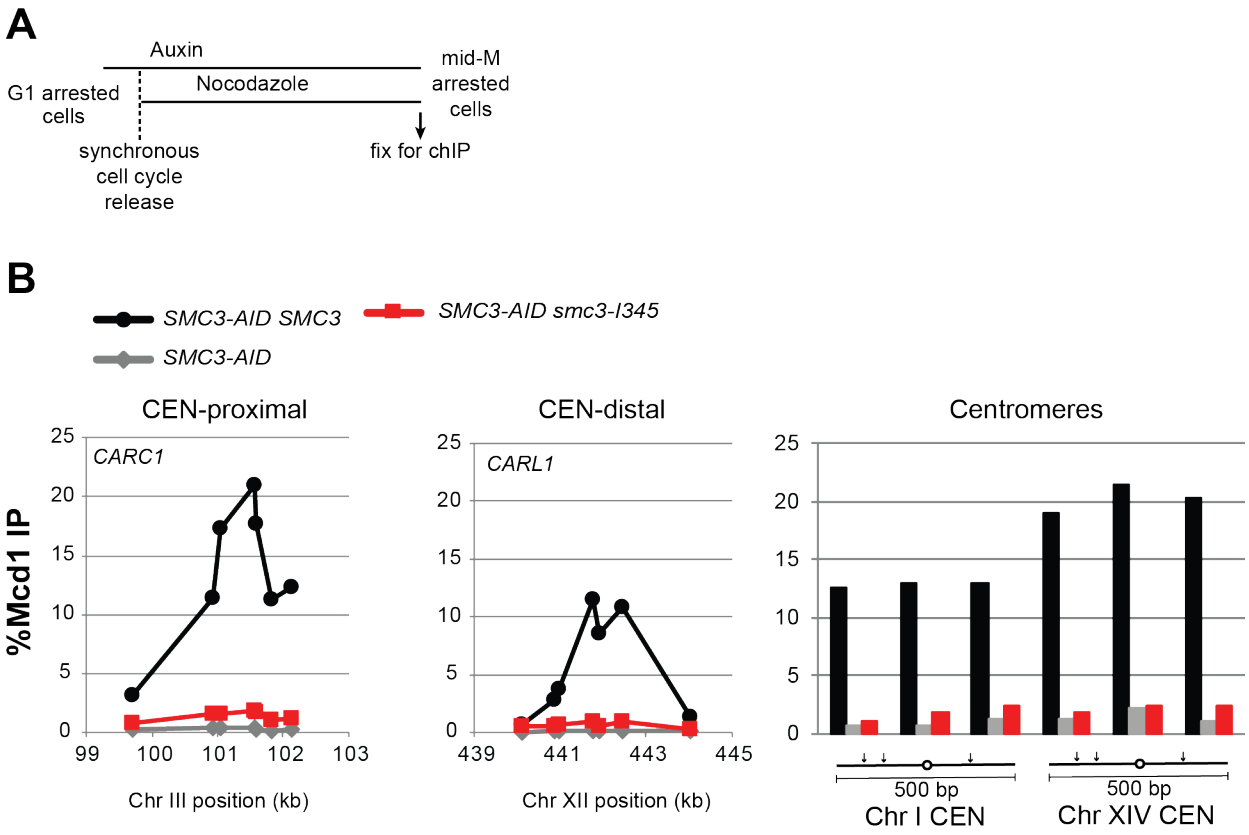
A
Auxin
Nocodazole
G1 arrested cells
mid-M arrested cells
synchronous cell cycle release
fix for chIP
B
SMC3-AID SMC3
SMC3-AID smc3-I345
SMC3-AID
CEN-proximal
CEN-distal
Centromeres
%Mcd1 IP
CARC1
CARL1
Chr III position (kb)
Chr XII position (kb)
500 bp
Chr I CEN
500 bp
Chr XIV CEN

Chapter Five: Discussion

The mechanism by which cohesin tethers two DNA molecules together remains unclear. This dissertation describes Smc3p functions that challenge cherished assumptions of cohesin function. First, I described a previously unappreciated role for the Smc3p/Mcd1p interface in loading of cohesin on DNA in Chapter 2. Second, I described a role for the Smc1p/Smc3p hinge in a post-DNA binding step necessary for the maintenance of sister chromatid cohesion. And third, I identified a specific region of the Smc3p coiled coil that is critical for cohesin function at a step after binding to the loader complex. Moreover, as a result of my screen for RID mutants of Smc3p, I obtained a comprehensive panel of mutants that can serve as a valuable tool to probe the mechanisms of cohesin function.

Revisiting the models for tethering of DNA by cohesin

My characterization of *smc3-D667* revealed that the Smc3p hinge participates in a critical step after cohesin binds chromosomes. Like *mcd1-Q266*, *mcd1-V137K*, and *pds5* mutants that also impair cohesion maintenance without disrupting cohesin binding to chromosomes, the *smc3-D667* mutant poses a challenge to the simple “embrace” model in which topologically bound cohesin is sufficient to tether sister chromatids (Eng et al. 2014). Instead, my observations of Smc3p hinge function support the “handcuff” model of tethering. In one version of the model, referred to as the intramolecular handcuff, a single cohesin has two DNA binding activities. A second version, the intermolecular handcuff, envisions two cohesins interacting while each bind a single DNA strand (Chang et al. 2005). Can my observations of *smc3-D667* rule out one of these versions of the handcuff model?

The intermolecular handcuff model predicts the existence of cohesin-cohesin interactions. Recently, interallelic complementation between pairs of *SMC3* or *MCD1* alleles provided the first evidence in support of cohesin-cohesin interactions (Eng et al. 2015). Two *SMC3* alleles that exhibit interallelic complementation are the temperature-sensitive *smc3-42* allele and *smc3-K113R*. I observed that when introduced into the temperature-sensitive *smc3-42* haploid, *smc3-D667* does not support interallelic complementation for viability. One explanation for the failure of *smc3-D667* to exhibit interallelic complementation may be that, unlike *smc3-K113R*, this allele abolishes multiple functions of Smc3p. Alternatively, *smc3-D667* may impair a single function of Smc3p necessary for interallelic complementation. Although I cannot yet distinguish between these two possibilities, a separate observation suggests a role for the Smc3p hinge in interallelic complementation. Unlike *smc3-K113R*, the double mutant *smc3-K112R, K113R* cannot support interallelic complementation. I discovered that internally HA-tagging *smc3-K112R, K113R* following Asn607, within the hinge domain, generated an allele that exhibits interallelic complementation. This is the first example of a mutation that restores interallelic complementation in *cis*. I hypothesized that, by extension, internally HA-tagging *smc3-D667* might restore its ability to support *smc3-42* viability through interallelic complementation. This did not turn out to be the case. Since internally HA-tagging *smc3-K112R, K113R* restored its interallelic complementation but

not that of *smc3-D667*, I consider it more likely that *smc3-D667* impairs a function necessary for interallelic complementation. These observations suggest the possibility that hinge domains mediate cohesin-cohesin interactions that make interallelic complementation possible. A crucial test of the intermolecular handcuff model awaits development of an assay for cohesin-cohesin interaction in the presence of DNA. Stringent assays for the activities of purified cohesin complex with DNA have recently been published (Murayama and Uhlmann 2014, Çamdere et al. 2015, Murayama and Uhlmann 2015), and it is reasonable to think that an *in vitro* cohesion assay is in sight. Alternatively, close proximity of two cohesins in cells could be examined using fluorescence resonance energy transfer (FRET).

The intramolecular handcuff model predicts two DNA binding sites within a single cohesin. Do my observations of Smc3p hinge function rule out the intramolecular handcuff model? Evidence showing that cohesin can bind DNA topologically requires that at minimum one binding event be topological (Haering et al. 2008, Stigler et al. 2016). My observation that smc3-D667p stably binds chromosomes suggests that one of its DNA binding modes remains intact and that this intact mode is likely topological. Therefore, the Smc3p hinge could be required to maintain the second DNA binding event. This event could be a second topological entrapment or a non-topological affinity for DNA. Since my observations are consistent with either of these possibilities, I cannot rule out the intramolecular handcuff model. However, the stable binding of smc3-D667p to chromosomes and failure to maintain cohesion require a modification of the intramolecular handcuff model. This modification requires that one DNA binding mode be stable while a second be unstable. It is hard to see how this could be the case if both sister chromatids were trapped within the large Smc1p/Smc3p ring. Instead, it is consistent with DNA from one sister chromatid binding within the Smc1p/Smc3p ring and the second binding in the smaller Mcd1p loop. Alternatively, one chromatid could bind topologically within either the large ring or small loop and the second chromatid could bind non-topologically to the head or hinge domains, which have been shown to bind DNA *in vitro* (Murayama and Uhlmann 2015). If the stable DNA binding mode is topological, distinguishing whether it is through the large Smc loop or small Mcd1p loop is possible using cysteine-crosslinking reagents between each interface of both the large and small loops.

Regulation of the Mcd1p-Smc3p interface in response to DNA damage

I identified multiple mutations within the interface between Mcd1p and Smc3p, which has been described as the DNA “exit gate” of cohesin. While a point mutation in Smc3p, L1029R, is sufficient to eliminate the ability of Mcd1p to bind Smc3p (Gligoris et al. 2014), I demonstrated that five amino acid insertions at I196 and K1023 were unlikely to abolish this interaction (Chapter 2 of this dissertation). This interface and its regulation remain poorly understood. A fusion protein that joins Smc3p and Mcd1p can restore viability to *smc3*Δ *mcd1*Δ cells, indicating that opening of this interface is not required for viability *per se* (Gruber et al. 2006). Mcd1p is post-translationally modified in response to DNA damage, and these modifications are required for cohesion generation in M phase cells (Heidinger-Pauli et al. 2009). DNA damage causes phosphorylation of

Mcd1p at S83, and can be mimicked by the S83D mutation to allow constitutive cohesion generation in M phase. Interestingly, this mutation lies directly within the interface between Mcd1p and Smc3p and is predicted to abolish their association. I have modified a crosslinking protocol that allows specific detection of the interaction between this region of Mcd1p and Smc3p's coiled coil (Beckouet et al. 2016). My initial results suggest that Mcd1p-S83D does impair its association with Smc3p. This is surprising considering that the Mcd1p-Smc3p interaction is necessary for viability. Instead, I think that Mcd1p may have a second mode of binding to Smc3p that allows the *SMC3-S83D* mutant to survive as the sole source of *MCD1*. Further biochemical and genetic investigation will provide valuable insight into how cohesin responds to DNA damage through modulation of the Smc3p-Mcd1p interaction.

Search for suppressors of inviable *SMC3* RID alleles

One advantage of studying cohesin in yeast is the ease of genetic manipulation and screening. I attempted to identify spontaneous suppressors of *smc3-D667* and *smc3-I345* mutant inviability by screening strains supported by an *SMC3 URA3 CEN* plasmid for growth on 5-FOA plates. Unfortunately, I needed to screen all FOA+ colonies by PCR to check for the presence of the RID mutation. After multiple rounds and thousands of FOA+ colonies screened, I found no FOA+ colonies that retained the RID mutations, all were likely gene conversion events that restored wild-type *SMC3*. One possible explanation is that these mutations produce large effects on the protein, a five-amino-acid insertion, that might be difficult to correct by spontaneous point mutation. Screening for suppressors may be facilitated by reducing the length of insertion or making point mutations that recapitulate the *smc3-D667* and *smc3-I345* phenotypes. I propose three alternative approaches that could be used to identify suppressors. First, chemical mutagenesis with EMS could allow for a wider range of mutations. Second, to reduce the incidence of gene conversions to wild type *SMC3* by homologous recombination, the *SMC3* allele on the covering plasmid could be codon scrambled to reduce the efficiency of HR. Third, error prone PCR mutagenesis approaches could be used to specifically screen for suppressor mutations in *cis*.

To conclude, the results I have presented in this dissertation contribute to an increasingly complex mechanism of cohesin function. While I believe that to simplify is more preferable than to complicate, my hope is that this work contributes in its own small way to refine the simple models depicted for cohesin in textbooks to something that more reflects the complex truth of this remarkable molecular machine.

References

Beckouët, F., Srinivasan, M., Roig, M. B., Chan, K.-L., Scheinost, J. C., Batty, P., et al. (2016). Releasing Activity Disengages Cohesin's Smc3/Scc1 Interface in a Process Blocked by Acetylation. Molecular Cell, 61(4), 563–574.

Çamdere, G., Guacci, V., Stricklin, J., & Koshland, D. (2015). The ATPases of cohesin interface with regulators to modulate cohesin-mediated DNA tethering. eLife, 4, 13115.

Chang, C.-R., Wu, C.-S., Hom, Y., & Gartenberg, M. R. (2005). Targeting of cohesin by transcriptionally silent chromatin. Genes & Development, 19(24), 3031–3042.

Eng, T., Guacci, V., & Koshland, D. (2014). ROCC, a conserved region in cohesin's Mcd1 subunit, is essential for the proper regulation of the maintenance of cohesion and establishment of condensation. Molecular Biology of the Cell, 25(16), 2351–2364.

Eng, T., Guacci, V., & Koshland, D. (2015). Interallelic complementation provides functional evidence for cohesin-cohesin interactions on DNA. Molecular Biology of the Cell, 26(23), 4224–4235.

Gruber, S., Arumugam, P., Katou, Y., Kuglitsch, D., Helmhart, W., Shirahige, K., & Nasmyth, K. (2006). Evidence that loading of cohesin onto chromosomes involves opening of its SMC hinge. Cell, 127(3), 523–537.

Haering, C. H., Farcas, A.-M., Arumugam, P., Metson, J., & Nasmyth, K. (2008). The cohesin ring concatenates sister DNA molecules. Nature, 454(7202), 297–301.

Heidinger-Pauli, J. M., Ünal, E., & Koshland, D. (2009). Distinct Targets of the Eco1 Acetyltransferase Modulate Cohesion in S Phase and in Response to DNA Damage. Molecular Cell, 34(3), 311–321.

Murayama, Y., & Uhlmann, F. (2014). Biochemical reconstitution of topological DNA binding by the cohesin ring. Nature, 505(7483), 367–371.

Murayama, Y., & Uhlmann, F. (2015). DNA Entry into and Exit out of the Cohesin Ring by an Interlocking Gate Mechanism. Cell, 163(7), 1628–1640.

Stigler, J., Çamdere, G. Ö., Koshland, D. E., & Greene, E. C. (2016). Single-Molecule Imaging Reveals a Collapsed Conformational State for DNA-Bound Cohesin. Cell Reports, 15(5), 988–998.